



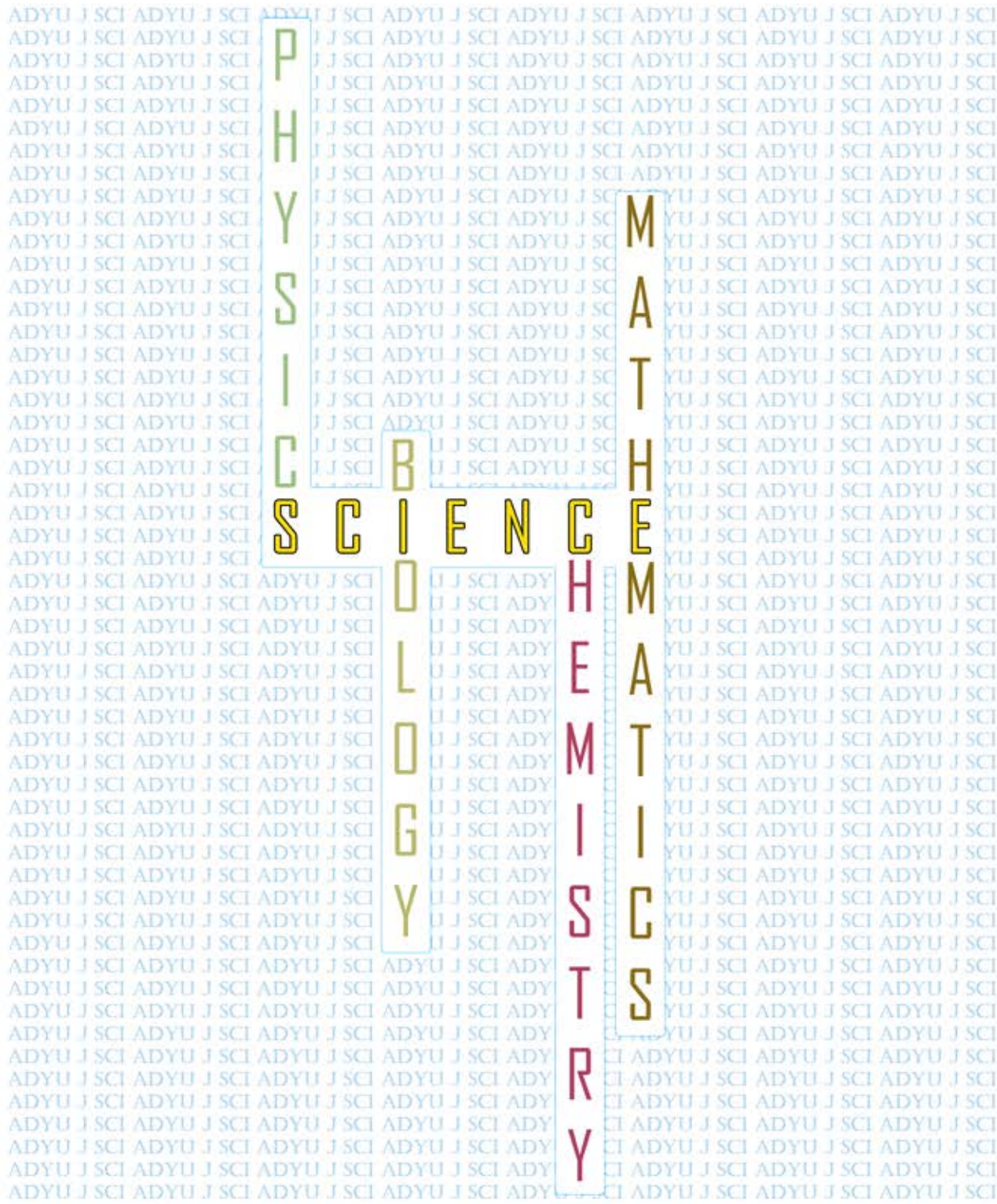
# Adiyaman University Journal of Science

Dec. 2023

Volume: 13

Issue: 1&2

An international peer reviewed journal of science



An open access, peer-reviewed, international journal of science. Biannual (June & December). ISSN 2147-1630 | e-ISSN 2146-586X. Publisher: Adiyaman University.

**Publication language:** English (with Turkish title and abstract)

**Issue published date:** 31.12.2023

**Privilege owner:** On Behalf of the Rectorate of Adiyaman University, Prof. Dr. Mehmet KELLEŞ (Rector)

**Web site:** EN: <https://dergipark.org.tr/en/pub/adyujsci>  
TR: <https://dergipark.org.tr/tr/pub/adyujsci>

#### EDITORIAL BOARD

**Editor-in-Chief** : Deniz SUNAR ÇERÇİ, Ph.D.

#### Editors:

**Biology** : Serdar SÖNMEZ, Ph.D.  
: Ertan YOLOĞLU, Ph.D.  
**Chemistry** : Cumhuri KIRILMIŞ, Ph.D.  
: Gökhan ELMACI, Ph.D.  
**Mathematics** : Selcen YÜKSEL PERKTAŞ, Ph.D.  
: Serbay DURAN, Ph.D.  
**Physics** : Salim ÇERÇİ, Ph.D.  
: Özge ERKEN, Ph.D.

**Statistics Editor:** : Tayfun SERVİ, Ph.D.

#### Section Editors

##### Biology:

Aydın AKBUDAK, Ph.D.  
Bahadır AKMAN, Ph.D.  
Birgül ÖZCAN, Ph.D.  
Deniz AYAS, Ph.D.  
Hasan YILDIZ, Ph.D.  
Olga SAK, Ph.D.  
Özkan ASLANTAŞ, Ph.D.  
Si Hong PARK, Ph.D.  
Süphan KARAYTUĞ, Ph.D.

##### Chemistry:

Sezgin BAKIRDERE, Ph.D.  
H. Mehmet KAYILI, Ph.D.  
Önder METİN, Ph.D.  
Zeynel SEFEROĞLU, Ph.D.  
Lokman UZUN, Ph.D.

##### Mathematics:

Ramazan AKGÜN, Ph.D.  
Murat CANDAN, Ph.D.  
FeYZa Esra ERDOĞAN, Ph.D.

Mehmet Onur FEN, Ph.D.  
Öznur GÖLBAŞI, Ph.D.  
Mehmet GÜLBAHAR, Ph.D.  
Bilge İNAN, Ph.D.  
Eylem GÜZEL KARPUZ, Ph.D.  
Aynur KESKİN KAYMAKCI, Ph.D.  
Mustafa Çağatay KORKMAZ, Ph.D.  
James F. PETERS, Ph.D.  
Tahsin ÖNER, Ph.D.

##### Physics:

Ahmet EKİCİBİL, Ph.D.  
Didar DOBUR, Ph.D.  
Daniel GREEN, Ph.D.  
Faruk KARADAĞ, Ph.D.  
Hakan ÖZTÜRK, Ph.D.  
Kristina RUSIMOVA, Ph.D.  
Latife ŞAHİN YALÇIN, Ph.D.  
Mustafa GÜNEŞ, Ph.D.  
Paolo GUNNELLINI, Ph.D.

**Technical Contact:** Serdar SÖNMEZ, Ph.D., [ssonmez@adiyaman.edu.tr](mailto:ssonmez@adiyaman.edu.tr), [sonmezserdar@gmail.com](mailto:sonmezserdar@gmail.com)

**Language Editors:** Münevver AKBAŞ



The articles published in this journal are licensed under a Creative Commons Attribution-NonCommercial-ShareAlike 4.0 International License.

**Table of Contents (İçindekiler)**  
Volume (Cilt): 13 Number (Sayı): 1&2  
December (Aralık) 2023

---

---

**BIOLOGY**

---

**Bioactivity Features of Novel Actinobacteria Isolated from Lichen and Orchid Plant**

Liken ve Orkide Bitkisinden İzole Edilen Aktinobakterilerin Biyoaktivite Özellikleri 43-58  
*Hilal ATEŞ, Hilal AY*

---

---

**MATHEMATICS**

---

**On the Interval Valued Cesaro Convergent Sequences Space**

Aralık Değerli Cesaro Yakınsak Diziler Uzayı Üzerine 1-17  
*Gülşen KILINÇ, Mehmet Sezai YILDIRIM*

**A Note on The Some Class of Symmetric Numerical Semigroups**

Bazı Simetrik Sayısal Yarı Grup Sınıflarına İlişkin Bir Not 18-27  
*Ahmet ÇELİK*

**A Numerical Application of the Chebyshev Operational Matrix Method for HIV Infection of CD4+T-cells**

CD4+T Hücrelerindeki HIV Enfeksiyonunun Yayılım Modelinin Chebyshev Operasyonel Matris Metodu ile bir Nümerik Uygulaması 59-73  
*Yalçın ÖZTÜRK, Ayşe Anapalı ŞENEL, Ceren LİMONCU, Mustafa GÜLSU*

**A Chen-like Inequalities on Submanifolds of Cosymplectic 3-Space Forms**

Kosimplektik 3-Uzay Formlarının Altmanifoldları Üzerinde Chen-tipi Eşitsizlikler 89-109  
*Mehmet GÜLBAHAR, Esra ERKAN*

---

---

**PHYSICS**

---

**The Sintering Temperature Effect on Magnetocaloric Effect in La<sub>2</sub>MnNiO<sub>6</sub> Double Perovskite Manganite Material**

La<sub>2</sub>MnNiO<sub>6</sub> Çift Katlı Perovskit Manganit Malzemede Sinterleme Sıcaklığının Manyetik Soğutma Parametrelerinin Üzerindeki Etkisi 28-42  
*İbrahim Barış SEVER, Arda KANDEMİR, Ali Osman AYAS, Ahmet EKİCİBİL*

**Structural, Magnetic and Catalytic Properties of FeCo Nanoparticles Synthesized by Polyol Process**

Poliol Yöntemi ile Sentezlenen FeCo Nanopartiküllerinin Yapısal, Manyetik ve Katalitik Özellikleri 74-88  
*Emre Can TAYFUN, Kaan ERMAN, Dogan KAYA, Faruk KARADAG, Ahmet EKİCİBİL*

---

---



## On the Interval Valued Cesaro Convergent Sequences Space

Gülşen KILINÇ<sup>1</sup>, Mehmet Sezai YILDIRIM<sup>2</sup>

<sup>1</sup>Adiyaman University Faculty of Education,  
Department of Mathematics and Science Education, Adiyaman, Türkiye  
[gkilinc@adiyaman.edu.tr](mailto:gkilinc@adiyaman.edu.tr), ORCID: 0000-0002-9657-2577

<sup>2</sup>Mathematics Teacher, Ministry of National Education, Adiyaman, Türkiye  
[sezai63songul@gmail.com](mailto:sezai63songul@gmail.com), ORCID: 0000-0001-8520-2610

Received: 14.05.2023

Accepted: 06.07.2023

Published: 31.12.2023

### Abstract

The concept of quasilinear space is a field that needs to be matured, the foundations of which were laid by S. M. Aseev's published work in 1986. The simplest nonlinear quasi linear space example is the set  $P$  which is a class of closed intervals of real numbers. In this study, it was given an interval-valued sequence space using the Cesàro limitation method's matrix domain. Also, its quasilinear space structure, some topological characteristics, and some inclusion relations were examined.

**Keywords:** Quasilinear Space; Interval Valued Sequence; Hausdorff Metric; Cesàro Convergence.

### Aralık Değerli Cesaro Yakınsak Diziler Uzayı Üzerine

#### Öz

Quasilineer uzay kavramı, temelleri S. M. Aseev'in 1986 yılında yayınlanan çalışmasıyla atılan, olgunlaşması gereken bir alandır. Lineer olmayan Quasilineer uzayın en basit örneği, gerçek sayıların kapalı aralıklar sınıfı olan  $P$  kümesidir. Bu çalışmada Cesàro limitleme yönteminin matris etki alanı kullanılarak aralık değerli bir dizi uzayı verildi. Ayrıca bu uzayın quasilineer uzay yapısı, bazı topolojik özellikleri ve bazı kapsama ilişkileri incelendi.

<sup>1</sup> Corresponding Author

DOI: 10.37094/adyujsci.1296930



**Anahtar Kelimeler:** Quasilinear Uzay; Aralık Değerli Dizi; Hausdorff Metrik; Cesàro yakınsaklık.

## 1. Introduction

Aseev [13] introduced the concept of quasilinear spaces in 1986, which generalized linear spaces. The partial order relation he used in the definition made it easy to give a consistent response to some basic concepts and results of linear algebra. His study has also inspired the presentation of many studies on set valued analysis [14], set differential equations [15], fuzzy quasilinear spaces [16]. Yılmaz has many studies on quasilinear spaces and has made important contributions to the literature [17, 18, 24-31].

After Zadeh [1] introduced the concept of fuzzy set to the literature, interval numbers and fuzzy numbers have also been used in the construction of mathematical structures. One of these structures is sequence spaces. Interval arithmetic, which was founded by Dwyer [2], was further developed by Moore [3, 4]. Chiao introduced sequence of interval numbers and defined the usual convergence of sequence interval numbers [23]. Some other studies on this topic: [12], [13].

Some studies in which fuzzy sequence spaces are defined and some of their properties are examined [6-11, 20]:

In this paper, we introduce interval valued Cesàro convergent sequence spaces and discuss some of their properties.

## 2. Preliminaries

Throughout this study,  $\mathbb{N}$ ,  $\mathbb{R}$  and  $\mathbb{C}$  will represent the set of natural, real and complex numbers, respectively. Closed interval is a subset of the real numbers  $\{x \in \mathbb{R} : \underline{D} \leq x \leq \overline{D}\}$  and the interval  $D$  is denoted as  $D = [\underline{D}, \overline{D}]$ , where  $\underline{D}$  and  $\overline{D}$  are the left and right endpoints of an interval  $D$ , respectively [5]. Although other types of intervals (open, half-open) appear in mathematics, our focus will be on closed intervals. The interval term in this study refers to a closed interval.

$D$  is said to be degenerate, if  $\underline{D} = \overline{D}$ . An interval of this type contains a single real number  $d$ , [5].

A closed subset of real numbers is an interval number. It is denoted as a set of all real valued interval numbers by  $P$  in this study. That is, each element of  $P$  is  $D$ , represented as

$$D = \{x \in \mathbb{R} : \underline{D} \leq x \leq \overline{D}\}. \quad (1)$$

The set of all real valued interval numbers  $P$  is metric space with the metric  $h$  called the hausdorff metric, [5] where  $h$  is defined as

$$h(D_1, D_2) = \max \left\{ \left| \underline{D}_1 - \underline{D}_2 \right|, \left| \overline{D}_1 - \overline{D}_2 \right| \right\}. \quad (2)$$

It is easily obtained that  $P$  is complete metric space with the function  $h$ . The usual metric of  $\mathbb{R}$  is obtained when  $D_1$  and  $D_2$  are degenerate intervals.

Also, the set of all real-valued interval numbers  $P$  is the normed space with the norm function defined [5]:

$$\|D\|_P = \sup \|t\|_{\mathbb{R}}, \quad t \in D, \quad D \in P, \quad \|t\|_{\mathbb{R}} = |t|.$$

Let us now go over Aseev's [13] definition of a quasilinear space and some of its basic properties.

The operations of addition, scalar multiplication, and a partial order relation on the set  $P$  of intervals are defined as follows:

For all  $U, V \in P$ ,  $U = [\underline{U}, \overline{U}]$ ,  $V = [\underline{V}, \overline{V}]$  and  $\lambda \in \mathbb{R}$ ,

$$U + V = [\underline{U}, \overline{U}] + [\underline{V}, \overline{V}] = [\underline{U} + \underline{V}, \overline{U} + \overline{V}]$$

$$\lambda U = \lambda [\underline{U}, \overline{U}] = \begin{cases} [\lambda \underline{U}, \lambda \overline{U}], & \text{if } \lambda \geq 0, \\ [\lambda \overline{U}, \lambda \underline{U}], & \text{if } \lambda < 0, \end{cases}$$

$$U \leq V \Leftrightarrow [\underline{U}, \overline{U}] \subseteq [\underline{V}, \overline{V}].$$

Let us continue by defining quasilinear space.

**Definition 1:** [13] When the addition, scalar multiplication, and partial order relation defined on a set  $X$  satisfy the following conditions,  $X$  is called quasilinear space:

- i)  $u \leq u$ ,
- ii)  $u \leq w$ , if  $u \leq v$  and  $v \leq w$ ,
- iii)  $u = v$  if  $u \leq v$  and  $v \leq u$ ,
- iv)  $u + v = v + u$ ,
- v)  $u + (v + w) = (v + u) + w$ ,
- vi) There is a  $\theta$  element of  $X$  that satisfies  $x + \theta = x$ ,
- vii)  $\mu. (\lambda u) = (\mu. \lambda)u$ ,

- viii)  $\mu \cdot (u + v) = \mu \cdot u + \mu \cdot v$ ,
- ix)  $1 \cdot u = u$ ,
- x)  $0 \cdot u = \theta$ ,
- xi)  $(\mu + \lambda) \cdot u \leq \mu \cdot u + \lambda \cdot v$ ,
- xii)  $u + v \leq w + \varphi$  if  $u \leq w$  and  $v \leq \varphi$ ,
- xiii)  $\mu \cdot u \leq \mu \cdot v$  if  $u \leq v$ ,

where for all  $u, v, w, \varphi \in X$  and  $\mu, \lambda \in \mathbb{R}$ .

In this study, quasilinear space is abbreviated as QLS.

When we use " $=$ " as a partial order relation, then the QLS transforms into a linear space. The set of all closed intervals of real numbers is a famous understandable example of a non-linear QLS.

**Definition 2:** [13] A norm is a  $n$  function defined from an  $X$  QLS to  $\mathbb{R}$  that satisfies the following conditions, in this case  $X$  is called a normed quasilinear space. That is  $n: X \rightarrow \mathbb{R}$ ,

For all  $u, v \in X$  and  $\mu$  scalar,

- i.  $n(u) > 0$ , if  $u \neq \theta$
- ii.  $n(u + v) \leq n(u) + n(v)$ ,
- iii.  $n(\mu \cdot u) = |\mu|n(u)$ ,
- iv.  $n(u) \leq n(v)$ , if  $u \leq v$ ,
- v. For any positive number  $\delta$ , If  $X$  has an  $u_\delta$  element that satisfies  $n(u_\delta) \leq \delta$  and,  $u \leq v + u_\delta$  then  $u \leq v$ .

Now let us define definition of the concept of interval number sequence.

An interval number sequence is a function whose domain set is  $\mathbb{N}$ , and the range set is the set of closed intervals  $P$ . That is, the function  $f$  defined as follows:

$$f: N \rightarrow P, \quad f(k) = (D_k),$$

is called an interval number sequence, where  $D_k = [\underline{D}_k, \overline{D}_k]$ , for each  $k$ , and  $\underline{D}_k \leq \overline{D}_k$ , [12].

The class of all interval sequences will be denoted by  $w(P)$  in this study.

$$w(P) = \{(D_k): k \in N, D_k \in P\},$$

The space  $w(P)$  is a quasilinear space with the following operations defined on interval term sequences: For all  $U, V \in w(P)$ ,

$$U = (U_k) = ([\underline{U}_1, \overline{U}_1], [\underline{U}_2, \overline{U}_2], \dots, [\underline{U}_k, \overline{U}_k], \dots)$$

$$V = (V_k) = ([\underline{V}_1, \overline{V}_1], [\underline{V}_2, \overline{V}_2], \dots, [\underline{V}_k, \overline{V}_k], \dots)$$

$$U + V = ([\underline{U}_k + \underline{V}_k, \overline{U}_k + \overline{V}_k]) \tag{3}$$

$$\lambda U = \lambda([\underline{U}_k, \overline{U}_k]) = (\lambda[\underline{U}_k, \overline{U}_k])$$

$$\lambda[\underline{U}_k, \overline{U}_k] = \begin{cases} [\lambda\underline{U}, \lambda\overline{U}], & \lambda \geq 0 \\ [\lambda\overline{U}, \lambda\underline{U}], & \lambda < 0 \end{cases} \tag{4}$$

$$U \leq V \Leftrightarrow [\underline{U}_k, \overline{U}_k] \subseteq [\underline{V}_k, \overline{V}_k]. \tag{5}$$

The following is a definition of the convergence of interval number sequences, [23]:

Let  $(U_k)$  be a sequence of interval numbers and  $U_0$  be an interval number. If there is a  $k_0 = k_0(\varepsilon) \in \mathbb{N}$  for which the inequality  $h(U_k, U_0) < \varepsilon$  is provided for all  $\varepsilon > 0$  and for all  $k > k_0$ , then the sequence  $(U_k)$  is said to be convergent to  $U_0$ . This convergence is displayed as

$$\lim_k U_k = U_0 \text{ or } (U_k) \rightarrow U_0, (k \rightarrow \infty),$$

where the limit is taken on the Hausdorff metric  $h$  given by equation 2.

We can conclude that  $\lim_{k \rightarrow \infty} U_k = U_0 \Leftrightarrow \lim_{k \rightarrow \infty} \underline{U}_k = \underline{U}_0$  ve  $\lim_{k \rightarrow \infty} \overline{U}_k = \overline{U}_0$ .

For example, let us consider the interval number sequence  $(U_k) = [-\frac{1}{k+3}, \frac{1}{k+3}]$ . If we examine the convergence of this sequence of intervals, we get that

$\lim_{k \rightarrow \infty} U_k = \lim_{k \rightarrow \infty} [-\frac{1}{k+3}, \frac{1}{k+3}] = [0,0] = \theta$ . This means that the sequence  $(U_k)$  is convergent to the interval number  $[0,0] = \theta$ .

The spaces of null, convergent, and bounded sequences of interval numbers are defined as follows, respectively:

$$P_{c_0} = \{(U_k) \in w(P) : \lim_k U_k = [0,0] = \theta\},$$

$$P_c = \left\{ (U_k) \in w(P) : \lim_k U_k = U_0, \quad U_0 \in P \right\},$$

$$P_{\ell_\infty} = \left\{ (U_k) \in w(P) : \sup_k \{ | \underline{U}_k |, | \overline{U}_k | \} < \infty \right\}.$$

These spaces are complete metric spaces with the function  $d$  defined as follows for each  $U$  and  $V$  sequence taken from these spaces: [12].

$$d(U_k, V_k) = \sup_k \{ \max \{ | \underline{U}_k - \underline{V}_k |, | \overline{U}_k - \overline{V}_k | \} \}.$$

An interval valued sequence is Cesàro convergent to  $V \in P$  if and only if  $h(\frac{1}{n} \sum_{k=1}^n U_k, V) \rightarrow 0$  for  $n \rightarrow \infty$ .

### 3. Main Results

$C_I(1)$  and  $C_{I_0}(1)$  represent the spaces of interval valued Cesàro convergent sequences and interval valued Cesàro null convergent sequences, respectively, in this study. That is,

$$C_I(1) = \{ (U_k) \in w(P) : \lim_{n \rightarrow \infty} h \left( \frac{1}{n} \sum_{k=1}^n [ \underline{U}_k, \overline{U}_k ], [ \underline{V}, \overline{V} ] \right) = 0, \text{ for some } [ \underline{V}, \overline{V} ] \in P \}$$

$$C_{I_0}(1) = \{ (U_k) \in w(P) : \lim_{n \rightarrow \infty} h \left( \frac{1}{n} \sum_{k=1}^n [ \underline{U}_k, \overline{U}_k ], [ 0, 0 ] \right) = 0 \}$$

Now let us show that this set is well defined, that is, it has at least one element.

For instance, the sequence  $([-1, \frac{1}{n}])$  belongs to the set  $C_I(1)$ . Really it can be easily seen that

$$\lim_n \frac{1}{n} \sum_{i=1}^n \left[ -1, \frac{1}{i} \right] = [-1, 0]$$

Therefore  $C_I(1) \neq \emptyset$ .

**Theorem 1:** The space  $C_I(1)$  is a metric space with the function  $d$  defined as

$$d(U, V) = \sup_n \{ \max \left\{ \frac{1}{n} \sum_{i=1}^n | \underline{U}_i - \underline{V}_i |, \frac{1}{n} \sum_{i=1}^n | \overline{U}_i - \overline{V}_i | \right\} \}. \tag{6}$$

**Proof:** i) For all  $U, V \in C_I(1)$ , when  $U \neq V$ , it is easy to see that  $d(U, V) > 0$ ,

Let us prove that  $U = V \Leftrightarrow d(U, V) = 0$ .

$$U = V \Leftrightarrow U_i = V_i, \text{ for each } i \in \mathbb{N},$$

$$\Leftrightarrow \underline{U}_i = \underline{V}_i \text{ and } \overline{U}_i = \overline{V}_i, \text{ for each } i \in \mathbb{N},$$

From here

$$|\underline{U}_j - \underline{V}_j| = 0, \text{ and } |\overline{U}_i - \overline{V}_i| = 0 \Leftrightarrow d(U, V) = 0$$

ii) It is clear that  $d(U, V) = d(V, U)$

$$\begin{aligned} \text{iii) } d(U, V) &= \sup_n \left\{ \max \left\{ \frac{1}{n} \sum_{i=1}^n |\underline{U}_i - \underline{V}_i|, \frac{1}{n} \sum_{i=1}^n |\overline{U}_i - \overline{V}_i| \right\} \right\} \\ &= \sup_n \left\{ \max \left\{ \frac{1}{n} \sum_{i=1}^n |\underline{U}_i - \underline{V}_i - \underline{Z}_i + \underline{Z}_i|, \frac{1}{n} \sum_{i=1}^n |\overline{U}_i - \overline{V}_i - \overline{Z}_i + \overline{Z}_i| \right\} \right\} \\ &\leq \sup_n \left\{ \max \left\{ \frac{1}{n} \sum_{i=1}^n (|\underline{U}_i - \underline{Z}_i| + |\underline{Z}_i - \underline{V}_i|), \frac{1}{n} \sum_{i=1}^n (|\overline{U}_i - \overline{Z}_i| + |\overline{Z}_i - \overline{V}_i|) \right\} \right\} \\ &= \sup_n \left\{ \max \left\{ \frac{1}{n} \sum_{i=1}^n (|\underline{U}_i - \underline{Z}_i|, |\overline{U}_i - \overline{Z}_i|) + \frac{1}{n} \sum_{i=1}^n (|\underline{Z}_i - \underline{V}_i|, |\overline{Z}_i - \overline{V}_i|) \right\} \right\} \\ &= \sup_n \left\{ \max \left\{ \frac{1}{n} \sum_{i=1}^n (|\underline{U}_i - \underline{Z}_i|, |\overline{U}_i - \overline{Z}_i|) \right\} + \max \left\{ \frac{1}{n} \sum_{i=1}^n (|\underline{Z}_i - \underline{V}_i|, |\overline{Z}_i - \overline{V}_i|) \right\} \right\} \\ &\leq \sup_n \left\{ \max \left\{ \frac{1}{n} \sum_{i=1}^n (|\underline{U}_i - \underline{Z}_i|, |\overline{U}_i - \overline{Z}_i|) \right\} \right\} + \sup_n \left\{ \max \left\{ \frac{1}{n} \sum_{i=1}^n (|\underline{Z}_i - \underline{V}_i|, |\overline{Z}_i - \overline{V}_i|) \right\} \right\} \\ &= d(U, Z) + d(Z, V) \end{aligned}$$

Thus, it can be written that

$$d(U, V) \leq d(U, Z) + d(Z, V).$$

That is,  $d$  is a metric.

**Theorem 2:** The spaces  $(C_I(1), d)$ ,  $(C_{I_0}(1), d)$  are complete metric spaces with the metric  $d$  defined in (6).

**Proof:** Consider  $(U^m)$  as a Cauchy sequence in  $C_I(1)$  space. We get

$$d(U^r, U^m) \rightarrow 0, (r, m \rightarrow \infty),$$

where  $U^r = (U_k^r) = (U_1^r, U_2^r, \dots, U_k^r, \dots)$ ,  $U^m = (U_k^m)$  and  $U_k^r = [\underline{U}_k^r, \overline{U}_k^r]$ . From here, for  $(r, m \rightarrow \infty)$

$$\sup_n \left\{ \max \left\{ \frac{1}{n} \sum_{k=1}^n |\underline{U}_k^r - \underline{U}_k^m|, \frac{1}{n} \sum_{k=1}^n |\overline{U}_k^r - \overline{U}_k^m| \right\} \right\} \rightarrow 0.$$

It means that for each  $n$ ,

$$\max \left\{ \frac{1}{n} \sum_{k=1}^n |\underline{U}_k^r - \underline{U}_k^m|, \frac{1}{n} \sum_{k=1}^n |\overline{U}_k^r - \overline{U}_k^m| \right\} \rightarrow 0, (r, m \rightarrow \infty).$$

Hence, for each  $n$ ,

$$\frac{1}{n} \sum_{k=1}^n \left| \underline{U}_k^r - \underline{U}_k^m \right| \rightarrow 0, \text{ and } \frac{1}{n} \sum_{k=1}^n \left| \overline{U}_k^r - \overline{U}_k^m \right| \rightarrow 0.$$

This shows us that cesaro transform of the sequences of real numbers  $(\underline{U}_k^m)_{m=1}^{\infty}$  and  $(\overline{U}_k^m)_{m=1}^{\infty}$  is the cauchy sequence. If the space of Cesàro convergent classical real number sequences is denoted by  $c(1)$ , we know that this sequence space is complete. Therefore, suppose that the sequences  $(\underline{U}_k^m)$  and  $(\overline{U}_k^m)$  are Cesàro convergent to the numbers  $\underline{U}_k$  and  $\overline{U}_k$ , respectively. Since we know that for all  $k$ ,  $\underline{U}_k^m \leq \overline{U}_k^m$ , we write  $\underline{U}_k \leq \overline{U}_k$ . Take into account the interval  $U = [\underline{U}_k, \overline{U}_k]$  thus produced. Then, we get  $d(U^r, U^m) \rightarrow d(U, U^m)$ , for  $r \rightarrow \infty$ .

Because the sequences  $(\underline{U}_k^m)$  and  $(\overline{U}_k^m)$  are Cesàro convergent to the numbers  $\underline{U}_k$  and  $\overline{U}_k$ , respectively, we can say that for all positive numbers  $\varepsilon_1$  and  $\varepsilon_2$ , there are the numbers  $m_0(\varepsilon_1)$  and  $m_0(\varepsilon_2)$  such that

$$\frac{1}{n} \sum_{k=1}^n \left| \underline{U}_k - \underline{U}_k^m \right| \leq \varepsilon_1$$

when  $m > m_0(\varepsilon_1)$  and

$$\frac{1}{n} \sum_{k=1}^n \left| \overline{U}_k - \overline{U}_k^m \right| \leq \varepsilon_2,$$

when  $m > m_0(\varepsilon_2)$ .

Let us say  $\varepsilon$  to the maximum of  $\varepsilon_1$  and  $\varepsilon_2$  numbers, that is  $\varepsilon = \max\{\varepsilon_1, \varepsilon_2\}$ . In this case, for

$$m > \max\{m_0(\varepsilon_1), m_0(\varepsilon_2)\},$$

$$\max \left\{ \frac{1}{n} \sum_{k=1}^n \left| \underline{U}_k - \underline{U}_k^m \right|, \frac{1}{n} \sum_{k=1}^n \left| \overline{U}_k - \overline{U}_k^m \right| \right\} < \varepsilon. \quad (7)$$

If the course of the proof is followed, it is seen that the (7) inequality is provided for each  $n$ . It means that

$$d(U, U^m) = \sup_n \left\{ \max \left\{ \frac{1}{n} \sum_{k=1}^n \left| \underline{U}_k - \underline{U}_k^m \right|, \frac{1}{n} \sum_{k=1}^n \left| \overline{U}_k - \overline{U}_k^m \right| \right\} \right\} \leq \varepsilon.$$

This indicates that it is  $U \in C_I(1)$ . Thus, it has completed the proof.

**Theorem 3:** The spaces  $P_c$  and  $C_I(1)$  are not linear isomorphic.

**Proof:** To demonstrate that two spaces are linear isomorphic, we must demonstrate the existence of a one-to-one and onto a linear transformation between them.

Let us define the transform  $T, T: P_c \rightarrow C_I^{(1)}$ ,

$$U \rightarrow T(U) = V, \quad V = (V_n), \quad (V_n) = \frac{1}{n} \sum_{k=1}^n [\underline{U}_k, \bar{U}_k] \quad (n \in \mathbb{N}).$$

For all  $X = (X_k) = [\underline{X}_k, \bar{X}_k]$  and  $U = (U_k) = [\underline{U}_k, \bar{U}_k] \in P_c$ ,

$$\begin{aligned} T(X + U) &= \frac{1}{n} \sum_{k=1}^n [\underline{X}_k + \underline{U}_k, \bar{X}_k + \bar{U}_k] \\ &= T(X) + T(U) \\ T(\alpha \cdot X) &= \frac{1}{n} \sum_{k=1}^n [\alpha \underline{X}_k, \alpha \bar{X}_k] = \alpha \cdot \left( \frac{1}{n} \sum_{k=1}^n [\underline{X}_k, \bar{X}_k] \right) = \alpha \cdot T(X), \quad (\alpha \in \mathbb{R}). \end{aligned}$$

So, the transform  $T$  is linear.

Let us investigate the  $T$  transform's one-to-one. For this purpose, let us assume

$$T(X) = T(U). \text{ Then, we get } T(X) - T(U) = \theta$$

where  $\theta = [0,0]$ .  $T(X - U) = \theta$  is obtained, because the  $T$  transform is linear.

$$\begin{aligned} T(X - U) &= \frac{1}{n} \sum_{k=1}^n ([\underline{X}_k, \bar{X}_k] - [\underline{U}_k, \bar{U}_k]) = [0,0], \\ &= \frac{1}{n} \sum_{k=1}^n ([\underline{X}_k - \underline{U}_k, \bar{X}_k - \bar{U}_k]) = [0,0]. \end{aligned}$$

This requires  $\underline{X}_k = \underline{U}_k$ , and  $\bar{X}_k = \bar{U}_k$  for all  $k \in \mathbb{N}$ . This means  $[\underline{X}_k, \bar{X}_k] \neq [\underline{U}_k, \bar{U}_k]$ .

So,  $T$  is not 1: 1. Therefore, the spaces  $P_c$  and  $C_I(1)$  are not linear isomorphic.

**Theorem 4:** An interval valued convergent sequence is also Cesáro convergent.

**Proof:** Let us assume that the sequence  $X = (X_n)$  converges to an element  $Y = [\underline{Y}, \bar{Y}]$  in  $P$ . That is  $\lim_{n \rightarrow \infty} h(X_n, Y) = 0$ . We get from here that,

$$\lim_{n \rightarrow \infty} \max\{|\underline{X}_n - \underline{Y}|, |\bar{X}_n - \bar{Y}|\} = 0$$

This means that  $\lim_{n \rightarrow \infty} |\underline{X}_n - \underline{Y}| = 0$  ve  $\lim_{n \rightarrow \infty} |\overline{X}_n - \overline{Y}| = 0$ . Thus, the real sequences  $(\underline{X}_n)$  and  $(\overline{X}_n)$  are convergent. We know that sequences of convergent real numbers are Cesàro convergent.

Let us assume that the sequences  $(\underline{X}_n)$  and  $(\overline{X}_n)$  of real numbers Cesàro converge to  $\underline{U}$  and  $\overline{U}$ . Where  $\underline{U}$  and  $\overline{U}$  are real numbers. Since for all  $n \in \mathbb{N}$ ,  $\underline{X}_n \leq \overline{X}_n$ , we know that  $\lim_{n \rightarrow \infty} \underline{X}_n \leq \lim_{n \rightarrow \infty} \overline{X}_n$ . From here, we have  $\underline{U} \leq \overline{U}$ . In addition, since the Cesàro limit and the limit of a convergent sequence in sequences with real terms are equal,

$$\begin{aligned} \lim_{n \rightarrow \infty} h([\underline{X}_n, \overline{X}_n], [\underline{U}, \overline{U}]) &= \lim_{n \rightarrow \infty} (\max\{|\underline{X}_n - \underline{U}|, |\overline{X}_n - \overline{U}|\}) \\ &= \lim_{n \rightarrow \infty} (\max\{|\underline{X}_n - \underline{Y}|, |\overline{X}_n - \overline{Y}|\}) \quad (n \rightarrow \infty). \end{aligned}$$

It means that the sequence  $X = (X_n)$  Cesàro converges to  $Y = [\underline{Y}, \overline{Y}]$ .

Consequently, we can say that the sequence space  $C_I(1)$  contains the sequence space  $P_c$ . That is,  $P_c \subset C_I(1)$ . Similarly,  $P_{c_0} \subset C_{I_0}(1)$  inclusion relation is also valid.

**Example 1:** Consider the following sequence  $(X_n) = \left(1 + \frac{1}{n}, 3\right)$ . We see that it converges to  $[1, 3]$ . We can prove easily. Really,

$$\begin{aligned} h\left(\left[1 + \frac{1}{n}, 3\right], [1, 3]\right) &= \max\left\{\left|1 + \frac{1}{n} - 1\right|, |3 - 3|\right\} \\ &= \max\left\{\frac{1}{n}, 0\right\} = \frac{1}{n} \rightarrow 0, \quad (n \rightarrow \infty). \end{aligned}$$

Now, let us investigate Cesàro convergence. We must demonstrate that

$$\begin{aligned} h\left(\frac{1}{n} \sum_{k=1}^n X_k, [1, 3]\right) &\rightarrow 0, \quad (n \rightarrow \infty). \\ h\left(\frac{1}{n} \sum_{k=1}^n X_k, [1, 3]\right) &= h\left(\frac{1}{n} \sum_{k=1}^n \left[1 + \frac{1}{k}, 3\right], [1, 3]\right) \\ &= h\left(\frac{1}{n} ([1 + 1, 3] + [1 + \frac{1}{2}, 3] + \dots + [1 + \frac{1}{n}, 3]), [1, 3]\right) \\ &= h\left(\left[\frac{1}{n} + \frac{1}{n}, \frac{3}{n}\right] + \left[\frac{1}{n} + \frac{1}{2n}, \frac{3}{n}\right] + \dots + \left[\frac{1}{n} + \frac{1}{n \cdot n}, \frac{3}{n}\right], [1, 3]\right) \end{aligned}$$

$$\begin{aligned}
&= h\left(\left[1 + \frac{1}{n}\left(1 + \frac{1}{2} + \dots + \frac{1}{n}\right), 3\right], [1, 3]\right) \\
&= \max\left\{\left|1 + \frac{1}{n}\left(1 + \frac{1}{2} + \dots + \frac{1}{n}\right) - 1\right|, |3 - 3|\right\} \\
&= \frac{1}{n}\left(1 + \frac{1}{2} + \dots + \frac{1}{n}\right) \rightarrow 0, (n \rightarrow \infty)
\end{aligned}$$

So, the proof is completed.

Now, let us see with an example that an interval sequence that is divergent can be convergent according to the Hausdorff metric in the Cesàro sense.

**Example 2:** Although the sequence  $X = (X_n) = ([-1, 0], [0, 1], [-1, 0], [0, 1], \dots)$  is divergent, it is Cesàro convergent to  $\left[-\frac{1}{2}, \frac{1}{2}\right]$  according to the Hausdorff metric. Let us examine the Cesàro convergence depending on  $n$  is even or odd which stamps the terms of the sequence.

If  $n$  is an odd number, then  $X_{2n+1} = \left[-\frac{n+1}{2n+1}, \frac{n}{2n+1}\right]$ .

Let us try to demonstrate that  $\lim_{n \rightarrow \infty} h(X_{2n+1}, \left[-\frac{1}{2}, \frac{1}{2}\right]) = 0$ .

$$\begin{aligned}
\lim_{n \rightarrow \infty} h(X_{2n+1}, \left[-\frac{1}{2}, \frac{1}{2}\right]) &= \lim_{n \rightarrow \infty} h\left(\left[-\frac{n+1}{2n+1}, \frac{n}{2n+1}\right], \left[-\frac{1}{2}, \frac{1}{2}\right]\right) \\
&= \lim_{n \rightarrow \infty} (\max\left\{\left|-\frac{n+1}{2n+1} - \left(-\frac{1}{2}\right)\right|, \left|\frac{n}{2n+1} - \frac{1}{2}\right|\right\}) \\
&= \lim_{n \rightarrow \infty} (\max\left\{\left|-\frac{n+1}{2n+1} + \frac{1}{2}\right|, \left|\frac{n}{2n+1} - \frac{1}{2}\right|\right\})
\end{aligned}$$

If here the maximum expression is  $\left|-\frac{n+1}{2n+1} + \frac{1}{2}\right|$ , we get  $\lim_{n \rightarrow \infty} \left|-\frac{n+1}{2n+1} + \frac{1}{2}\right| = 0$ .

If here the maximum expression is  $\left|\frac{n}{2n+1} - \frac{1}{2}\right|$ , then  $\lim_{n \rightarrow \infty} \left|\frac{n}{2n+1} - \frac{1}{2}\right| = 0$ .

Let us now consider, the case where  $n$  is an even number. In this case, since

$$X_{2n} = \left[-\frac{1}{2}, \frac{1}{2}\right],$$

$$\lim_{n \rightarrow \infty} h(X_{2n}, \left[-\frac{1}{2}, \frac{1}{2}\right]) = \lim_{n \rightarrow \infty} \max\left\{\left|-\frac{1}{2} + \frac{1}{2}\right|, \left|\frac{1}{2} - \frac{1}{2}\right|\right\} = \lim_{n \rightarrow \infty} \max\{0, 0\} = 0.$$

As a result, the goal is accomplished.

Thus, we gave an example of an interval sequence that is Cesàro convergent even though it is divergent. This indicates that the coverage of  $P_c \subset C_I(1)$  is certain.

**Theorem 5:** The space  $C_I(1)$  is a subspace of  $P_{\ell_\infty}$ .

**Proof:** We will show that when  $U = (U_k) \in C_I(1)$ ,  $U$  is the element of  $P_{\ell_\infty}$ .

$$U \in C_I^{(1)} \Leftrightarrow \lim_{n \rightarrow \infty} h\left(\frac{1}{n} \sum_{k=1}^n U_k, V\right) = 0, \text{ for any } V \in P.$$

$$\begin{aligned} h\left(\frac{1}{n} \sum_{k=1}^n [U_k, \bar{U}_k], V\right) &= h\left(\frac{1}{n} ([\underline{U}_1, \bar{U}_1] + \dots + [\underline{U}_n, \bar{U}_n]), [\underline{V}, \bar{V}]\right), \\ &= h\left(\left[\frac{\underline{U}_1 + \dots + \underline{U}_n}{n}, \frac{\bar{U}_1 + \dots + \bar{U}_n}{n}\right], [\underline{V}, \bar{V}]\right), \\ &= \max \left\{ \left| \frac{1}{n} (\underline{U}_1 + \dots + \underline{U}_n) - \underline{V} \right|, \left| \frac{1}{n} (\bar{U}_1 + \dots + \bar{U}_n) - \bar{V} \right| \right\} \rightarrow 0, \quad (n \rightarrow \infty) \\ &\Leftrightarrow \left| \frac{1}{n} (\underline{U}_1 + \dots + \underline{U}_n) - \underline{V} \right| \rightarrow 0 \text{ and } \left| \frac{1}{n} (\bar{U}_1 + \dots + \bar{U}_n) - \bar{V} \right| \rightarrow 0, \quad (n \rightarrow \infty). \end{aligned}$$

From here the sequences  $(U_k)$  and  $(\bar{U}_k)$  are Cesàro convergent in  $\mathbb{R}$ . Therefore, they are also bounded. Since for all  $k \in \mathbb{N}$ ,  $\underline{U}_k \leq \bar{U}_k$ , the interval  $[U_k, \bar{U}_k]$  is bounded and we get that  $U = (U_k)$  belongs to  $P_{\ell_\infty}$ . We have, the space  $C_I(1)$  is covered by  $P_{\ell_\infty}$ .

$$X \in C_I(1) \Leftrightarrow h\left(\frac{1}{n} (\underline{X}_1 + \dots + \underline{X}_n), \frac{1}{n} (\bar{X}_1 + \dots + \bar{X}_n)\right), [\underline{U}, \bar{U}] \rightarrow 0 (n \rightarrow \infty),$$

$$Y \in C_I(1) \Leftrightarrow h\left(\frac{1}{n} (\underline{Y}_1 + \dots + \underline{Y}_n), \frac{1}{n} (\bar{Y}_1 + \dots + \bar{Y}_n)\right), [\underline{V}, \bar{V}] \rightarrow 0 (n \rightarrow \infty),$$

where  $U, V \in P$ . Now, let us show that for  $X, Y \in C_I(1)$ ,  $X + Y \in C_I(1)$ . Since

$$\begin{aligned} &h\left(\frac{1}{n} (\underline{X}_1 + \underline{Y}_1 + \dots + \underline{X}_n + \underline{Y}_n), \left(\frac{1}{n} (\bar{X}_1 + \bar{Y}_1 + \dots + \bar{X}_n + \bar{Y}_n)\right), [\underline{U} + \underline{V}, \bar{U} + \bar{V}]\right) \\ &= h\left(\left[\frac{1}{n} (\underline{X}_1 + \dots + \underline{X}_n), \frac{1}{n} (\bar{X}_1 + \dots + \bar{X}_n)\right] + \left[\frac{1}{n} (\underline{Y}_1 + \dots + \underline{Y}_n), \frac{1}{n} (\bar{Y}_1 + \dots + \bar{Y}_n)\right], [\underline{U}, \bar{U}] + [\underline{V}, \bar{V}]\right) \rightarrow 0 \text{ (for } n \rightarrow \infty), \text{ we get} \end{aligned}$$

$$h\left(\frac{1}{n} (\underline{X}_1 + \underline{Y}_1 + \dots + \underline{X}_n + \underline{Y}_n), \left(\frac{1}{n} (\bar{X}_1 + \bar{Y}_1 + \dots + \bar{X}_n + \bar{Y}_n)\right), [\underline{U} + \underline{V}, \bar{U} + \bar{V}]\right) \rightarrow 0,$$

so  $X + Y \in C_I(1)$ .

For  $X \in C_I(1)$  and  $\lambda \in \mathbb{R}$ , let us show that  $\lambda X \in C_I(1)$

$$\lambda X = \lambda[\underline{X}, \overline{X}] = \begin{cases} [\lambda\underline{X}, \lambda\overline{X}], & \text{if } \lambda \geq 0 \\ [\lambda\overline{X}, \lambda\underline{X}], & \text{if } \lambda < 0 \end{cases}$$

Since  $X \in C_I(1) \Leftrightarrow h\left(\left[\frac{1}{n}(\underline{X}_1 + \dots + \underline{X}_n), \frac{1}{n}(\overline{X}_1 + \dots + \overline{X}_n)\right], [\underline{U}, \overline{U}]\right) \rightarrow 0 (n \rightarrow \infty)$ ,

( $U \in C_I(1)$ ). If  $\lambda \geq 0$ ,  $\lambda X = [\lambda\underline{X}, \lambda\overline{X}]$ . We have

$$\begin{aligned} & h\left(\left[\frac{1}{n}(\lambda\underline{X}_1 + \dots + \lambda\underline{X}_n), \frac{1}{n}(\lambda\overline{X}_1 + \dots + \lambda\overline{X}_n)\right], [\lambda\underline{U}, \lambda\overline{U}]\right) \\ &= h\left(\lambda\left[\frac{1}{n}(\underline{X}_1 + \dots + \underline{X}_n), \frac{1}{n}(\overline{X}_1 + \dots + \overline{X}_n)\right], \lambda[\underline{U}, \overline{U}]\right) \\ &= \lambda h\left(\left[\frac{1}{n}(\underline{X}_1 + \dots + \underline{X}_n), \frac{1}{n}(\overline{X}_1 + \dots + \overline{X}_n)\right], [\underline{U}, \overline{U}]\right) \rightarrow 0 \text{ (for } n \rightarrow \infty). \end{aligned}$$

If  $\lambda < 0$ ,  $\lambda X = [\lambda\overline{X}, \lambda\underline{X}]$ . We have

$$\begin{aligned} & h\left(\left[\frac{1}{n}(\lambda\overline{X}_1 + \dots + \lambda\overline{X}_n), \frac{1}{n}(\lambda\underline{X}_1 + \dots + \lambda\underline{X}_n)\right], [\lambda\overline{U}, \lambda\underline{U}]\right) \\ &= h\left(\left[\frac{1}{n}(-\lambda)(\overline{X}_1 + \dots + \overline{X}_n), \frac{1}{n}(-\lambda)(\underline{X}_1 + \dots + \underline{X}_n)\right], (-\lambda)[\overline{U}, \underline{U}]\right) \\ &= (-\lambda)h\left(\left[\frac{1}{n}(\overline{X}_1 + \dots + \overline{X}_n), \frac{1}{n}(\underline{X}_1 + \dots + \underline{X}_n)\right], [\overline{U}, \underline{U}]\right) \rightarrow 0 (n \rightarrow \infty) \end{aligned}$$

We have shown that when  $X \in C_I(1)$ ,  $\lambda X \in C_I(1)$ .

**Theorem 6:** The space  $C_I(1)$  is a QLS with the operations given by (3), (4) and the partial order relation given by (5).

**Proof:** For all  $U, V, Z \in C_I(1)$  and  $\lambda \in \mathbb{R}$  also, for  $k \in \mathbb{N}$ ,

- i) It is trivial that  $U \preceq U$ .
- ii) When  $U \preceq V$  and  $V \preceq Z$  for all  $1 \leq k < \infty$ , we have  $U_k \subseteq V_k$  and  $V_k \subseteq Z_k$  due to (5). Since  $U_k, V_k, Z_k \in P$  and  $P$  is a QLS, it becomes  $U_k \subseteq Z_k$ , for all  $1 \leq k < \infty$ . Because of (5),  $U \preceq Z$ .
- iii) Let  $U \preceq V$  and  $V \preceq U$ . In this case, for all  $1 \leq k < \infty$ ,  $U_k \subseteq V_k$  and  $V_k \subseteq U_k$ . Since  $U_k, V_k \in P$ , and  $P$  is a QLS, equality  $U_k = V_k$  is obtained. So,  $U = V$ .

It can be easily seen that these two equations are satisfied:

- iv)  $U + V = V + U$ ,
- v)  $U + (V + Z) = (U + V) + Z$ ,

- vi) There is  $\theta = (\theta_p, \theta_p, \dots, \theta_p, \dots) \in C_I(1)$  to be provided  $U + \theta = U$ , where  $\theta_p = 0$ .
- vii) It is very easy to see that
 
$$\lambda.(\beta.U) = \lambda.(\beta.U_1, \beta.U_2, \dots, \beta.U_n, \dots)$$

$$= (\lambda\beta.U_1, \lambda\beta.U_2, \dots, \lambda\beta.U_n, \dots) = (\lambda\beta).U,$$
- viii)  $\lambda(U + V) = \lambda(U_1 + V_1, U_2 + V_2, \dots, U_n + V_n, \dots)$ 

$$= (\lambda U_1 + \lambda V_1, \lambda U_2 + \lambda V_2, \dots, \lambda U_n + \lambda V_n, \dots)$$

$$= \lambda U + \lambda V,$$
- ix)  $1.U = U,$
- x)  $0.U = 0.(U_1, U_2, \dots, U_n, \dots) = (0.U_1, 0.U_2, \dots, 0.U_n, \dots) = (0, 0, \dots, 0) = \theta,$
- xi)  $(\lambda + \beta).U = (\lambda + \beta).(U_1, U_2, \dots, U_n, \dots)$ 

$$= ((\lambda + \beta).U_1, (\lambda + \beta).U_2, \dots, (\lambda + \beta).U_n, \dots),$$

and it is obtained that

$$\lambda.U + \beta.U = \lambda.(U_1, U_2, \dots, U_n, \dots) + \beta.(U_1, U_2, \dots, U_n, \dots)$$

$$= (\lambda.U_1 + \beta.U_1, \lambda.U_2 + \beta.U_2, \dots, \lambda.U_n + \beta.U_n, \dots).$$

For all  $1 \leq k < \infty$ , when  $U \in C_I(1)$ , since  $U_k, V_k \in P$  and  $P$  is a QLS, we have

$$(\lambda + \beta).U_k \subseteq \lambda.U_k + \beta.U_k,$$

and thus, it is obtained that  $(\lambda + \beta).U \subseteq \lambda.U + \beta.U$ ,

- xii) If  $U \preceq V$  and  $Z \preceq W$ , for  $1 \leq k < \infty$ , then  $U_k \subseteq V_k$  and  $Z_k \subseteq W_k$ . It is founded that
 
$$U_k + Z_k \subseteq V_k + W_k, \text{ and } U + Z \preceq V + W.$$
- xiii) If  $U \preceq V$ , since  $U_k \subseteq V_k$ , for  $\lambda \in \mathbb{R}$ , we get  $\lambda.U_k \subseteq \lambda.V_k$ . From here  $\lambda.U \preceq \lambda.V$  obtained.  
So,  $C_I(1)$  is a quasilinear space with operations (3), (4) and (5).

**Theorem 7:** The space  $C_I(1)$  is a normed quasilinear space with the function  $n$  defined

as

$$n: C_I(1) \rightarrow \mathbb{R}, n(U) = \sup_k \|U_k\|_P,$$

where  $\|U_k\|_P = \max\{|U_k|, |\bar{U}_k|\}$ .

**Proof:** For all  $U, V \in C_I(1)$  and  $\beta \in \mathbb{R}$ ,

- i) It is clear that  $n(U) \geq 0$ .
- ii)  $n(U) = 0 \Leftrightarrow \sup_k \|U_k\|_P = 0, (k \in \mathbb{N})$

$\Leftrightarrow$  For all  $k \in \mathbb{N}$ ,  $\|U_k\|_P = 0$ ,

$\Leftrightarrow U = \theta$ .

$$\begin{aligned} \text{iii)} \quad n(U + V) &= \sup_k \|U_k + V_k\|_P, \quad (k \in \mathbb{N}) \\ &\leq \sup_k \{\|U_k\|_P + \|V_k\|_P\}, \\ &= \sup_k \{\|U_k\|_P\} + \sup_k \{\|V_k\|_P\} \\ &= n(U) + n(V), \end{aligned}$$

$$\begin{aligned} \text{iv)} \quad n(\beta U) &= \sup_k \|\beta U_k\|_P, \quad (k \in \mathbb{N}) \\ &= \sup_k \{|\beta| \|U_k\|_P\}, \quad (k \in \mathbb{N}), \\ &= |\beta| \cdot \sup_k \{\|U_k\|_P\}, \quad (k \in \mathbb{N}) \\ &= |\beta| n(U). \end{aligned}$$

v) Let us assume that  $U \preceq V$ . This implies it to be  $U_k \subseteq V_k$ , and  $\|U_k\|_P \leq \|V_k\|_P$  for each  $k \in \mathbb{N}$ ,  $U_k, V_k \in P$ , since  $P$  is a normed QLS. From here it is obtained  $\sup_k \|U_k\|_P \leq \sup_k \|V_k\|_P$ , and it means  $n(U) \leq n(V)$ .

vi) Let  $\delta > 0$  be given and let  $U, V \in C_I(1)$ . Assume that there exists an element  $U_\delta \in C_I(1)$  such that  $U \preceq V + U_\delta$  and  $n(U_\delta) \leq \delta$ . To verify the last case, we must show that  $U \preceq V$  in these conditions. From the hypothesis, we get  $U_k \subseteq V_k + U_{\delta_k}$  and  $\sup_k \|U_{\delta_k}\|_P \leq \delta$  for each positive integer  $k$ . Since  $P$  is a normed QLS, we can say  $U_k \subseteq V_k$  for each positive integer  $k$ . Hence, this means  $U \preceq V$ . This completes the proof.

#### 4. Conclusion

We define an interval valued space and then present some topological characteristics and inclusion relations of this space. By demonstrating that, this sequence space has the quasilinear space structure described by Aseev, we also made a contribution to the study of quasilinear spaces. The paper serves as a guide for future research in a related field.

#### Acknowledgments

This article has been created from the second author's master's thesis, which was overseen by the first author.

## References

- [1] Zadeh, L.A., *Fuzzy sets*, Information and Control 8, 338–353, 1965.
- [2] Dwyer, P.S., *Linear computations*, New York, Wiley, 1951.
- [3] Moore, R.E., *Automatic error analysis in digital computation*, Lockheed Missiles and Space Co. Technical Report LMSD-48421, Palo Alto, CA, 1959.
- [4] Moore, R.E. and Yang, C.T., *Interval analysis I*, LMSD285875, Lockheed Missiles and Space Company, 1962.
- [5] Moore, R.E., Kearfott, R.B. and Cloud, M.J., *Introduction to interval analysis*, Society for Industrial and Applied Mathematics, Philadelphia, 2009.
- [6] Nanda, S., *On sequences of fuzzy numbers*, Fuzzy Sets and Systems 33, 123–126, 1989.
- [7] Talo, Ö. and Başar, F., *Determination of the duals of classical sets of sequences of fuzzy numbers and related matrix transformations*, Computers and Mathematics with Applications 58, 717–733, 2009.
- [8] Altın, Y., Mursaleen, M. and Altınok, H., *Statistical summability  $(C, 1)$  for sequences of fuzzy real numbers and a Tauberian theorem*, Journal of Intelligent & Fuzzy Systems 21 (6), 379–384, 2010.
- [9] Altınok, H., Çolak, R. and Altın, Y., *On the class of  $\lambda$ -statistically convergent difference sequences of fuzzy numbers*, Soft Computing 16 (6), 1029–1034, 2012.
- [10] Altınok, H., Çolak, R. and Et, M.,  *$\lambda$ -difference sequence spaces of fuzzy numbers*, Fuzzy sets and Systems 160, 3128–3139, 2009.
- [11] Hong, D.H. and Lee, S., *Some algebraic properties and a distance measure for interval-valued fuzzy numbers*, Information Sciences 148, 1-10, 2002.
- [12] Şengönül, M. and Eryılmaz, A., *On the sequence spaces of interval numbers*, Thai Journal of Mathematics, 8(3), 503-510, 2010.
- [13] Aseev, S.M., *Quasilinear operators and their application in the theory of multivalued mappings*, Proc. Steklov Inst. Math., 167, 23–52, 1986.
- [14] Alefeld, G. and Mayer, G., *Interval analysis: Theory and applications*, J. Comput. Appl. Math., 121, 421–464, 2000.
- [15] Lakshmikantham, V., Gnana Bhaskar, T. and Vasundhara Devi, J., *Theory of set differential equations in metric spaces*, Cambridge Scientific Publishers, Cambridge, 2006.
- [16] Rojas-Medar, M.A., Jiménez-Gamero, M.D., Chalco-Cano, Y., & Viera-Brandão, A.J., *Fuzzy quasilinear spaces and applications*, Fuzzy Sets and Systems, 152, 173 –190, 2005.
- [17] Yılmaz, Y., Bozkurt, H., Çakan, S., *On orthonormal sets in inner product quasilinear spaces*, Creat. Math. Inform. 25 (2), 237-247, 2016.
- [18] Yılmaz, Y., Bozkurt, H., Levent, H., Çetinkaya, Ü., *Inner product fuzzy quasilinear spaces and some fuzzy sequence spaces*, Journal of Mathematics, No.2466817, 1-15, 2022.
- [19] Kreyszig, E., *Introductory functional analysis with applications*, John Wiley & Sons. Inc., 1978.
- [20] Şengönül, M., *On the Zweier sequence spaces of fuzzy numbers*, International Journal of Mathematics and Mathematical Sciences, 2014, Article ID 439169, 1-9, 2014.
- [21] Şengönül, M., Başar, F., *Some new Cesàro sequence spaces of non-absolute type which include the spaces  $c_0$  and  $c$* , Soochow J. Math. 31 (1), 107-119, 2005.

[22] Zararsız, Z., Şengönül, M., *The Application Domain of Cesàro Matrix on Some Sequence Spaces of Fuzzy Numbers*, International Journal of Mathematical Analysis, 9 (1), 1–14, 2015.

[23] Chiao, K., *Fundamental properties of interval vector max-norm*, Tamsui Oxford J. Math. Sci., 18 (2), 219-233, 2002.

[24] Yılmaz, Y., Bozkurt, H., Levent, H., Çetinkaya, Ü., *Inner product fuzzy quasilinear spaces and some fuzzy sequence spaces*, Journal of Mathematics, 2022, Article ID 2466817, 1-15, 2022.

[25] Bozkurt, H., Yılmaz, Y., *New inner products quasilinear spaces on interval numbers*, Journal of Function Spaces, 2016, Article ID:2619271, 1-9, 2016.

[26] Levent, H., Yılmaz, Y., *Inner-product quasilinear spaces with applications in signal processing*, Euro-Tbilisi Mathematical Journal, 14, (4), 25-146, 2021.

[27] Levent, H., Yılmaz, Y., *Translation, modulation and dilation systems in set-valued signal processing*, Carpathian Math. Publ. 10, (1), 143-164, 2018.

[28] Bozkurt, H., Yılmaz, Y., *Some new results on inner product quasilinear spaces*, Cogent Mathematics, 3, 1194801, 2016.

[29] Levent, H., Yılmaz, Y., *Analysis of signals with inexact data by using interval-valued functions*, The Journal of Analysis, 30 (4), 1635-1651, 2022.

[30] Levent, H., Yılmaz, Y., Bozkurt, H., *On the inner-product spaces of complex interval sequences*, Communication in Advanced Mathematical Sciences, 5,4, 180-188, 2022.

[31] Levent, H., Yılmaz, Y., *Fourier transform of interval sequences and its applications*, Journal of Intelligent & Fuzzy Systems, (Accepted) 2023.



## A Note on The Some Class of Symmetric Numerical Semigroups

Ahmet ÇELİK\*

*Adiyaman University, Vocational School of Technical Sciences, Department of Computer Technologies,  
Adiyaman, Türkiye  
acelik@adiyaman.edu.tr, ORCID: 0000-0001-5980-0625*

Received: 04.01.2023

Accepted: 06.07.2023

Published: 31.12.2023

### Abstract

In this article, we will examine some classes of symmetric numerical semigroups and half of them, which are a class of irreducible numerical semigroups such that  $U = \langle a, a + 1 \rangle$  and  $U = \langle a, a + 2 \rangle$  symmetric numerical semigroups, respectively.

**Keywords:** Numerical semigroup; Gap; Perfect; Symmetric; Irreducible numerical semigroup.

### Bazı Simetrik Sayısal Yarı Grup Sınıflarına İlişkin Bir Not

#### Öz

Bu makalede, indirgenemez sayısal yarıgrupların bir sınıfı olan sırasıyla  $U = \langle a, a + 1 \rangle$  ve  $U = \langle a, a + 2 \rangle$  şeklindeki simetrik sayısal yarıgrupları ve onların yarısı olan sayısal yarıgrupları inceleyeceğiz.

**Anahtar Kelimeler:** Sayısal yarıgrup; Boşluk; Mükemmel; Simetrik; İndirgenemez sayısal yarıgrup.



## 1. Introduction

Numerical semigroups naturally arose as the set of values of  $d$  which have nonnegative integer solutions to Diophantine equations of the form  $c_1x_1 + c_2x_2 + \dots + c_nx_n = d$ , where  $c_1, c_2, \dots, c_n \in \mathbb{N}$  (here  $\mathbb{N}$  denotes the nonnegative integers). We reduce to the case  $\gcd(c_1, c_2, \dots, c_n) = 1$ . Frobenius asked what is the largest integer  $d$  such that a given equation has no solutions over the nonnegative integers. Sylvester and others solved the  $n = 2$  case, and since then finding the largest such  $d$  has been known as the Frobenius problem (The case  $n = 2$  corresponds to a numerical semigroup  $S$  produced with two elements, which is called a symmetric numerical semigroup). A through introduction to the Frobenius problem and related topics are given in [1].

The numerical semigroups have an important role in commutative algebra and algebraic geometry. In addition, Bertin and Carbonne [2], Delorme [3], Watanabe [4] et al. have successfully described the properties of numerical semigroups that are compatible with numerical semigroup rings related to various classifications in ring theory.

Numerical semigroups are also used to analyze singularities on planar algebraic curves. The numerical semigroups associated with these planar curves are irreducible.

A numerical semigroup is irreducible if it cannot be expressed as an intersection of two numerical semigroups containing it properly. There are two families of numerical semigroups of particular importance in the theory of irreducible numerical semigroups. These are symmetric and pseudo-symmetric numerical semigroups (for details, see [5-7]).

Recently, some applications to coding theory and cryptography have emerged. The reason for this is the use of algebraic codes and Weierstrass numerical semigroups. The goal here is to find the properties of the codes in terms of a corresponding numerical semigroup (for details see [8, 9]).

Let  $\mathbb{N}$  and  $\mathbb{Z}$  be non-negative integers and integers set, respectively.  $U \subseteq \mathbb{N}$  is called a numerical semigroup if it satisfies following conditions

- 1)  $0 \in U$ ,
- 2)  $u_1 + u_2 \in U$  for all  $u_1, u_2 \in U$ ,
- 3)  $\text{Card}(\mathbb{N} \setminus U)$  is finite.

The Frobenius number of  $S$  is

$$f(U) = \max\{x \in \mathbb{Z}: x \notin U\}$$

and the element number of  $U$  is

$$n(U) = \text{Card}(\{0,1,2,\dots,f(U)\} \cap U) .$$

If  $U$  is a numerical semigroup such that  $U = \langle u_1, u_2, \dots, u_n \rangle$ , then we write that

$$U = \langle u_1, u_2, \dots, u_n \rangle = \{c_0 = 0, c_1, c_2, \dots, c_{n-1}, c_n = f(U) + 1, \rightarrow \dots\}$$

where  $u_t < u_{t+1}$ ,  $n = n(U)$ , and the arrow means that every integer greater than  $f(U) + 1$  belongs to  $U$ , for  $t = 1, 2, \dots, n = n(U)$ . Here, we say the number  $C(U) = f(U) + 1$  is conductor of  $U$  ([10, 11]).

Let  $U = \langle u_1, u_2, \dots, u_k \rangle$  be a numerical semigroup. Then the numbers  $m(U) = \min\{x \in U: x \neq 0\} = u_1$  and  $e(U) = k$  are called multiplicity and embedding dimension of  $U$ , respectively. On the other hand, for numerical semigroup  $S$  it is known that  $e(U) \leq m(U)$ . If  $e(U) = m(U)$ , then we say  $U$  has maximal embedding dimension. The numerical semigroup  $U$  is called symmetric if  $f(U) - b \in U$  for all  $b \in \mathbb{Z} \setminus U$ . It is known that  $U = \langle u_1, u_2 \rangle$  is symmetric numerical semigroup and  $f(U) = u_1 u_2 - u_1 - u_2$ . Also, a numerical semigroup  $U$  is pseudo-symmetric if  $f(U)$  is even and the only integer such that  $b \in \mathbb{Z} \setminus U$  and  $f(U) - b \notin U$  is  $b = \frac{f(U)}{2}$  (for details see, [12, 13, 14]). On the other hand, we define the numerical semigroup  $\frac{U}{q} = \{x \in \mathbb{N}: qx \in U\}$ . It is clear that  $U \subseteq \frac{U}{q}$ , for  $q > 0$ ,  $q \in \mathbb{N}$ . If  $q = 2$  then the numerical semigroup  $\frac{U}{2}$  is called half of  $U$ . If  $v|m$  then  $\frac{U}{m} \subseteq \frac{U}{v}$  for  $v, m \in \mathbb{N} \setminus \{0\}$  and also if  $q \in U$  then we find  $\frac{U}{q} = \mathbb{N}$  ([15]).

Let  $U$  be a numerical semigroup. The element  $z$  is a gap of  $U$  if  $z \in \mathbb{N}$  but  $z \notin U$ , we denote the set of gaps of  $U$ , by  $H(U)$ , i.e.  $H(U) = \{z \in \mathbb{N}: z \notin U\}$ . Here,  $z \in H(U)$  is called isole gap if  $z - 1, z + 1 \in U$ . The set of isole gaps of  $U$  is denoted by  $I(U)$ , i.e.  $I(U) = \{z \in H(U): z - 1, z + 1 \in U\}$ . Also, the numerical semigroup  $U$  is called perfect if  $I(U) = \emptyset$  (for details see [16, 17, 18]).

In this study, we will examine some classes of symmetric numerical semigroups and half of them, which are a class of irreducible numerical semigroups such that  $U = \langle a, a + 1 \rangle$  and  $U = \langle a, a + 2 \rangle$  symmetric numerical semigroups, respectively.

## 2. Main Results

**Theorem 2.1.** ([5]) Let  $U$  be a numerical semigroup. Then,

(a) If  $f(U)$  is a odd integer then  $U$  is irreducible if and only if for all  $h, h' \in \mathbb{Z}$ , such that  $h + h' = f(U)$ , we have that either  $h \in U$  or  $h' \in U$  (that is,  $U$  is symmetric).

(b) If  $f(U)$  is an even integer then  $U$  is irreducible if and only if for all  $h, h' \in \mathbb{Z} \setminus \left\{ \frac{f(U)}{2} \right\}$  such that  $h + h' = f(U)$ , we have that either  $h \in U$  or  $h' \in U$  (that is,  $U$  is pseudo-symmetric).

**Theorem 2.2.** If  $U = \langle a, a + 1 \rangle$ , where  $a > 1$  and  $a \in \mathbb{N}$ , then we have  $I(U) = \{f(U)\}$ .

**Proof.** Let  $U = \langle a, a + 1 \rangle$  be a symmetric numerical semigroup. Then, we write

$$U = \langle a, a + 1 \rangle = \{0, a, a + 1, 2a, 2a + 1, 2a + 2, \dots, a^2 - a - 2, a^2 - a, \dots\},$$

$$f(U) = a^2 - a - 1$$

and

$$H(U) = \{1, 2, 3, \dots, a - 1, a + 2, \dots, a^2 - a - 1\}.$$

In this case, we have

$$I(U) = \{z \in H(U) : z - 1, z + 1 \in U\} = \{a^2 - a - 1\} = \{f(U)\}.$$

**Corollary 2.3.** If  $U = \langle a, a + 1 \rangle$ , where  $a > 1$  and  $a \in \mathbb{N}$ , then  $U$  is not perfect.

**Theorem 2.4.** Let  $U = \langle a, a + 1 \rangle$  be a symmetric numerical semigroup, where  $a > 1$  and  $a \in \mathbb{N}$ . In this case,

(1) If  $a > 2$  is even number then  $\frac{U}{2} = \langle \frac{a}{2}, a + 1 \rangle$ ,

(2) If  $a > 1$  is odd number then  $\frac{U}{2} = \langle \frac{a+1}{2}, a \rangle$ .

**Proof.** Let  $U = \langle a, a + 1 \rangle$  be a symmetric numerical semigroup, where  $a > 1$  and  $a \in \mathbb{N}$ . In this case,

(1) If  $a > 2$  is even number then  $\frac{a}{2} \in \mathbb{N}$ . Thus,

$$x \in \langle \frac{a}{2}, a + 1 \rangle \Leftrightarrow \exists p_1, p_2 \in \mathbb{N}, x = \left(\frac{a}{2}\right)p_1 + (a + 1)p_2$$

$$\Leftrightarrow 2x = (a)p_1 + (a + 1)2p_2 \in \langle a, a + 1 \rangle = U$$

$$\Leftrightarrow x \in \frac{U}{2}.$$

(2) If  $a > 1$  is odd number then  $\frac{a+1}{2} \in \mathbb{N}$ . So,

$$y \in \langle \frac{a+1}{2}, a \rangle \Leftrightarrow \exists v_1, v_2 \in \mathbb{N}, y = (\frac{a+1}{2})v_1 + (a)v_2$$

$$\Leftrightarrow 2y = (a+1)v_1 + (a)2v_2 \in \langle a, a+1 \rangle = U$$

$$\Leftrightarrow y \in \frac{U}{2}.$$

**Theorem 2.5.** If  $U = \langle a, a+1 \rangle$  be a symmetric numerical semigroup, where  $a > 1$  and  $a \in \mathbb{N}$ , then the numerical semigroup  $\frac{U}{2}$  is not perfect.

**Proof.** Let  $U = \langle a, a+1 \rangle$  be a symmetric numerical semigroup, where  $a > 1$  and  $a \in \mathbb{N}$ . Then, from Theorem 2.4 we write that

(1) If  $a > 2$  is even number then  $\frac{U}{2} = \langle \frac{a}{2}, a+1 \rangle$ ,

(2) If  $a > 1$  is odd number then  $\frac{U}{2} = \langle \frac{a+1}{2}, a \rangle$ .

In this case,

(1) If  $a > 2$  is even number then

$$\frac{U}{2} = \langle \frac{a}{2}, a+1 \rangle = \left\{ 0, \frac{a}{2}, a, a+1, \frac{3a}{2}, \frac{3a}{2} + 1, 2a, 2a+1, \dots, \frac{a^2}{2} - a - 2, \frac{a^2}{2} - a, \dots \right\}$$

and

$$H(\frac{U}{2}) = \left\{ 1, 2, 3, \dots, \frac{a}{2} - 1, \frac{a}{2} + 1, a - 1, \dots, \frac{a^2}{2} - a - 1 \right\}.$$

Thus, we obtain

$$f(\frac{U}{2}) = \frac{a^2}{2} - a - 1 \in I(\frac{U}{2})$$

since

$$I(\frac{U}{2}) = \left\{ x \in H(\frac{U}{2}) : x - 1, x + 1 \in \frac{U}{2} \right\}.$$

So,  $I(\frac{U}{2}) \neq \emptyset$ .

(2) If  $a > 1$  is odd number then

$$\begin{aligned} \frac{U}{2} &= \langle \frac{a+1}{2}, a \rangle \\ &= \left\{ 0, \frac{a+1}{2}, a, a+1, \frac{3a}{2} + 1, 2a, 2a+2, \dots, \frac{a^2-1}{2} - a - 1, \frac{a^2-1}{2} - a + 1, \rightarrow \dots \right\} \end{aligned}$$

and

$$H\left(\frac{U}{2}\right) = \left\{ 1, 2, 3, \dots, \frac{a+1}{2} - 1, \frac{a+1}{2} + 1, a - 1, \dots, \frac{a^2-1}{2} - a \right\}.$$

Thus, we obtain

$$f\left(\frac{U}{2}\right) = \frac{a^2-1}{2} - a \in I\left(\frac{U}{2}\right),$$

since

$$I\left(\frac{U}{2}\right) = \left\{ x \in H\left(\frac{U}{2}\right) : x - 1, x + 1 \in \frac{U}{2} \right\}$$

and  $I\left(\frac{U}{2}\right) \neq \emptyset$ . So, we find that the numerical semigroup  $\frac{U}{2}$  is not perfect.

**Theorem 2.6.** Let  $U = \langle a, a + 2 \rangle$  be a numerical semigroup, where  $a \in \mathbb{N}$  and  $a > 1$  is odd. Then  $U$  is not perfect numerical semigroup.

**Proof.** Let  $U = \langle a, a + 2 \rangle$  be a symmetric numerical semigroup. Then, we write

$$U = \langle a, a + 2 \rangle = \{0, a, a + 2, 2a, 2a + 2, \dots, a^2 - 3, a^2 - 1, \rightarrow \dots\},$$

$$f(U) = a^2 - 2$$

and

$$H(U) = \{1, 2, 3, \dots, a - 1, a + 1, 2a + 1, \dots, a^2 - 2\}.$$

In this case, we have,

$$f(U) = a^2 - 2 \in I(U)$$

since

$$I(U) = \{z \in H(U) : z - 1, z + 1 \in U\}.$$

Thus,  $U$  is not perfect numerical semigroup.

**Theorem 2.7.** Let  $U = \langle a, a + 2 \rangle$  be a symmetric numerical semigroup for  $a \in \mathbb{N}, a > 1$  is odd. Then, we have  $\frac{U}{2} = \langle a, a + 1, a + 2 \rangle$ .

**Proof.** Let  $U = \langle a, a + 2 \rangle$  be a symmetric numerical semigroup, for  $a \in \mathbb{N}, a > 1$  is odd. Then,

$$\begin{aligned} u \in \langle a, a + 1, a + 2 \rangle &\Leftrightarrow \exists v_1, v_2, v_3 \in \mathbb{N}, u = (a)v_1 + (a + 1)v_2 + (a + 2)v_3 \\ &\Leftrightarrow 2u = (a)2v_1 + (a + 1)2v_2 + (a + 2)2v_3 \\ &\Leftrightarrow 2u = 2av_1 + 2av_2 + 2v_2 + 2av_3 + 4v_3 = a(2v_1 + v_2) + \\ &\quad (a + 2)(2v_3 + v_2) \\ &\Leftrightarrow 2u \in \langle a, a + 2 \rangle = U \Leftrightarrow u \in \frac{U}{2}. \end{aligned}$$

**Theorem 2.8.** Let  $U = \langle a, a + 2 \rangle$  be a symmetric numerical semigroup for  $a \in \mathbb{N}, a > 1$  is odd. Then, the numerical semigroup  $\frac{U}{2}$  is perfect.

**Proof.** Let  $U = \langle a, a + 2 \rangle$  be symmetric numerical semigroup for  $a \in \mathbb{N}, a > 1$  is odd. Then, we have  $\frac{U}{2} = \langle a, a + 1, a + 2 \rangle$  from Theorem 2.7. In this case, we write that

$$\begin{aligned} \frac{U}{2} &= \langle a, a + 1, a + 2 \rangle \\ &= \left\{ 0, a, a + 1, a + 2, 2a, 2a + 2, 2a + 3, \dots, \left(\frac{a-1}{2}\right)a - 3, \left(\frac{a-1}{2}\right)a, \right. \\ &\quad \left. \rightarrow \dots \right\} \end{aligned}$$

and

$$H\left(\frac{U}{2}\right) = \left\{ 1, 2, 3, \dots, a - 1, a + 3, a + 4, 2a - 1, \dots, f\left(\frac{U}{2}\right) = \left(\frac{a-1}{2}\right)a - 1 \right\}.$$

Thus, we obtain

$$I\left(\frac{U}{2}\right) = \left\{ x \in H\left(\frac{U}{2}\right) : x - 1, x + 1 \in \frac{U}{2} \right\} = \phi.$$

So, we find that the numerical semigroup  $\frac{U}{2}$  is perfect.

**Example 2.9.** Let  $U = \langle 4, 5 \rangle = \{0, 4, 5, 8, 9, 10, 12, \rightarrow \dots\}$ . Then we have

$$f(U) = 11, m(U) = 4, n(U) = 6, e(U) = 2, H(U) = \{1, 2, 3, 6, 7, 11\}$$

and

$$I(U) = \{z \in H(U): z - 1, z + 1 \in U\} = \{f(U) = 11\}.$$

Thus, the numerical semigroup  $U$  is not perfect. Also,

$$\frac{U}{2} = \{u \in \mathbb{N}: 2u \in U\} = \{0, 2, 4, \rightarrow \dots\} = \langle 2, 5 \rangle, H\left(\frac{U}{2}\right) = \{1, 3\}$$

and

$$I\left(\frac{U}{2}\right) = \left\{g \in H\left(\frac{U}{2}\right): g - 1, g + 1 \in \frac{U}{2}\right\} = \{1, 3\} \neq \phi.$$

So,  $\frac{U}{2}$  is not perfect.

**Example 2.10.** Let  $U = \langle 5, 6 \rangle = \{0, 5, 6, 10, 11, 12, 15, 16, 17, 18, 20, \rightarrow \dots\}$ . Then we write

$$H(U) = \{1, 2, 3, 4, 7, 8, 9, 13, 14, 19\}$$

and

$$I(U) = \{z \in H(U): z - 1, z + 1 \in U\} = \{f(U) = 19\}.$$

Thus, the numerical semigroup  $U$  is not perfect. Also,

$$\frac{U}{2} = \{u \in \mathbb{N}: 2u \in U\} = \{0, 3, 5, 6, 8, \rightarrow \dots\} = \langle 3, 5 \rangle, H\left(\frac{U}{2}\right) = \{1, 2, 4, 7\}$$

and

$$I\left(\frac{U}{2}\right) = \left\{g \in H\left(\frac{U}{2}\right): g - 1, g + 1 \in \frac{U}{2}\right\} = \{4, 7\} \neq \phi.$$

So,  $\frac{U}{2}$  is not perfect.

**Example 2.11.** Let's  $U = \langle 5, 7 \rangle = \{0, 5, 7, 10, 12, 14, 15, 17, 19, 20, 21, 22, 24, \rightarrow \dots\}$ . Then we write

$$H(U) = \{1, 2, 3, 4, 6, 8, 9, 11, 13, 16, 18, 23\}$$

and

$$I(U) = \{z \in H(U): z - 1, z + 1 \in U\} = \{6, 11, 13, 16, 18, 23\}.$$

Thus, the numerical semigroup  $U$  is not perfect. Also,

$$\frac{U}{2} = \{u \in \mathbb{N}: 2u \in U\} = \{0, 5, 6, 7, 10, \rightarrow \dots\} = \langle 5, 6, 7 \rangle, H\left(\frac{U}{2}\right) = \{1, 2, 3, 4, 8, 9\}$$

and

$$I\left(\frac{U}{2}\right) = \left\{g \in H\left(\frac{U}{2}\right) : g - 1, g + 1 \in \frac{U}{2}\right\} = \phi.$$

So,  $\frac{U}{2}$  is perfect numerical semigroup.

## References

- [1] Ojeda, I., Vigneron-Tenorio, A., *Simplicial complexes and minimal free resolution of monomial algebras*, Journal of Pure and Applied Algebra, 214, 850–861, 2010.
- [2] Bertin, J., Carbonne, P., *Semi-groupes d'entiers et application aux branches*, Journal of Algebra, 49, 81–95, 1977.
- [3] Delorme, C., *Sous-monoïdes d'intersection complète de  $N$* , Annales Scientifiques de l'École Normale Supérieure, 4(9), 145–154, 1976.
- [4] Watanabe, K., *Some examples of one dimensional Gorenstein domains*, Nagoya Mathematical Journal, 49, 101–109, 1973.
- [5] Rosales, J.C., Branco, M.B., *Irreducible numerical semigroups*, Pacific Journal Of Mathematics, 209(1), 131-143, 2003.
- [6] Blanco, V., Rosales, J.C., *m-irreducible numerical semigroups*, Forum Mathematicum, 25, 1249 – 1261, 2013.
- [7] Süer, M., Yeşil, M., *Symmetric and pseudo-symmetric numerical semigroups via young diagrams and their semigroup rings*, Journal of the Korean Mathematical Society, 58 (6), 1367-1383, 2021.
- [8] Barucci, V., Dobbs, D.E., Fontana, M., *Maximality properties in numerical semigroups and applications to one-dimensional analytically irreducible local domains*, Memoirs of the American Mathematical Society 598, 1997.
- [9] Delgado, M., Farrán, J.I., García-Sánchez, P.A., Llena, D., *On the weight hierarchy of codes coming from semigroups with two generators*, IEEE Transactions on Information Theory, 60, 282–295, 2014.
- [10] Froberg, R., Gotlieb C., Haggkvist, R., *On numerical semigroups*, Semigroup Forum, 35, 63-68, 1997.
- [11] Rosales, J.C., Garcia-Sanchez, P.A., *Developments in Mathematics Series Numerical semigroups.*, Springer New York, 181 pp, 2009.
- [12] Assi, A., Garcia-Sanchez, P.A., *RSME Springer Series Numerical semigroups and Applications*, Springer New York, 106 pp, 2016.
- [13] Rosales, J.C., *Symmetric numerical semigroups with arbitrary multiplicity and embedding dimension*, Proceedings of the American Mathematical Society, 129(8), 2197-2203, 2001.
- [14] Rosales, J.C., Garcia-Sanchez, P.A., *Pseudo-symmetric numerical semigroups with three generators*, Journal of Algebra, 291, 46-54, 2005.
- [15] Harold, J.S., *Numerical semigroups that are fractions of numerical semigroups of maximal embedding dimension*, JP Journal of Algebra Number Theory and App., 17(1), 69-96, 2010.

[16] Harold, J.S., *On isolated gaps in numerical semigroups*, Turkish Journal of Mathematics, 46,123 –129, 2022.

[17] Frias, M.A.M., Rosales, J.C., *Perfect numerical semigroups*, Turkish Journal of Mathematics, 43, 1742 – 1754, 2019.

[18] İlhan, S., *On the set gaps in numerical semigroups*, International Journal of Algebra, 1(3), 145-149, 2007.



## The Sintering Temperature Effect on Magnetocaloric Effect in La<sub>2</sub>MnNiO<sub>6</sub> Double Perovskite Manganite Material

İbrahim Barış SEVER<sup>1</sup>, Arda KANDEMİR<sup>2</sup>, Ali Osman AYAŞ<sup>3,\*</sup>, Ahmet EKİCİBİL<sup>4</sup>

<sup>1</sup>Adiyaman University, Faculty of Science and Letters, Department of Physics, 02040, Adiyaman, Türkiye  
*ibrahim.baris02@gmail.com, ORCID: 0000-0001-6745-2472*

<sup>2</sup>Çukurova University, Faculty of Science and Letters, Department of Physics, 01250, Adana, Türkiye  
*ardakandemir88@gmail.com, ORCID: 0000-0002-9439-0366*

<sup>3</sup>Adiyaman University, Faculty of Science and Letters, Department of Physics, 02040, Adiyaman, Türkiye  
*aayas@adiyaman.edu.tr, ORCID: 0000-0002-6186-8191*

<sup>4</sup>Çukurova University, Faculty of Science and Letters, Department of Physics, 01250, Adana, Türkiye  
*ahmetcan@cu.edu.tr, ORCID: 0000-0003-3071-0444*

Received: 19.07.2023

Accepted: 09.08.2023

Published: 31.12.2023

### Abstract

La<sub>2</sub>NiMnO<sub>6</sub> double-perovskite manganite samples were produced with sol-gel method to investigate structural, morphological, magnetic and magnetocaloric properties. They were sintered at 1000 and 1100 °C for LNM-1000 and LNM-1100 sample, respectively. The crystal structure of the samples was determined as Rhombohedral with R $\bar{3}c$  space group. Morphological analyses revealed that LNM-1000 sample included different polygonal shaped grains with small magnitudes, while grain boundaries became unclear for the LNM-1100 sample. The Curie temperatures were determined as 200 and 220 K while effective magnetic moment values were calculated as 1.75 and 2.13 for LNM-1000 and LNM-1100 samples, respectively. Arrot plots showed that samples exhibited second order magnetic phase transition. Maximum magnetic entropy change and relative cooling power values were calculated as 0.21, 0.25 J kg<sup>-1</sup> K<sup>-1</sup> and 46.2, 50.5 J kg<sup>-1</sup> for LNM-1000 and LNM-1100 samples, respectively. Although the samples have the Curie temperature around sub-room temperature range that is much higher than Gd<sub>2</sub>NiMnO<sub>6</sub>



(5 K) and they have second order magnetic phase transition, relatively low value of magnetic entropy change values of these samples limit their usage as a magnetic coolant material.

**Keywords:** Magnetic refrigeration; Magnetocaloric effect; Curie temperature; Double perovskite manganites.

## **La<sub>2</sub>MnNiO<sub>6</sub> Çift Katlı Perovskit Manganit Malzemede Sinterleme Sıcaklığının Manyetik Soğutma Parametrelerinin Üzerindeki Etkisi**

### **Öz**

La<sub>2</sub>NiMnO<sub>6</sub> çift peroksit manganit örnekleri yapısal, morfolojik, manyetik ve manyetokalorik özelliklerini araştırmak için sol-jel yöntemi ile üretildi. LNM-1000 ve LNM-1100 numuneleri sırasıyla 1000 ve 1100 °C'de sinterlenmişlerdir. Numunelerin kristal yapısı R $\bar{3}c$  uzay grubuna sahip Rhombohedral olarak belirlenmiştir. Morfolojik analizler, LNM-1000 numunesinin küçük boyutlara sahip farklı poligonal şekilli taneler içerdiğini, LNM-1100 numunesinde ise tane sınırlarının belirsizleştiğini ortaya koymuştur. Curie sıcaklıkları 200 ve 220 K olarak belirlenirken, etkin manyetik moment değerleri LNM-1000 ve LNM-1100 numuneleri için sırasıyla 1.75 ve 2.13 olarak hesaplanmıştır. Arrot grafikleri örneklerin ikinci dereceden manyetik faz geçişi sergilediğini göstermiştir. Maksimum manyetik entropi değişimi ve bağıl soğutma gücü değerleri LNM-1000 ve LNM-1100 numuneleri için sırasıyla 0.21, 0.25 J kg<sup>-1</sup> K<sup>-1</sup> ve 46.2, 50.5 J kg<sup>-1</sup> olarak hesaplanmıştır. Örneklerin Curie sıcaklığının oda sıcaklığının altında Gd<sub>2</sub>NiMnO<sub>6</sub>'dan (5 K) çok daha yüksek olması ve ikinci dereceden manyetik faz geçişine sahip olması gibi avantajlarına rağmen, bu örneklerin manyetik entropi değişim değerlerinin nispeten düşük olması manyetik soğutucu malzeme olarak kullanımlarını sınırlamaktadır.

**Anahtar Kelimeler:** Manyetik soğutma; Manyetokalorik etki; Curie sıcaklığı; Çift-katmanlı perovskitler.

### **1. Introduction**

Increasing energy demand and energy related environmental problems which adversely affect our health are one of the provocative problems of the modern humanity [1]. Due to this fact, many governments pay considerable attention to reduce these adverse effects [2]. It should be noted that refrigeration devices have relatively high energy consumption rate among other energy consuming technologies with approximately 15% [3] of the total energy consumption rate in the world. Moreover, current refrigeration systems also have some other hazardous effects on the environment like ozone-depleting and/or greenhouse effect [4, 5]. By considering given disadvantages of current cooling devices, many scientists focus on alternative cooling

technologies like magnetic cooling due to possible energy efficiency and environmentally green nature [6-8]. Magnetic cooling technology is mainly based on Magnetocaloric Effect (MCE). For this reason, it is important to define MCE which can be defined as thermal response of magnetic material under the influence of applied magnetic field change [1, 5, 7, 9]. MCE can be measured by adiabatic temperature change ( $\Delta T_{AD}$ ) and/or magnetic entropy change ( $\Delta S_M$ ) [6, 8, 10].  $\Delta S_M$  is mainly related to magnetic moment alignment and maximum change of these parameters occurs around the magnetic phase transition temperature [1, 5, 7, 9].

Although many studies about several magnetocaloric material families in the literature report results of the cooling performance parameters of these families, it is not reached an optimization on all parameters yet [7, 9, 11-13]. The closest results of the targeted properties were observed in Gd element and its alloys [14]. On the other hand, Gd element has the high-cost problem that limits its usage as a magnetic coolant materials. Similar handicaps exist in other potential candidate coolant materials and therefore researchers continue to search new candidates. Among these candidates, perovskite manganites reach considerable attention due to exposing rich physical and magnetic properties [1, 15-19]. The general formula of the perovskite manganites is given as  $A_{1-x}B_xMnO_3$ , where A means rare-earth elements and B for the alkaline earth elements. This stoichiometric structure allows researchers to use this family in very large scale of technological application topics like spintronic devices [20], magnetic sensors [21, 22], and coolants for magnetic refrigeration [16, 23-27].

Perovskite manganites have also a slightly different form than  $A_{1-x}B_xMnO_3$  type called double perovskite manganite and the chemical formula of this type is given as  $A_{2-x}B_xMn_2O_6$  [15, 24, 25, 28]. Although a lot of Research about  $A_{1-x}B_xMnO_3$  type perovskites have been performed, research about  $A_{2-x}B_xMn_2O_6$  type double perovskite is relatively rare. Physical mechanism about this form should be explained and extra data about the sintering treatment is needed by characterizing some new and novel members. Due to this reason, in this work we have produced  $La_2MnNiO_6$  sample under two different sintering temperature. The morphological, structural, magnetic, and magnetocaloric properties of this novel compound were characterized and explained in detail. Previous studies about this structure have reported some properties like photocatalytic activity, adsorption of mono-crotophos from aqueous environment etc., but as far as we know, there is no report in the literature that investigate all these properties. Additionally, sintering temperature effect on this structure was also investigated firstly in this work. The result of this study can yield useful understandings to obtain room temperature range magnetocaloric materials for magnetic cooling applications.

## 2. Experimental Procedure

Polycrystalline  $\text{La}_2\text{MnNiO}_6$  Double perovskite manganite sample was sol-gel method. To obtain sample with desired stoichiometry required quantities of  $\text{La}(\text{NO}_3)_3 \cdot x\text{H}_2\text{O}$  (99.9% purity), NiO (99.9% purity) and  $\text{MnO}_2$  ( $\geq 99\%$  purity). Monoethylene glycol with 99.9% purity, Hydrochloric acid with 37 % purity, nitric acid with 70 % purity, and citric acid monohydrate with 99.9% purity were used as a chelating substance. All materials were heated and mixed by magnetic stirrer at 300 °C. This process continues to obtain gel-like precipitation. This form was burned at 500 °C for 1 h, then calcined at 600 °C for 6 h. To obtain fine powders, the obtained materials were grounded by an agate mortar. After this process, powder samples were pressed to make disc-shaped samples. Then, disc-shaped samples were sintered at 1000 and 1100 °C for 24 h in the air and these samples are labelled as LNM-1000 and LNM-1100, respectively.

The crystal structure of the samples was performed with X-Ray Diffraction (XRD) method. The  $\text{CuK}\alpha$  with  $\lambda=1.5406 \text{ \AA}$  at room temperature was used as radiation source. X'Pert High Score Plus software was used to determine potential candidate structure and the Rietveld refinement method ready in Fullprof software was used to determine the crystal structure of the samples. Morphological properties of the samples were analyzed by Scanning Electron Microscope (SEM) technique. Elemental analyses of the samples were performed by Energy Dispersive X-Ray Spectroscopy (EDS) method.

The magnetic properties of the samples have been analyzed by two measurements called temperature dependent  $M(T)$  and isothermal magnetization curves  $M(H)$  measurements. These measurements performed with a Vibration Sample Magnetometer (VSM) equipped Physical Properties Measurement System (PPMS). The  $M(T)$  of the samples measured from 10 to 350 K temperature range under two regimes called zero-field cooled (ZFC) and field-cooled (FC).  $M(H)$  curves performed from 0 to 5 T magnetic field at 4 K temperature steps around phase transition temperature region. All measurements, analyzes, methods and techniques were carried out at Çukurova University Central Research Laboratory (ÇÜMERLAB).

### 3. Results and Discussions

The crystallographic information of the samples was investigated by using XRD data collected at room temperature. The Rietveld's refinement method [29] via Fullprof software has been used to analyze XRD data [30]. The refinement results are given in the Figs.1a-b for LNM-1000, LNM-1100 samples, respectively. The parameters about crystal structure obtained from the refinement analysis are tabulated in Table 1.

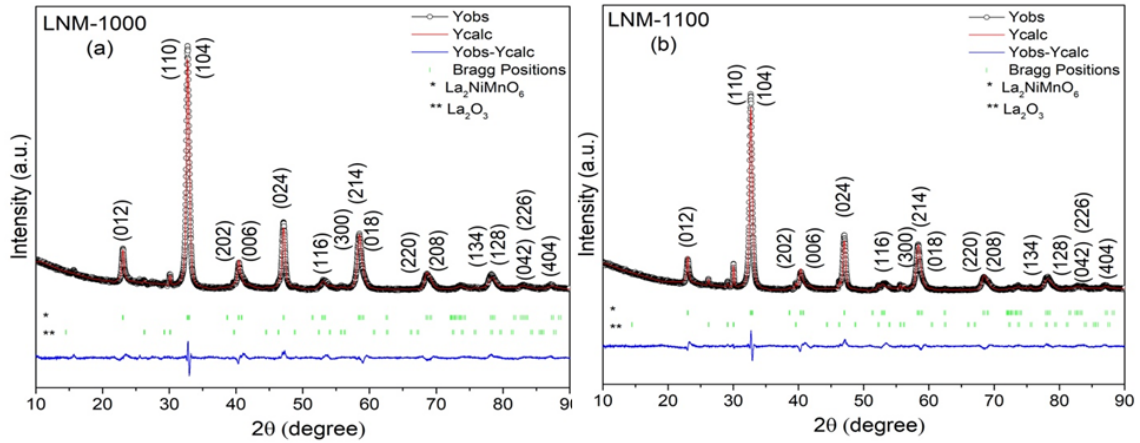


**Figure 1:** XRD Patterns for samples (a) LNM-1000, (b) LNM-1100. The red line, black circle, green bars, blue line, and asterisk represent calculated data, observed data, Bragg positions, differences between observed and calculated data, and impurity phases, respectively

**Table 1:** The structural parameters for samples LNM-1000 and LNM-1100 samples. The lattice parameters ( $a$ ,  $b$ ,  $c$ ), unit cell volume ( $V$ ), average bond angle of B-O-B (B: Mn, Ni), the average bond length of B-O (B: Mn, Ni), the crystallite size ( $D$ ), and the convergence factor ( $\chi^2$ ) values for each sample

Structural Parameters	Samples	
	LNM-1000	LNM-1100
$a$ (Å)	5.4743	5.4858
$b$ (Å)	5.4743	5.4858
$c$ (Å)	13.2607	13.2938
$V$ (Å <sup>3</sup> )	344.1534	346.4652
$\langle$ B-O-B $\rangle$ (°)	156.13	153.80
$\langle$ d <sub>B-O</sub> $\rangle$ (Å)	1.92861	1.93942
$D$ (nm)	21.74	24.04
$\chi^2$	3.97	3.93

The convergence between theoretical model and observed data known as chi-squared ( $\chi^2$ ) observed from Rietveld refinement for LNM-1000 and LNM-1100 samples are 3.83 and 3.60, respectively. These results mean ( $\chi^2 < 4$ ) observed and experimental data well match with each other. From this result, it can be argued that these samples have rhombohedral structure with  $R\bar{3}c$  space group. However, small amount of impurity phase belongs to  $La_2O_3$  structure also detected. The main crystal structure kept unchanged by increasing sintering temperature ( $T_s$ ) from 1000 °C to 1100 °C. As can be seen from Table 1, the lattice parameters increased by increasing  $T_s$ . The change of lattice parameters inevitably affected the average B-O bond length and average B-O-B bond angle (B: Mn, Ni) (See Table 1).

For magnetic and magnetocaloric properties the crystallite size ( $D$ ) plays an important role due to the indirect result of determining boundary lines that is known non-magnetic places in materials. For this reason, calculating  $D$  parameter is important and can be calculated by Debye-Scherrer equation given below [31, 32]:

$$D = \frac{\kappa\lambda}{\beta\cos\theta} \quad (1)$$

where  $\lambda$  is the wavelength of the x-ray ( $\lambda_{\text{Cu-K}\alpha} = 1.5406 \text{ \AA}$ ),  $\kappa$  is the crystallite shape factor (0.94 for each sample), and  $\beta$  is the peak full width at half maximum at the observed peak angle  $\theta$  (in radians). It can be seen from Table 1 that the average crystallite size value increases by increasing  $T_S$ . This increment is consistent with the results obtained from the literature [33-36] and may be due to the higher growth rate of crystallite size at higher temperatures below melting point [35, 36].

To investigate morphological and elemental properties of the samples SEM and EDS methods had been used. SEM images with EDS spectra graphs for LNM-1000 and LNM-1100 samples are given in Figs.2 (a-b).

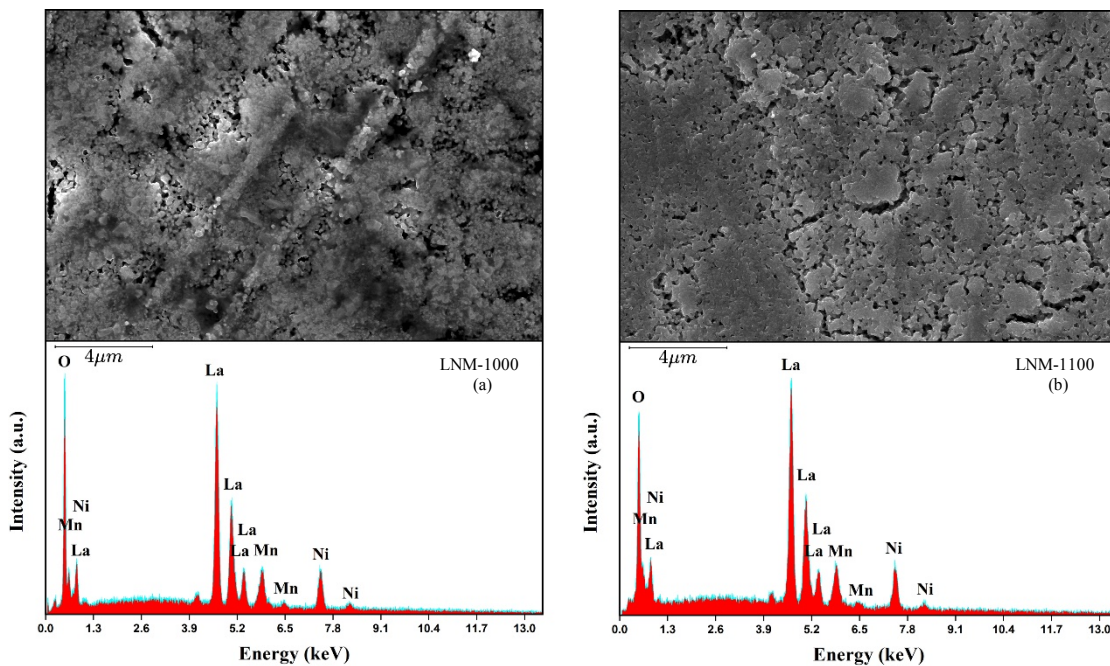


**Figure 2:** SEM images and EDS measurements for samples (a) LNM-1000, (b) LNM-1100

As can be seen from the SEM photo in the Fig. 2a, grains have different polygonal shapes with quite small magnitudes. In some places, small amount of aggregation that indicates liquid phase [24], is detected. By increasing  $T_S$ , the boundary lines become unclear that can be

interpreted as areas which includes liquid phase increases by increasing  $T_S$ . The liquid phase may play a role to get grains together that might be the reason of unclear boundary lines in LNM-1100 sample [24]. From EDS spectra, it is understood that both samples include all starting elements that means no element loss during preparation process and there is no impurity element in both samples.

Temperature dependent magnetization measurements ( $M(T)$ ) of LNM-100 and LNM-1100 samples measured in FC and ZFC modes were carried out under 25 mT external magnetic field to examine the magnetic behavior and to determine the phase transition temperatures. The results are shown in Figs. 3 (a-b) (left axes).

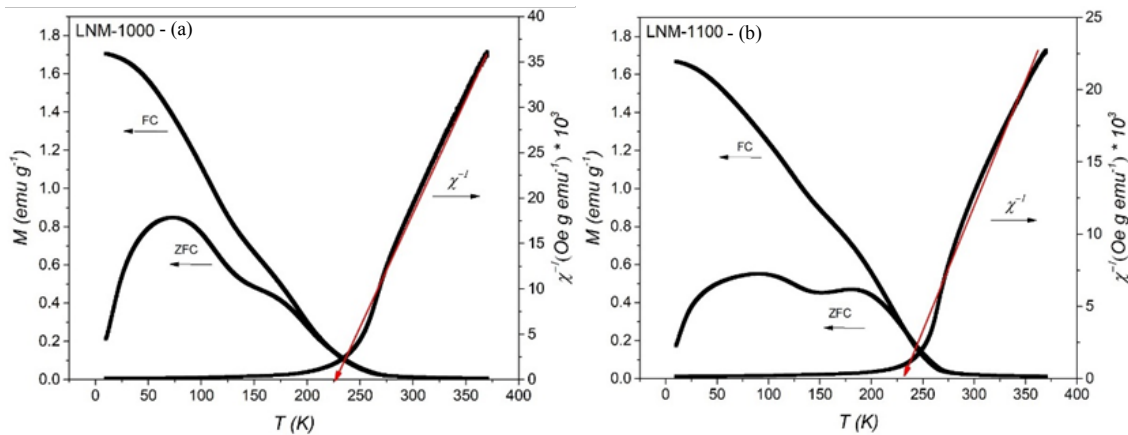


**Figure 3:** The  $M(T)$  curves obtained at both FC and ZFC modes and inverse susceptibility for (a) LNM-1000 and (b) LNM-1100 samples

It can be seen from left axes of the Figs. 3 (a-b) magnetization of the samples decreases by increasing the temperature in FC mode. On the other hand, in ZFC mode, magnetization behavior is different at low temperature range where the magnetization increases at first and then starts to decrease by increasing temperature. Magnetization closes to zero value in both FC and ZFC mode at high temperature region. This behavior means magnetic phase transition from ferromagnetic to paramagnetic phase. Difference between ZFC and FC mode at low temperature range indicates existence of antiferromagnetic interaction, domain wall pinning effect and the spin-class like behavior in the matrix of the samples. Maximum magnetic entropy change occurs at the magnetic phase transition temperature  $T_C$ . For this reason, determining  $T_C$  is important and in this work, we have used two methods to determine it. At the first method, inverse susceptibility cure is used. Red straight line that is fitting the paramagnetic part of the graphs cuts the x axes at  $T_C$ . In the second method, we have used  $dM/dT$  graphs given in Figs 4 (a-b).

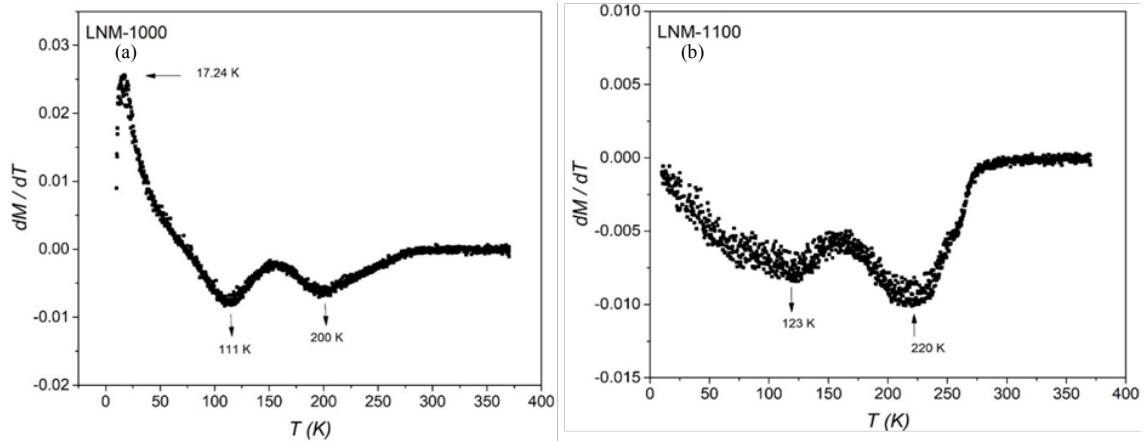


**Figure 4:** The  $dM/dT$ -( $T$ ) curves for (a) LNM-1000 and (b) LNM-1100 samples

The minimum point of the  $dM/dT$  graphs called as TC. Determined TC values of the samples are tabulated in Table 2. As can be seen from the Table 2, TC values are 200 and 220 K for LNM-1000 and LNM-1100, respectively. The increase in TC may come from decreasing boundary lines of grains that is also seen in SEM images as increasing aggregated areas. Boundary lines are known magnetically inactive places and decreasing this kind of areas leads to increase in magnetic nature of the sample and for this reason, TC value of the sample increases. To compare the phase transition temperatures of the samples, the phase transition temperature of the Gd<sub>2</sub>NiMnO<sub>6</sub> [37] sample was also gift in Table 2. It can be seen from the Table 2, TC values of the samples increase considerably with change of Gd with La. The TC values obtained from inverse susceptibility curves show very small differences that comes from antiferromagnetic interaction explained above. This fact can also be seen as a difference between inverse susceptibility curve of paramagnetic side and the red line extrapolated in this area. This discrepancy comes from co-existence of paramagnetic, ferromagnetic and/or antiferromagnetic clusters in this temperature range which is called Griffiths phase [38].

Another important magnetic parameter is effective magnetic moment ( $\mu_{eff}$ ). Left axes of the Figs.3 show linear behavior at high temperature range. This part can be fitted to Curie-Weiss law and  $\mu_{eff}$  can be calculated by this law given as:

$$\chi = \frac{C}{T - \theta} \quad (2)$$

where  $\theta$  is the paramagnetic curie temperature,  $C$  is the Curie constant and this value for the samples can be given as:

$$C = \frac{N\mu_{eff}^2\mu_B^2}{3k_B} \quad (3)$$

where  $\mu_B$  is the Bohr magneton,  $N$  is Avogadro's number,  $k_B$  is Boltzmann constant, and  $\mu_{eff}$  is the effective magnetic moment. By using given relations above,  $\mu_{eff}$  values are calculated and tabulated in Table 2. As can be seen from Table 2,  $\mu_{eff}$  value increases by increasing  $T_S$  that supports the strengthening of the magnetic nature of the samples.

**Table 2:** Magnetic and magnetocaloric parameters of the LNM-1000 and LNM-1100 samples

Sample	$T_C$ (K)	$\mu_{eff}$ ( $\mu_B$ )	$-\Delta S_M$ ( $J\ kg^{-1}K^{-1}$ )	RCP ( $J\ kg^{-1}$ )	Reference
LNM-1000	200	1.75	0.21	46.2	This work
LNM-1100	220	2.13	0.25	50.5	This work
$Gd_2NiMnO_6$	5	-	26	-	[33]

Another measurement to investigate magnetic properties is isothermal magnetization curves ( $M(H)$ ) that measured up to 5 T magnetic fields around phase transition range with 4 K temperature steps. Measured  $M(H)$  curves are given in Figs. 5.

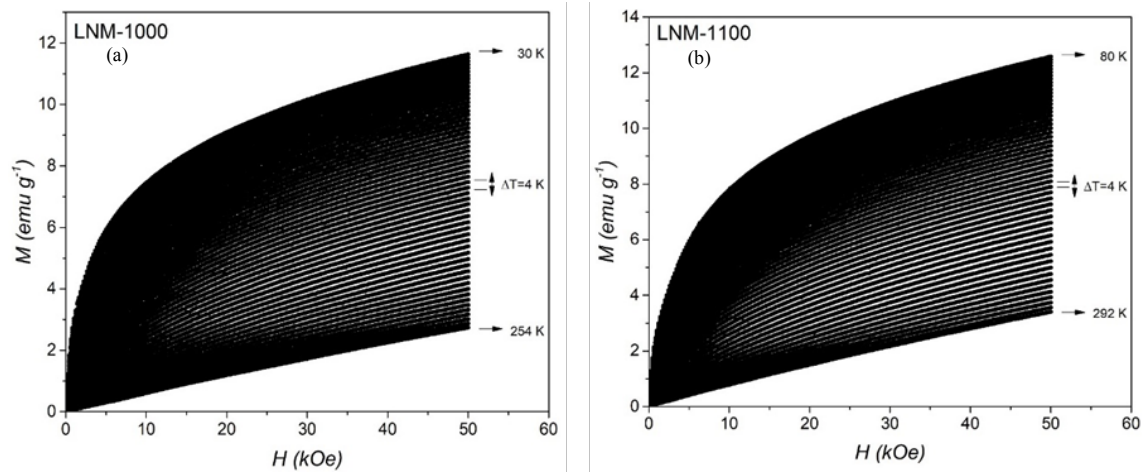


**Figure 5:** Isothermal magnetization curves measured at various temperatures around  $T_C$  with a step of 4 K for (a) LNM-1000 and (b) LNM-1100 samples

It can be seen from the Figs.5 (a-b) that magnetization curves increase suddenly by increasing the applied magnetic field at low temperature measurements. These curves close to linear behavior for measurements at measured high temperature side. This behavior indicates magnetic phase transition from ferromagnetic (FM) to paramagnetic (PM) phase that is also observed in  $M(T)$  part. In all curves saturation is not reached that may come from such parameters

like short-range FM interaction, magnetic inhomogeneity or low level of applied magnetic field [39].

To determine the magnetic cooling capacity of a magnetic material, magnetic entropy change parameter is a frequently used parameter and can be calculated with using isothermal magnetization curves and Eqn. (4) given below. Application of this equation explained anywhere else [1, 5]

$$-\Delta S_M = \int_0^H \left( \frac{\partial M}{\partial T} \right)_H dT \quad (4)$$

The  $-\Delta S_M$ - $T$  curves obtained from Eqn. (4) are given in Figs. 6 (a-b) and maximum  $\Delta S_M$  values are also listed in Table 2.

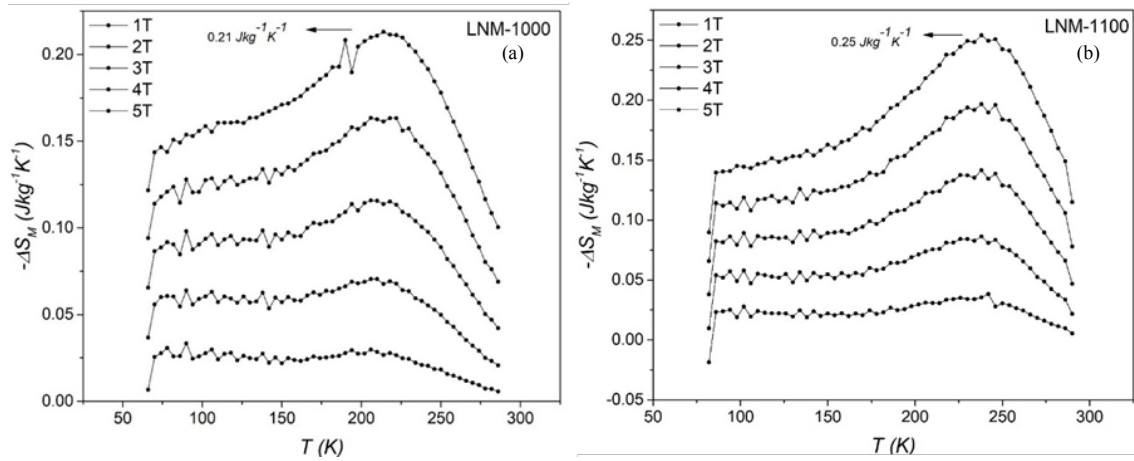


**Figure 6:**  $-\Delta S_M$ -( $T$ ) curves for (a) LNM-1000 and (b) LNM-1100 samples

As can be seen also in other magnetic properties,  $-\Delta S_M$  value increases with increasing  $T_S$  value (see Table 2). This increase in magnetic nature of the samples can be explained with increasing aggregated sites which leads to increase the active magnetic field in samples. It can be said that maximum  $-\Delta S_M$  value of the samples is quite low level when the result is compared with the Gd based example given in Table 2. This result limits the usage of these samples as magnetic coolant material. It should be noted that keeping  $-\Delta S_M$  value of the samples at high level as in Gd based example is important while the  $T_C$  value is increased.

Reversible magnetic phase transition is another important parameter that is expected from a candidate coolant material. Magnetic materials that show second order magnetic phase transition also exhibit negligible thermal and magnetic hysteresis and vice versa for materials that exhibit first order magnetic phase transition type. Banerjee's criterion is the known method of

determining the magnetic phase transition type of materials [40]. In this method,  $H/M$  vs  $M^2$  graph called Arrot plot obtained from  $M(H)$  data is used to determine magnetic phase transition nature of the samples. Obtained graphs are given in Figs. 7 (a-b).

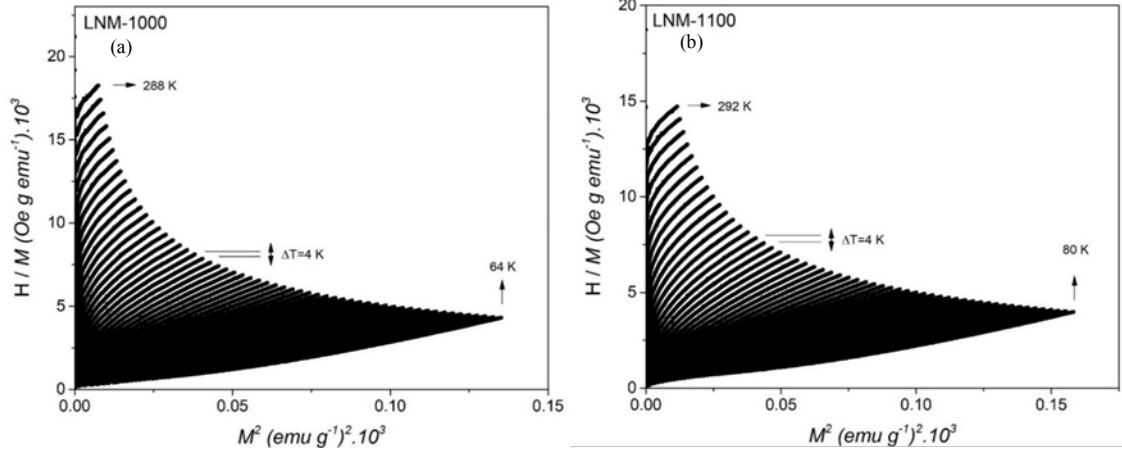


**Figure 7:** Arrot plots for (a) LNM-1000 and (b) LNM-1100 samples.

According to Arrot graphs, the slope of the curves is positive that indicates that the samples have second order magnetic phase transition nature. Due to this property, ignorable thermal and magnetic hysteresis accommodate to the magnetic phase transition of the samples that makes these samples more suitable for magnetic cooling applications.

Relative Cooling Power (RCP) is also an important parameter for MCE and is calculated by equation below:

$$RCP = -\Delta S_M^{max} \times \delta T_{FWHM} \quad (5)$$

where  $\delta T_{FWHM}$  is the full width at half maximum of the  $-\Delta S_M(T)$  curve. In ideal thermodynamic cycle the amount of heat that can be transferred between heat and cold sides could be represented by RCP. The RCP values calculated under  $\Delta H = 5$  T are listed in Table 2. As also in other parameters, the RCP value increases with increasing  $T_S$ .

#### 4. Conclusion

As a conclusion, LNM-1000 and LNM-1100 samples were produced with sol-gel method successfully and their structural, magnetic, and magnetocaloric properties were also characterized. From the Rietveld's refinement method, crystal structure of the samples was determined as Rhombohedral structure with  $R\bar{3}c$  space group. LNM-1000 sample has quite small, different polygonal shaped grains with clear grain boundaries and by increasing temperature, in

the LNM-1100 sample, areas that have a melting form of the grains increases which means grain boundaries are not seen clearly in these areas. Both samples show a second-order magnetic phase transition from ferromagnetic to paramagnetic phase by increasing temperature.  $T_C$  values were determined as 200 and 220 K for LNM-1000 and LNM-1100 samples, respectively.  $-\Delta S_M^{max}$  and RCP values were calculated as 0.21, 0.25, and 46.2, 50.5 for the LNM-1000 and LNM-1100 samples, respectively.

By considering the magnetic cooling results of the samples and  $Gd_2NiMnO_6$  sample, obtaining magnetic cooling samples that exhibit second order magnetic phase transition at high temperature range is acceptable. On the other hand, in future works, it should be investigated some substitution effects to increase the  $-\Delta S_M^{max}$  values of the samples while keeping or increasing  $T_C$  values. From the results of the samples, it can be said that increasing particle and grain sizes mainly has a positive effect on the magnetocaloric effect parameters of the samples.

### Acknowledgments

This work is supported by the Research Project Unit of the Adiyaman University Under Grant Contract no FEFYL/2021-0004.

This work was produced from a master's thesis called " $La_{2-x}Na_xNiMnO_6$  ( $x=0.0, 0.1, 0.2, 0.3, 0.5, 1.0$ ) Çift Katmanlı Perovskit Malzemelerin Yapısal, Manyetik Ve Manyetokalorik Özelliklerinin İncelenmesi", which is being carried out at Adiyaman University Graduate Education Institute.

### References

- [1] Ayaş, A.O., Kılıç Çetin, S., Akça, G., Akyol, M., Ekicibil, A., *Magnetic refrigeration: current progress in magnetocaloric properties of perovskite manganite materials*, Materials Today Communications, 35, 105988, 2023.
- [2] Gross, R., Leach, M., Bauen, A., *Progress in renewable energy*, Environment International, 29,105-122, 2003.
- [3] Tassou, S.A., Ge, Y., Hadawey, A., Marriott, D., *Energy consumption and conservation in food retailing*, Applied Thermal Engineering, 31, 147-156, 2011.
- [4] Gschneidner Jr, K.A., Pecharsky, V.K., Pecharsky, A.O., Zimm, C.B., *Recent developments in magnetic refrigeration*, Materials Science Forum, 315-317, 69-76, 1999.
- [5] Ayaş, A.O., Akyol, M., Ekicibil, A., *Structural and magnetic properties with large reversible magnetocaloric effect in  $(La_{1-x}Pr_x)_{0.85}Ag_{0.15}MnO_3$  ( $0.0 \leq x \leq 0.5$ ) compounds*, Philosophical Magazine, 96, 922-937, 2016.
- [6] Gschneidner Jr, K.A., Pecharsky, V.K., Tsokol, A.O., *Recent developments in magnetocaloric materials*, Reports on Progress in Physics, 68, 1479, 2005.

- [7] Phan, M.-H., Yu, S.-C., *Review of the magnetocaloric effect in manganite materials*, Journal of Magnetism and Magnetic Materials, 308, 325-340, 2007.
- [8] Gutfleisch, O., Willard, M.A., Brück, E., Chen, C.H., Sankar, S.G., Liu, J.P., *Magnetic materials and devices for the 21st century: stronger, lighter, and more energy efficient*, Advanced Materials, 23, 821-842, 2011.
- [9] Gschneidner Jr, K.A, Pecharsky, V.K., *Magnetocaloric materials*, Annual Review of Materials Science, 30, 387-429, 2000.
- [10] Zhang, Y., Tian, Y., Zhang, Z., Jia, Y., Zhang, B., Jiang, M., Wang, J., Ren, Z., *Magnetic properties and giant cryogenic magnetocaloric effect in B-site ordered antiferromagnetic  $Gd_2MgTiO_6$  double perovskite oxide*, Acta Materialia, 226, 117669, 2022.
- [11] Ram, N.R., Prakash, M., Naresh, U., Kumar, N.S., Sarmash, T.S., Subbarao, T., Kumar, R.J., Kumar, G.R., Naidu, K.C.B., *Review on magnetocaloric effect and materials*, Journal of Superconductivity and Novel Magnetism, 31,1971-1979, 2018.
- [12] Franco, V., Blázquez, J.S., Ipus, J.J., Law, J.Y., Moreno-Ramírez, L.M., Conde, A., *Magnetocaloric effect: from materials research to refrigeration devices*, Progress in Materials Science, 93, 112-232, 2018.
- [13] Lyubina, J., *Magnetocaloric materials for energy efficient cooling*, Journal of Physics D: Applied Physics, 50, 53002-53002, 2017.
- [14] Pecharsky, V.K., Gschneidner Jr, K.A., *Giant magnetocaloric effect in  $Gd_5(Si_2Ge_2)$* , Physical Review Letters, 78, 4494-4497, 1997.
- [15] Ayaş, A.O., Kandemir, A., Kılıç Çetin, S., Akça, G., Akyol, M., Ekicibil, A., *Investigation of the effect of sintering temperature on structural, magnetic and magnetocaloric properties in  $PrCaMn_2O_6$  double perovskite manganite system*, Journal of Materials Science: Materials in Electronics, 33, 7357-7370, 2022.
- [16] Kılıç Çetin, S., Akça, G., Ayaş, A.O., Akyol, M., Ekicibil, A., *Structural, magnetic, and magnetocaloric properties of pb-substituted  $La_{0.7}(Te_{1-x}Pb_x)_{0.3}MnO_3$  ( $0.0 \leq x \leq 0.3$ ) manganites*, Journal of Superconductivity and Novel Magnetism, 33, 527-538, 2020.
- [17] Ayaş, A.O., Kılıç Çetin, S., Akyol, M., Akça, G., Ekicibil, A., *Effect of B site partial Ru substitution on structural magnetic and magnetocaloric properties in  $La_{0.7}Pb_{0.3}Mn_{1-x}Ru_xO_3$  ( $x = 0.0, 0.1$  and  $0.2$ ) perovskite system*, Journal of Molecular Structure, 1200, 127120-127120, 2020.
- [18] Kanikırmızı, T., İzgi, T., Bayri, N., Gencer, H., Kolat, V.S., Pektas, M., Atalay, S., *Structural, magnetic and magnetocaloric properties of Ru doped  $Pr_{0.67}Ca_{0.33}Mn_{1-x}Ru_xO_3$  manganites*, Journal of Materials Science: Materials in Electronics, 33, 21778-21795, 2022.
- [19] Kılıç Çetin, S., Akça, G., Aslan, M.S., Ekicibil, A., *Role of nickel doping on magnetocaloric properties of  $La_{0.7}Sr_{0.3}Mn_{1-x}Ni_xO_3$  manganites*, Journal of Materials Science: Materials in Electronics, 32, 10458-10472, 2021.
- [20] Privitera, A., Righetto, M., Cacialli, F., Riede, M.K., *Perspectives of organic and perovskite-based spintronics*, Advanced Optical Materials, 9, 2100215, 2021.
- [21] Balcells, L., Carrillo, A.E., Martínez, B., Sandiumenge, F., Fontcuberta, J., *Room temperature magnetoresistive sensor based on thick films manganese perovskite*, Journal of Magnetism and Magnetic Materials, 221, 224-230, 2000.
- [22] Balcells, L., Fontcuberta, J., Martínez, B., Obradors, X., *High-field magnetoresistance at interfaces in manganese perovskites*, Physical Review B, 58, R14697-R14700, 1998.

- [23] Barman, A., Kar-Narayan, S., Mukherjee, D., *Caloric effects in perovskite oxides*, *Advanced Materials Interfaces*, 6, 1900291-1900291, 2019.
- [24] Ayaş, A.O., *Observation of room-temperature range magnetocaloric effect in  $PrSr_{1-x}Pb_xMn_2O_6$  ( $0.4 \leq x \leq 0.6$ ) double-perovskite manganite system*, *Journal of Superconductivity and Novel Magnetism*, 32, 393-403, 2019.
- [25] Ayaş, A.O., *Structural and magnetic properties with reversible magnetocaloric effect in  $PrSr_{1-x}Pb_xMn_2O_6$  ( $0.1 \leq x \leq 0.3$ ) double perovskite manganite structures*, *Philosophical Magazine*, 98, 2782-2796, 2018.
- [26] Akça, G., Ayaş, A.O., Kılıç Çetin, S., Akyol, M., Ekicibil, A., *Effect of monovalent cation doping on structural, magnetic, and magnetocaloric properties of  $Pr_{0.85}A_{0.15}MnO_3$  ( $A = Ag$  and  $K$ ) manganites*, *Journal of Superconductivity and Novel Magnetism*, 30, 1515-1525, 2017.
- [27] Kılıç Çetin, S., Acet, M., Ekicibil, A., Sarıkürkçü, C., Kıymaç, K., *Reversibility in the adiabatic temperature-change of  $Pr_{0.73}Pb_{0.27}MnO_3$* , *Journal of Alloys and Compounds*, 565, 139-143, 2013.
- [28] Ayaş, A.O., Akyol, M., Kılıç Çetin, S., Kaya, M., Dinçer İ., Ekicibil, A., Elerman, Y., *Room temperature magnetocaloric effect in  $Pr_{1.75}Sr_{1.25}Mn_2O_7$  double-layered perovskite manganite system*, *Philosophical Magazine*, 97, 671-682, 2017.
- [29] Rietveld, H., *A profile refinement method for nuclear and magnetic structures*, *Journal of Applied Crystallography*, 2, 65-71, 1969.
- [30] Rodríguez-Carvajal, J., *Recent advances in magnetic structure determination by neutron powder diffraction*, *Physica B: Condensed Matter*, 192, 55-69, 1993.
- [31] Debye, P., Scherrer, P., *Interference on inordinate orientated particles in Roentgen light*, *Physikalische Zeitschrift*, 17, 277-283, 1996.
- [32] Debye, P., Scherrer, P., *Interference on inordinate orientated particles in X-ray light III*, *Physikalische Zeitschrift*, 18, 291-301, 1997.
- [33] Chandra, K., Singhal, S., Goyal, S., *Magnetic and Mössbauer spectral studies of nano crystalline cobalt substituted magnesium ferrites ( $Mg_xCo_{1-x}Fe_2O_4$ )*, *Hyperfine Interactions*, 183, 75-80, 2008.
- [34] Rajendran, M., Pullar, R.C., Bhattacharya, A.K., Das, D., Chintalapudi, S.N., Majumdar, C.K., *Magnetic properties of nanocrystalline  $CoFe_2O_4$  powders prepared at room temperature: variation with crystallite size*, *Journal of Magnetism and Magnetic Materials*, 232, 71-83, 2001.
- [35] Barati, M.R., *Characterization and preparation of nanocrystalline MgCuZn ferrite powders synthesized by Sol-Gel Auto-Combustion Method*, *Journal of Sol-Gel Science and Technology*, 52, 171-178, 2009.
- [36] Kumar, V., Rana, A., Yadav, M.S., Pant, R.P., *Size-induced effect on nano-crystalline  $CoFe_2O_4$* , *Journal of Magnetism and Magnetic Materials*, 320, 1729-1734, 2008.
- [37] Krishna Murthy, J., Devi Chandrasekhar, K., Mahana, S., Topwal, D., Venimadhav, A., *Giant magnetocaloric effect in  $Gd_2NiMnO_6$  and  $Gd_2CoMnO_6$  ferromagnetic insulators*, *Journal of Physics D: Applied Physics*, 48, 355001-355001, 2015.
- [38] Phong, P.T., Manh, D.H., Hoan, L.C., Ngai, T.V., Phuc, N.X., Lee, I.-J., *Particle size effects on  $La_{0.7}Ca_{0.3}MnO_3$ : Griffiths phase-like behavior and magnetocaloric study*, *Journal of Alloys and Compounds*, 662, 557-565, 2016.

[39] Phong, P.T., Dang, N.V., Bau, L.V., An, N.M., Lee, I.-J., *Landau mean-field analysis and estimation of the spontaneous magnetization from magnetic entropy change in  $La_{0.7}Sr_{0.3}MnO_3$  and  $La_{0.7}Sr_{0.3}Mn_{0.95}Ti_{0.05}O_3$* , *Journal of Alloys and Compounds*, 698, 451-459, 2017.

[40] Banerjee, B.K., *On a Generalised approach to first and second order magnetic transitions*, *Physics Letters*, 12, 16-17, 1964.



## Bioactivity Features of Novel Actinobacteria Isolated from Lichen and Orchid Plant

Hilal ATEŞ<sup>1</sup>, Hilal AY<sup>2,\*</sup>

<sup>1</sup>Ondokuz Mayıs University, Faculty of Science, Department of Biology, 55270, Samsun, Türkiye  
[hilal.ates@omu.edu.tr](mailto:hilal.ates@omu.edu.tr), ORCID: 0000-0002-5460-2360

<sup>2</sup>Yildiz Technical University, Faculty of Arts and Sciences, Department of Molecular Biology and Genetics, 34220, Istanbul, Türkiye  
[hilal.ay@yildiz.edu.tr](mailto:hilal.ay@yildiz.edu.tr), ORCID: 000-0002-8735-4703

Received: 20.12.2022

Accepted: 26.09.2023

Published: 31.12.2023

### Abstract

A total of 10 actinobacterial strains were isolated from a lichen and an orchid species by employing a selective isolation procedure for actinobacteria. Antimicrobial activities of the isolates were evaluated against *Aspergillus niger* ATCC 16404, *Candida albicans* ATCC 10231, *Enterococcus faecalis* ATCC 29212, *Bacillus subtilis* ATCC 6633, *Escherichia coli* ATCC 25922, *Klebsiella pneumoniae* ATCC 700603, *Pseudomonas aeruginosa* ATCC 27853, *Salmonella enterica* ATCC 13311, *Staphylococcus aureus* ATCC 29213 and *Listeria monocytogenes* NCTC 5348. Out of the 10 isolates, eight showed antimicrobial activity against at least one pathogen. For molecular identification of the strains, 16S rRNA gene sequence analysis was performed. The pairwise comparison of the 16S rRNA gene sequences of the strains with the databases showed that the strains are members of the genus *Streptomyces* by sharing 98.9 – 100% gene sequence similarities. Phylogenetic relationships of the strains within the genus



*Streptomyces* were revealed by maximum likelihood and maximum parsimony phylogenetic trees. The results revealed that unexplored environmental habitats like lichens and plant tissues may represent a potential reservoir for novel actinobacteria with promising bioactivity features.

**Keywords:** 16S rRNA Gene; Actinobacteria; Antimicrobial Activity; Lichen; Orchid Tuber.

## Liken ve Orkide Bitkisinden İzole Edilen Aktinobakterilerin Biyoaktivite Özellikleri

### Öz

Aktinobakteriler için seçici bir izolasyon prosedürü kullanılarak bir liken ve orkide türünden toplam 10 aktinobakteri izole edilmiştir. İzolatların antimikrobiyal aktiviteleri *Aspergillus niger* ATCC 16404, *Candida albicans* ATCC 10231, *Enterococcus faecalis* ATCC 29212, *Bacillus subtilis* ATCC 6633, *Escherichia coli* ATCC 25922, *Klebsiella pneumoniae* ATCC 700603, *Pseudomonas aeruginosa* ATCC 27853, *Salmonella enterica* ATCC 13311, *Staphylococcus aureus* ATCC 29213 ve *Listeria monocytogenes* NCTC 5348 patojenlerine karşı değerlendirilmiştir. On izolattan sekizi, en az bir patojene karşı antimikrobiyal aktivite göstermiştir. İzolatları moleküler olarak tanımlamak amacıyla 16S rRNA gen dizi analizi yapılmıştır. 16S rRNA geni karşılaştırmalı analizleri bütün izolatların *Streptomyces* cinsi üyesi olduklarını ve %98,9 – 100 gen dizi benzerliği taşıdıklarını göstermiştir. İzolatların *Streptomyces* cinsi içerisindeki filogenetik ilişkileri maksimum olabilirlik ve maksimum sıklık filogenetik ağaçları ile ortaya çıkarılmıştır. Sonuçlar, likenler ve bitki dokuları gibi henüz çalışılmamış çevresel habitatların önemli biyoaktivite özelliklerine sahip yeni aktinobakteriler için potansiyel bir kaynak olabileceğini göstermektedir.

**Anahtar Kelimeler:** 16S rRNA Geni; Aktinobakteriler; Antimikrobiyal Aktivite; Liken; Orkide Yumrusu.

### 1. Introduction

Novel drug leads, notably antimicrobial compounds, are needed to combat diseases such as increased antibiotic resistance and cancer that threaten human life [1, 2]. Although compounds with antimicrobial and therapeutic effects are produced by chemical synthesis, nature is still the richest and most important source for therapeutic compounds [3]. Microbial natural products with distinct biological activities are the most significant source for novel pharmaceutical compounds, including antimicrobial and antioxidant drugs. The numerous reports of the reappearance of

pathogenic microorganisms resistant to antibiotics increase the requirement for more powerful antimicrobials having new modes of action. Among the diverse resources, the advantageous chemical scaffolds and metabolic potential of actinobacteria have made it one of the most promising resources for bioprospecting. Roughly, more than half of the known antibiotics used in clinics today are produced by bacteria from the phylum *Actinomycetota*, formerly known as the phylum *Actinobacteria* [4, 5]. Notably, the genus *Streptomyces* alone constitutes 80% of the bioactive natural products produced by the members of the phylum *Actinomycetota* [6, 7].

The phylum *Actinomycetota*, also known as actinobacteria, comprises a diverse group of Gram-positive bacteria with high G+C content in their genomes. These bacteria, mostly producing substrate and aerial mycelia, are abundant in soil and have been isolated from various ecosystems, including alkaline soils [8], marine sponges [9], deep-sea sediments [10], hot springs [11], and medicinal plants [12]. Since most actinobacteria serve significant ecological functions, they have wide application potential in agriculture and environmental protection in addition to the production of antibiotics. However, the increasing emergence of new diseases and pathogens as well as antibiotic resistance has led to a reappearance of fascination for the discovery of new bioactive compounds for therapeutic applications. Therefore, the search for unexplored or extreme ecological habitats as sources of new actinobacteria with biological activity against pathogens has the utmost importance for discovering novel bioactive compounds with antimicrobial and/or anticancer activity. In this respect, lichens and plant tissues appear to have a good potential source for novel actinobacteria [13].

Lichens are the symbiotic communities of fungi and green algae or cyanobacteria. They have diverse morphologies and can be found in a wide variety of areas ranging from poles to tropical areas, especially in terrestrial areas [14, 15]. Most lichens are capable of producing bioactive substances with antioxidant, cytotoxic and antimicrobial activity [16].

Although the fungi and algae or cyanobacteria diversity in the symbiotic lichen community is often described, there is little information about the microorganisms found in the association of lichen as a bioactive secondary metabolite producer [17]. Recent reports have revealed that there is a large number of microorganisms in the lichen association [18, 19]. These lichen and related microorganisms form stable and specific populations, which represent a third form of lichen symbiosis as a whole [20].

Another promising source for the discovery of novel actinobacteria having bioactivity potential is plant tissues. Endophytic actinobacteria have great potential for the production of new natural compounds essential for commercial and medical use [21]. Currently, many studies have

focused on the isolation of novel actinobacteria producing bioactive secondary metabolites which have potential use in medicine, industry, and agriculture [22, 23].

In this study, our objectives were to isolate possible novel actinobacteria with antimicrobial and/or antibiofilm activities from unexploited sources of *Xanthoria* sp., a lichen collected from tree barks, and endophytic tissues of a *Serapias* sp., an orchid genus distributed in north Anatolia. The results underline novel *Actinobacteria* from plant and lichen samples have a high potential for bioactive secondary metabolites as well as the importance of exploitation of symbiotic actinobacteria from understudied sources for bioprospecting.

## **2. Materials and Methods**

### **2.1. Isolation of actinobacteria**

The lichen and orchid samples were collected from the campus of Ondokuz Mayıs University. The collected samples were delivered to the laboratory in sterile bags. In order to isolate actinobacteria from a lichen sample of *Xanthoria* sp., and an orchid species of *Serapias* sp., three selective media were prepared under aseptic conditions. The selective media used were the R2A medium [24], Czapek's Dox medium [25], and soil extract medium [26].

The lichen samples were brought to the laboratory and then incubated at 100 °C for an hour. Each lichen sample was then crushed in a sterile mortar and weighed 1 g and transferred to a 9-ml sterile Ringer's (Oxoid) solution under aseptic conditions. After good vortexing, the solutions were kept at 60 °C in a water bath for 15 min and then diluted to prepare  $10^{-2}$  and  $10^{-3}$  concentration tubes. For selective isolation of actinobacteria, 200 µl from each tube was spread onto the media. Both the rhizosphere and endophytic parts of the orchid tuber were used for actinobacteria isolation. The orchid tuber was kept in 100 ml sterile Ringer's solution (Oxoid) in a flask overnight. It was then transferred to a water bath at 60 °C and incubated for 20 min. After incubation, 200 µl Ringer's solution was spread onto selective isolation media. For isolation of endophytic actinobacteria, the orchid tuber removed from the Ringer's solution was crushed in sterile mortar and pestle and then transferred to a 9-ml sterile Ringer's solution. Then it was kept in a water bath for 15 min at 60 °C. After preparation of  $10^{-2}$  and  $10^{-3}$  concentration tubes, 200 µl of each tube was inoculated onto selective media. All plates were inoculated in triplicate and incubated at 28 °C for three weeks.

## 2.2. Antimicrobial activity test

Antimicrobial activity of the isolated actinobacteria was tested against *Aspergillus niger* ATCC 16404, *Candida albicans* ATCC 10231, *Enterococcus faecalis* ATCC 29212, *Bacillus subtilis* ATCC 6633, *Escherichia coli* ATCC 25922, *Klebsiella pneumoniae* ATCC 700603, *Pseudomonas aeruginosa* ATCC 27853, *Salmonella enterica* ATCC 13311, *Staphylococcus aureus* ATCC 29213, and *Listeria monocytogenes* NCTC 5348. The actinobacteria isolates were grown at 28 °C for a week on the ISP2 agar medium [27]. An amount of actinobacterial mycelia was taken and transferred into a 9-ml sterile Ringer's solution. A 7- $\mu$ l of suspended bacterial solution was inoculated onto Bennett's Agar [28] without antibiotic supplementation and then incubated at 28 °C for 3 days. At the end of the incubation period, 1 ml chloroform was poured on the colonies which were developed under sterile conditions, and chloroform was expected to evaporate after 40 minutes. Subsequently, fresh pathogens developed on semi-solid nutrient agar were inoculated by spreading plates. After 48 hours of incubation under appropriate incubation conditions, the zone diameter of the region around the colonies was measured. Amphotericin B (5 mg ml<sup>-1</sup>) was used for *A. niger*, and chloramphenicol (30  $\mu$ g ml<sup>-1</sup>) was used for other test pathogens as positive controls. The experiments were performed in duplicate, and the data are expressed as a mean value  $\pm$  standard deviation.

## 2.3. Biofilm inhibition test

Antibiofilm activity of the isolates against pathogen *S. aureus* ATCC 29213 was evaluated in 96-well plates. The pathogen organism was incubated overnight in 100 ml LB medium. Test isolates were developed in ISP 2 medium, and supernatants were removed after centrifugation at 13000 rpm for 5 min. 100  $\mu$ l of supernatants were placed in each well, and a volume of 100  $\mu$ l of the pathogen grown in the LB medium was added to the wells and incubated at 37 °C for 18 hours. The bacteria-supernatant mixture was then removed from the wells and allowed to dry at room temperature for 15 min. Then, a volume of 200  $\mu$ l of crystal violet dye (1%, w:v) was added to the wells and kept for 45 minutes. At the end of the period, the dye was removed, and the wells were washed with sterilized distilled water. Then, 200  $\mu$ l of ethanol (95%, v:v) was added and the absorbance at 595 nm was measured [29].

## 2.4. Identification of the isolates and phylogenetic analysis

The actinobacteria with antimicrobial and/or antibiofilm activities were identified by 16S rRNA gene analysis. The genomic DNA extraction from the isolates was performed as described by Chun and Goodfellow [30]. The PCR amplifications of the 16S rRNA gene region of the isolates were performed using the 27F (5'AGAGTTTGATCTGGCTCAG3') and 1525R

(5'AAGGAGGTGWTCCARCC3') universal primers. The purified PCR products were sequenced using 518F (5'CCAGCAGCCGCGTAATACG3'), 800R (5'TACCAGGGTATCTAATCC3') and MG5F (5'AAACTCAAAGGAATTGACGG3') primers on an ABI PRISM 3730 XL automated sequencer in Macrogen Inc. (The Netherlands). The obtained sequences were assembled using the ChromasPro Version 1.7.6 (Technelysium Pty Ltd) program. The nearly complete 16S rRNA gene sequences were aligned with those of the closely related type strains downloaded from the EzBioCloud server [31]. The pairwise sequence similarities between the strains and their relatives within the genus *Streptomyces* were estimated by following the method described by Meier-Kolthoff et al. (2013) for the 16S rRNA gene on the GGDC web server (<http://ggdc.dsmz.de/>) [32]. The phylogenetic relationships between the strains and their close neighbours within the genus *Streptomyces* determined by pairwise gene comparisons were also inferred by the GGDC web server [32] by employing the DSMZ phylogenomics pipeline as described in previous works [33, 34]. Briefly, a multiple sequence alignment for the 16S rRNA gene sequences was built with MUSCLE [35]. The maximum likelihood (ML) and maximum parsimony (MP) phylogenetic trees were constructed from the alignment obtained through RAxML [36] and TNT algorithms [37], respectively. A rapid bootstrapping together with the autoMRE bootstrapping criterion [38] and a succeeding search for the best tree was employed to build the maximum likelihood tree. For the maximum parsimony tree, 1000 bootstrapping replications were applied combined with tree-bisection-and-reconnection branch swapping and ten arbitrary sequence addition replications. The aligned sequences were examined for compositional discrepancies by applying the test executed in PAUP\* [39].

### **3. Results and Discussion**

#### **3.1. Antimicrobial activity**

The antimicrobial properties of 10 isolates were tested against *E. coli* ATCC 25922, *B. subtilis* ATCC 6633, *S. aureus* ATCC 29213, *K. pneumoniae* ATCC 700603, *P. aeruginosa* ATCC 27853, *S. enterica* ATCC 13311, *A. niger* ATCC 16404, *C. albicans* ATCC 10231, *E. faecalis* ATCC 29212 and *L. monocytogenes* NCTC 5348 pathogens. It was determined that eight isolates showed antimicrobial activity against at least one pathogen. The results are given in Table 1 and show that actinobacteria obtained from lichen and orchid bulbs have a significant antimicrobial effect on pathogens.

**Table 1:** Inhibition zone diameters of actinobacteria obtained from lichen and orchid bulbs against the pathogens

Strain No	1	2	3	4	5	6	7	8	9	10
IC12A	-	-	-	-	-	-	-	-	-	-
IC12B	39.5±0.7	26±6.3	16.5±0.7	-	21.5±0.7	29±1.4	16.5±2.1	33.5±0.7	28.5±2.1	-
IC13	32.5±3.5	-	29±0	-	-	25.5±0.7	-	24±1.4	17±2.8	-
IC15A	-	-	-	-	-	-	-	15±1.4	13.5±2.1	-
IS21	-	-	-	-	-	-	-	17±4.2	17±4.2	-
IC21	36.5±6.3	24±1.4	30±1.4	-	13.5±2.1	25±5.6	-	30±5.6	27.5±3.5	-
SR31	14±1.4	32.5±9.6	-	-	-	47.5±9.6	-	43±4.2	46±5.6	-
SR22	-	-	-	-	-	32.5±3.5	-	-	-	-
SS31	33±2.8	-	-	15±1.4	-	-	-	-	-	-
SR32	-	-	-	-	-	-	-	-	-	-
Positive control	20.5±1.4	24±1.4	33.5±2.1	14.5±2.1	16.5±3.5	10±0	21.5±3.5	22.5±2.1	15±2.1	34.5±1.4

1; *C. albicans* ATCC 10231, 2; *B. subtilis* ATCC 6633, 3; *A. niger* ATCC 16404, 4; *E. faecalis* ATCC 29212, 5; *E. coli* ATCC 25922, 6; *S. aureus* ATCC 29213, 7; *K. pneumoniae* ATCC 700603, 8; *S. enterica* ATCC 13311, 9; *L. monocytogenes* NCTC 5348, 10; *P. aeruginosa* ATCC 27853.

The results show that strains IC12B, IC13 and IC21 exhibited high level of antimicrobial activity against *C. albicans*, *S. aureus*, *S. enterica* and *L. monocytogenes* pathogens while relatively lower against the *A. niger* pathogen. Strains IC12B and SR31 showed high antimicrobial activity against *B. subtilis* by forming an inhibition zone of 26 mm and 32.5 mm, respectively, compared to positive control (24 mm), while strain IC21 showed moderate antimicrobial activity. The strains SR22 and SR31 showed significantly higher antimicrobial activities against *S. aureus* compared to the positive control. Strain SR31 showed high antimicrobial activity against *B. subtilis*, *S. aureus*, *S. enterica* and *L. monocytogenes*. This strain was a highly bioactive microorganism against the pathogens *S. aureus*, *S. enterica* and *L. monocytogenes* by forming inhibition zones over 40 mm, which implies its bioactivity potential, particularly against foodborne infections. In addition, strain SR31 inhibited the growth of *C. albicans* moderately. On the other hand, strain SS31 showed higher inhibition activity against *C. albicans* and *E. faecalis* compared to the positive control. Strain IC12B exhibited high antimicrobial activity against *E. coli* and moderate activity against *K. pneumoniae*, while strains IC15A and IS21 exhibited moderate antimicrobial activity against *S. enterica* and *L. monocytogenes* by forming inhibition zones ranging from 13 – 17 mm in diameter. None of the isolates showed antimicrobial activity against *P. aeruginosa*. When the antimicrobial activity test results are evaluated in general, especially strain IC12B showed activity in a broad spectrum since

strain IC12B showed antimicrobial activity against all pathogens tested except *E. faecalis* and *P. aeruginosa*. Strain IC21 seemed to be effective as a promising source of antifungal agents.

### 3.2. Biofilm inhibition

Biofilm inhibition test was performed against the *S. aureus* ATCC 29213 pathogen for 10 isolates, and the results were evaluated with One-Way Anova program. Compared to the positive control group, strain IC12B significantly inhibited biofilm formation at the 95% significance level.

### 3.3. Phylogenetic characterization of actinobacteria

The strains were identified by the 16S rRNA gene pairwise sequence analysis. These strains were determined to be members of the genus *Streptomyces*. The most closely related type species according to the 16S rRNA gene pairwise sequence analysis were given in Table 2.

**Table 2:** The 16S rRNA gene sequence identity values to the closely related type species

Isolates	GenBank accession number	Closest type strain	Identity (%)	Isolation source
IC12A	MK503625	<i>Streptomyces aureus</i> NBRC 100912	99.93	Endophytic tissues of <i>Serapias</i> sp.
IC13	MK503627	<i>Streptomyces antimycoticus</i> NBRC 12839	100.00	Endophytic tissues of <i>Serapias</i> sp.
IC15A	MK503628	<i>Streptomyces aureocirculatus</i> NRRL ISP-5386	99.52	Endophytic tissues of <i>Serapias</i> sp.
IC21	MK503629	<i>Streptomyces antimycoticus</i> NBRC 12839	100.00	Endophytic tissues of <i>Serapias</i> sp.
IS21	MK503630	<i>Streptomyces aureocirculatus</i> NRRL ISP-5386	99.52	Endophytic tissues of <i>Serapias</i> sp.
IC12B	MK503626	<i>Streptomyces antimycoticus</i> NBRC 12839	100.00	Endophytic tissues of <i>Serapias</i> sp.
SR22	MK503631	<i>Streptomyces nanshensis</i> SCSIO 01066	99.57	<i>Xanthoria</i> sp.
SR31	MK503632	<i>Streptomyces decoyicus</i> NRRL 2666	100.00	<i>Xanthoria</i> sp.
SS31	MK503634	<i>Streptomyces daghestanicus</i> NRRL B-5418	99.58	<i>Xanthoria</i> sp.
SR32	MK503633	<i>Streptomyces nanshensis</i> SCSIO 01066	98.99	<i>Xanthoria</i> sp.

The phylogenetic tree based on comparative analysis of the 16S rRNA gene sequences of the strains and their close neighbours within the genus *Streptomyces* revealed that the strains were separated into six clades (Fig. 1). The strains IC12B, IC21 and IC13 were clustered together with *S. geldanamycininus* NRRL B-3602<sup>T</sup>, *S. yatensis* NBRC 101000<sup>T</sup>, *S. mordarskii* NRRL B-1346<sup>T</sup> as well as with *S. antimycoticus* NBRC 12839<sup>T</sup>. All three strains were observed to have similar antimicrobial activity profiles by having strong inhibition against *C. albicans*, *A. niger*, *E. coli*, *S. aureus*, *S. enterica* and *L. monocytogenes* (Table 1). Similarly, their most closely related phylogenetic neighbour *S. antimycoticus* was reported to be used as a biocontrol agent [40] and a source organism for bioactive terpenoids napyradiomycins [41]. In addition, *S. yatensis* was also reported to produce bioactive metabolites with antifungal [42] and nematocidal activities [43]. Considering the bioactivity profiles of the *Streptomyces* species within the same clade as well as high antimicrobial activities, the strains can be considered as potential sources for new bioactive compounds. The close phylogenetic relationship of the strains with the type strain of *S. antimycoticus* was also confirmed by the phylogenetic tree. The pairwise comparison of the 16S rRNA gene sequences of the strains indicated that the strains have 100% identity with each other.

Strain SR31 formed a cluster with the type strains of *S. decoyicus* NRRL B-2666<sup>T</sup>, *S. siyoensis* NRRL B-5408<sup>T</sup>, *S. caniferus* NBRC 15389<sup>T</sup>, *S. platensis* JCM 4662<sup>T</sup> and *S. monumycini* NRRL B-24309<sup>T</sup>. The antimicrobial activity tests showed that strain SR31 have strong inhibitory activity against *B. subtilis*, *S. aureus*, *S. enterica* and *L. monocytogenes* compared to the positive control. The type species in the same clade were also reported to produce antimicrobial and antitumor metabolites such as decoyinin, psicofuranine [44], siomycin [45] and caniferolide [46], which implies a high potential of strain SR31 to produce novel bioactive metabolites.

Strain SS31 was differentiated from the type species of *S. daghestanicus* NRRL B-5418<sup>T</sup>, *S. albidoflavus* DSM 40455<sup>T</sup> and *S. violascens* ISP 5183<sup>T</sup> within the cluster they formed together. Considering the tree topology and antimicrobial activities against *C. albicans* and *E. faecalis*, strain SS31 may represent a novel species within the genus *Streptomyces*.

Strains SR22 and SR32 were clustered together with the type species of *S. nanshensis* SCSIO 01066<sup>T</sup>. Although both strains shared the highest 16S rRNA gene sequence identity levels with the type species of *S. nanshensis*, they were differentiated from each other by 99.46% gene sequence identity level. Thus, both strains SR22 and SR32 may represent two novel species for the genus *Streptomyces*.

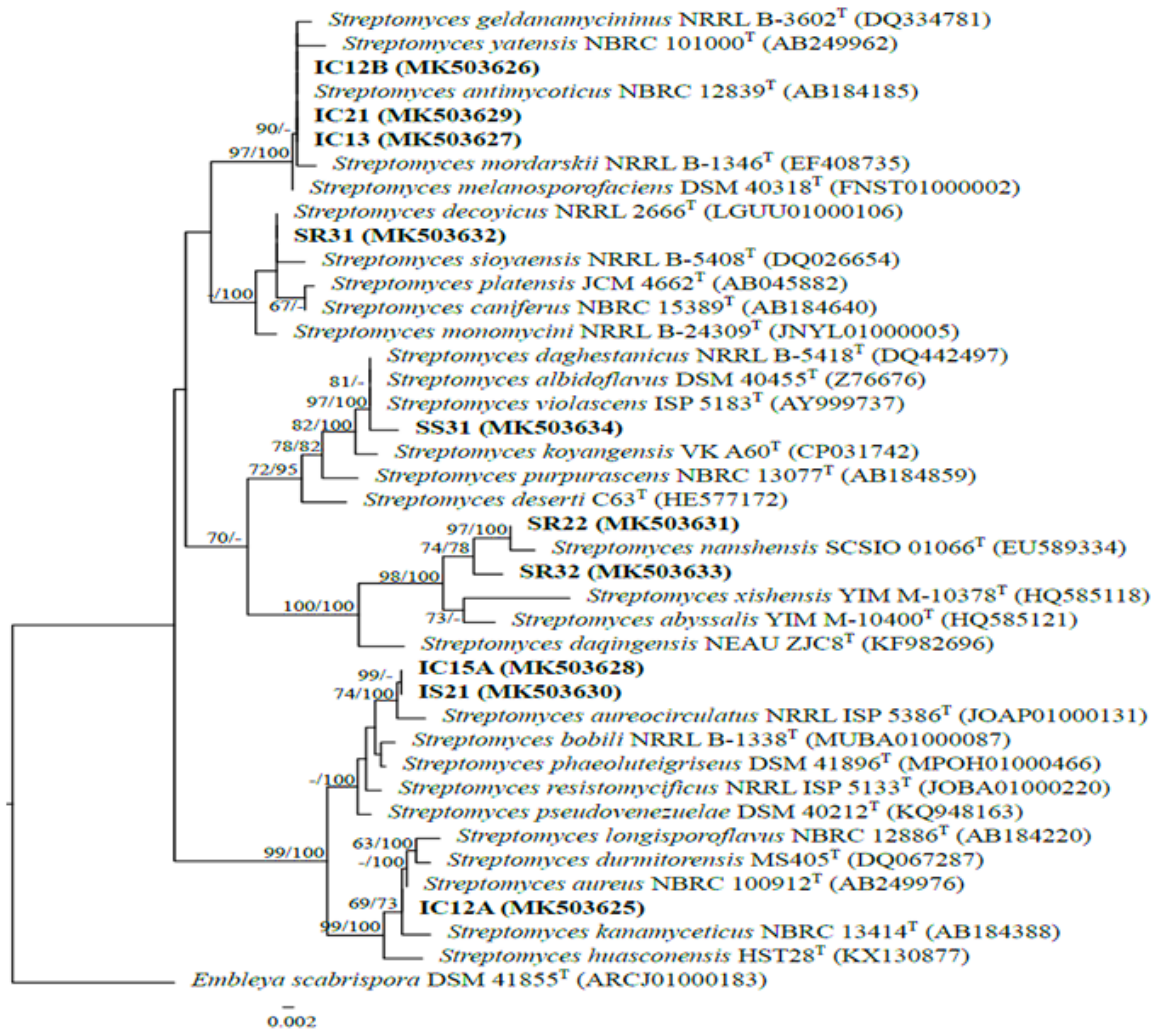


**Figure 1:** Phylogenetic tree of the *Streptomyces* strains based on the 16S rRNA gene sequence analysis. The tree was derived under the General Time Reversible with gamma distribution model and rooted through the midpoint. The scale indicates the expected number of nucleotide substitutions per site. The numbers above the branches are support levels when more than 60% bootstraps with maximum likelihood (left) and maximum parsimony (right). *Embleya scabriscora* DSM 41855<sup>T</sup> was used as an outgroup.

Strains IC15A and IS21 were clustered with their most closely related species *S. aureocirculatus* NRRL ISP 5386<sup>T</sup>, while their 16S rRNA gene sequence identity level with each other was calculated as 100%. Therefore, strains IC15A and IS21 might be representatives of a novel species within the genus *Streptomyces*. Sahu et al. (2007) reported that *S. aureocirculatus* produced a bioactive sugar molecule that inhibits the growth of pathogens [47]. Consistently, strains IC15A and IS21 showed antimicrobial activity against *S. enterica* and *L. monocytogenes*. Considering phylogenetic positions on the tree as well as the relatively low level of 16S rRNA gene sequence similarity, strains IC15A and IS21 have the possibility to be novel species of the genus *Streptomyces*, and hence, their bioactivity might result from structurally new metabolites.

Strain IC12A formed a large cluster with the type strains of *S. aureus* NBRC 100912<sup>T</sup>, *S. durmitorensis* MS405<sup>T</sup>, *S. longisporoflavus* NBRC 12886<sup>T</sup>, *S. kanamyceticus* NBRC 13414<sup>T</sup> and *S. huasconensis* HST28<sup>T</sup>. Although the strain showed no antimicrobial activity against the pathogens tested, the tree topology may suggest that strain IC12A might represent a novel species within the genus *Streptomyces*.

As actinobacteria are well-known for their ability to produce a myriad of bioactive secondary metabolites, the exploration of novel actinobacteria from unexplored or underexplored habitats is considered to be the most effective strategy to discover novel species with distinct biochemistry. Lichens are one of the underexplored microbial communities in terms of actinobacterial biodiversity and hold high promise for novel actinobacteria, as revealed by the present study. Selbmann et al. [48] investigated culturable bacteria from four Antarctic lichen species, i.e. *Lecanora fuscobrunnea* Dodge & Baker, *Umbilicaria decussata* (Villars) Zahlbruckner, *Usnea antarctica* Du Rietz, *Xanthoria elegans* (Link) Th. Fries, and reported 30 morphologically distinct bacterial strains, 20 of which were actinobacteria. The bioactivity of actinobacteria isolated from lichen samples was also reported by previous studies [49, 50]. Davies et al. [49] and Williams et al. [50] extracted novel bioactive metabolites, i.e. uncialamycin with antibiotic activity and cladoniamides A–G with cytotoxicity, from *Streptomyces uncialis* isolated from the surface of a lichen *Cladonia uncialis* collected near Pitt River, British Columbia. Consistently, Parrot et al. [51] showed that the littoral lichens are important sources of novel bioactive actinobacteria. However, there is no report on *Streptomyces* spp. isolated from the lichen genus *Xanthoria* (Fr.) Th. Fr.; thus, the present study is the first report revealing putatively novel *Streptomyces* spp. with significant antimicrobial activities from this lichen genus.

The endophytic actinobacteria from plant species also have distinct bioactivity characteristics, such as the endophytes of orchid plants [52]. Alibrandi et al. [53] revealed that over 25% of microbial symbionts in *Serapias* sp. were members of the actinobacteria in their culture-independent study, but they did not conduct any bioactivity screening for those actinobacteria. On the other hand, Saikia et al. [54] investigated the phylogenetic affiliation of actinobacteria isolated from various orchid species belonging to the genera *Cymbidium* Sw., *Dendrobium* Sw., *Micropera* Lindl., *Renanthera* Lour., *Rhynchostylis* Blume and *Vanda* R. Br. They identified 51 morphologically distinct actinobacterial isolates with multiple plant growth-promoting activities as well as broad-spectrum antifungal properties against various plant pathogens. Although similar works about bioactive actinobacteria from orchids species are reported in the literature, the present study is the first to show the *Streptomyces* spp. isolated from *Serapias* sp. have antimicrobial activity against human pathogens.

#### 4. Conclusion

Actinobacteria is a notable group of bacteria for researchers as they produce antibiotics and other therapeutically effective substances. In particular, the *Streptomyces* strains are known for their ability to produce new antibiotics and other biologically important compounds, including insecticides, herbicides, antiparasitics, immunosuppressants, and other compounds of industrial interest [55-57]. Thus, it is of utmost importance for the exploitation of this prolific group of bacteria isolated from unexplored or extreme habitats to discover novel bioactive metabolites.

In this study, the actinobacteria isolated from lichen and endophytic tissues of orchid tubers were revealed to have considerable antimicrobial activities against a number of human pathogens. From the phylogenetic point of view, moreover, these actinobacteria may represent novel species within the genus *Streptomyces*. However, a polyphasic approach involving morphological, biochemical, and phylogenetic characterization, as well as whole genome-based comparative analyses, must be employed to determine the taxonomic positions of these strains within the genus *Streptomyces*. Consequently, our present work on actinobacteria from lichen and orchid samples to search for promising natural sources for distinct bioactivity reveals that unexplored habitats are a real treasure for novel actinobacteria producing bioactive secondary metabolites waiting to be discovered. A comprehensive bioprospecting study supported by genome-based bioactivity estimation for these strains is required in the near future.

#### References

- [1] Payne, D.J., Gwynn, M.N., Holmes, D.J., Pompliano, D.L., *Drugs for bad bugs: confronting the challenges of antibacterial discovery*, Nature reviews Drug discovery, 6(1), 29-40, 2007.
- [2] Olano, C., Méndez, C., Salas, J.A., *Molecular insights on the biosynthesis of antitumour compounds by actinomycetes*, Microbial Biotechnology, 4(2), 144-164, 2011.
- [3] Manivasagan, P., Kang, K.H., Sivakumar, K., Li-Chan, E.C., Oh, H.M., Kim, S.K., *Marine actinobacteria: an important source of bioactive natural products*, Environmental toxicology and pharmacology, 38(1), 172-188, 2014.
- [4] Barka, E.A., Vatsa, P., Sanchez, L., Gaveau-Vaillant, N., Jacquard, C., Klenk, H.P., Clément, C., Ouhdouch, Y., van Wezel, G.P., *Taxonomy, physiology, and natural products of Actinobacteria*, Microbiology and Molecular Biology Reviews, 80(1), 1-43, 2016.
- [5] Lee, L.H., Goh, B.H., Chan, K.G., *Actinobacteria: Prolific producers of bioactive metabolites*, Frontiers Media SA, 1612, 2020.
- [6] Kumar, N., Singh, R.K., Mishra, S., Singh, A., Pachouri, U.C., *Isolation and screening of soil Actinomycetes as source of antibiotics active against bacteria*, International Journal of Microbiology Research, 2(2), 12, 2010.

- [7] Manivasagan, P., Venkatesan, J., Sivakumar, K., Kim, S.K., *Pharmaceutically active secondary metabolites of marine actinobacteria*, *Microbiological research*, 169(4), 262-278, 2014.
- [8] Ay, H., Nouioui, I., del Carmen Montero-Calasanz, M., Carro, L., Klenk, H.P., Goodfellow, M., Igual, J.M., Çetin, D., Şahin, N., Işık, K., *Actinomadura alkaliterrae sp. nov., isolated from an alkaline soil*, *Antonie van Leeuwenhoek*, 110(6), 787-794, 2017.
- [9] Khan, S.T., Tamura, T., Takagi, M., Shin-Ya, K., *Streptomyces tateyamensis sp. nov., Streptomyces marinus sp. nov. and Streptomyces haliclona sp. nov., isolated from the marine sponge Haliclona sp.*, *International journal of systematic and evolutionary microbiology*, 60(12), 2775-2779, 2010.
- [10] Xiao, J., Luo, Y., Xu, J., Xie, S., Xu, J., *Modestobacter marinus sp. nov., a psychrotolerant actinobacterium from deep-sea sediment, and emended description of the genus Modestobacter*, *International journal of systematic and evolutionary microbiology*, 61(7), 1710-1714, 2011.
- [11] Duan, Y.Y., Ming, H., Dong, L., Yin, Y.R., Zhang, Y., Zhou, E.M., Liu, L., Nie, G.X., Li, W.J., *Streptomyces calidiresistens sp. nov., isolated from a hot spring sediment*, *Antonie van Leeuwenhoek*, 106(2), 189-196, 2014.
- [12] Wang, Z., Tian, J., Li, X., Gan, L., He, L., Chu, Y., Tian, Y., *Streptomyces dioscori sp. nov., a Novel Endophytic Actinobacterium Isolated from Bulbil of Dioscorea bulbifera L.*, *Current microbiology*, 75(10), 1384-1390, 2018.
- [13] Parrot, D., Legrave, N., Delmail, D., Grube, M., Suzuki, M., Tomasi, S., *Review—Lichen-associated bacteria as a hot spot of chemodiversity: focus on unciamycin, a promising compound for future medicinal applications*, *Planta Medica*, 82(13), 1143-1152, 2016.
- [14] Lutzoni, F., Miadlikowska, J., *Lichens*. *Current Biology*, 19(13), R502-R503, 2009.
- [15] Asplund, J., Wardle, D.A., *How lichens impact on terrestrial community and ecosystem properties*, *Biological Reviews*, 92(3), 1720-1738, 2017.
- [16] Boustie, J., Tomasi, S., Grube, M., *Bioactive lichen metabolites: alpine habitats as an untapped source*, *Phytochemistry Reviews*, 10(3), 287-307, 2011.
- [17] Calcott, M.J., Ackerley, D.F., Knight, A., Keyzers, R.A., Owen, J.G., *Secondary metabolism in the lichen symbiosis*, *Chemical Society Reviews*, 47(5), 1730-1760, 2018.
- [18] Muggia, L., Vancurova, L., Škaloud, P., Peksa, O., Wedin, M., Grube, M., *The symbiotic playground of lichen thalli—a highly flexible photobiont association in rock-inhabiting lichens*, *FEMS Microbiology Ecology*, 85(2), 313-323, 2013.
- [19] Liu, C., Jiang, Y., Wang, X., Chen, D., Chen, X., Wang, L., Han, L., Huang, X., Jiang, C., *Diversity, antimicrobial activity, and biosynthetic potential of cultivable actinomycetes associated with lichen symbiosis*, *Microbial ecology*, 74(3), 570-584, 2017.
- [20] Grube, M., Cernava, T., Soh, J., Fuchs, S., Aschenbrenner, I., Lassek, C., Wegner, U., Becher, D., Riedel, K., Sensen, C.W., Berg, G., *Exploring functional contexts of symbiotic sustain within lichen-associated bacteria by comparative omics*, *The ISME journal*, 9(2), 412-424, 2015.
- [21] Liu, Y.H., Guo, J.W., Salam, N., Li, L., Zhang, Y.G., Han, J., Mohamad, O.A., Li, W.J., *Culturable endophytic bacteria associated with medicinal plant Ferula songorica: molecular phylogeny, distribution and screening for industrially important traits*, *3 Biotech*, 6(2), 1-9, 2016.

- [22] Li, J., Zhao, G.Z., Chen, H.H., Wang, H.B., Qin, S., Zhu, W.Y., Xu, L.H., Jiang, C.L., Li, W.J., *Antitumour and antimicrobial activities of endophytic streptomycetes from pharmaceutical plants in rainforest*, *Letters in applied microbiology*, 47(6), 574-580, 2008.
- [23] Golinska, P., Wypij, M., Agarkar, G., Rathod, D., Dahm, H., Rai, M., *Endophytic actinobacteria of medicinal plants: diversity and bioactivity*, *Antonie Van Leeuwenhoek*, 108(2), 267-289, 2015.
- [24] Reasoner, D.J., Geldreich, E.E., *A new medium for the enumeration and subculture of bacteria from potable water*, *Applied and environmental microbiology*, 49(1), 1-7, 1985.
- [25] Weyland, H., *Actinomycetes in North Sea and Atlantic ocean sediments*, *Nature*, 223(5208), 858-858, 1969.
- [26] Hamaki, T., Suzuki, M., Fudou, R., Jojima, Y., Kajiura, T., Tabuchi, A., Sen, K., Shibai, H., *Isolation of novel bacteria and actinomycetes using soil-extract agar medium*, *Journal of bioscience and bioengineering*, 99(5), 485-492, 2005.
- [27] Shirling, E.T., Gottlieb, D., *Methods for characterization of Streptomyces species*, *International journal of systematic bacteriology*, 16(3), 313-340, 1966.
- [28] Jones, K.L., *Fresh isolates of actinomycetes in which the presence of sporogenous aerial mycelia is a fluctuating characteristic*, *Journal of bacteriology*, 57(2), 141-145, 1949.
- [29] Sankar Ganesh, P., Rai Vittal, R., *In vitro antibiofilm activity of Murraya koenigii essential oil extracted using supercritical fluid CO<sub>2</sub> method against Pseudomonas aeruginosa PAOI*, *Natural Product Research*, 29(24), 2295-2298, 2015.
- [30] Chun, J., Goodfellow, M., *A phylogenetic analysis of the genus Nocardia with 16S rRNA gene sequences*, *International Journal of Systematic and Evolutionary Microbiology*, 45(2), 240-245, 1995.
- [31] Yoon, S.H., Ha, S.M., Kwon, S., Lim, J., Kim, Y., Seo, H., Chun, J., *Introducing EzBioCloud: a taxonomically united database of 16S rRNA gene sequences and whole-genome assemblies*, *International journal of systematic and evolutionary microbiology*, 67(5), 1613, 2017.
- [32] Meier-Kolthoff, J.P., Carbasse, J.S., Peinado-Olarte, R.L., Göker, M., *TYGS and LPSN: a database tandem for fast and reliable genome-based classification and nomenclature of prokaryotes*, *Nucleic acids research*, 50(D1), D801-D807, 2022.
- [33] Ay, H., *Genomic insight into a novel actinobacterium, Actinomadura rubrisoli sp. nov., reveals high potential for bioactive metabolites*, *Antonie van Leeuwenhoek*, 114(2), 195-208, 2021.
- [34] Meier-Kolthoff, J.P., Hahnke, R.L., Petersen, J., Scheuner, C., Michael, V., Fiebig, A., Rohde, C., Rohde, M., Fartmann, B., Goodwin, L.A., Chertkov, O., Reddy, T., Pati, A., Ivanova, N.N, Markowitz, V., Kyrpides, N.C., Woyke, T., Göker M., Klenk, H.P., *Complete genome sequence of DSM 30083T, the type strain (U5/41T) of Escherichia coli, and a proposal for delineating subspecies in microbial taxonomy*, *Standards in Genomic Sciences*, 9(2), 2014.
- [35] Edgar, R.C., *MUSCLE: a multiple sequence alignment method with reduced time and space complexit*, *BMC bioinformatics*, 5(1), 1-19, 2004.
- [36] Stamatakis, A., *RAxML version 8: a tool for phylogenetic analysis and post-analysis of large phylogenies*, *Bioinformatics*, 30(9), 1312-1313, 2014.
- [37] Goloboff, P.A., Farris, J.S., Nixon, K.C., *TNT, a free program for phylogenetic analysis*, *Cladistics*, 24(5), 774-786, 2008.

- [38] Pattengale, N.D., Alipour, M., Bininda-Emonds, O.R., Moret, B.M., Stamatakis, A., *How many bootstrap replicates are necessary?* in *Annual International Conference on Research in Computational Molecular Biology*, pp.184-200, 2009.
- [39] Swofford, D.L., *PAUP: phylogenetic analysis using parsimony, version 4.0 b10*, Sinauer Associates, Sunderland, MA, 2002.
- [40] Koch, E., Löffler, I., *Partial characterization of the antimicrobial activity of Streptomyces antimycoticus FZB53*, *Journal of Phytopathology*, 157(4), 235-242, 2009.
- [41] Motohashi, K., Sue, M., Furihata, K., Ito, S., Seto, H., *Terpenoids produced by actinomycetes: Napyradiomycins from Streptomyces antimycoticus NT17*, *Journal of natural products*, 71(4), 595-601, 2008.
- [42] Benouagueni, S., Ranque, S., Kirane, D.G., *A non-polyenic antifungal produced by a Streptomyces yatensis strain isolated from Mellah Lake in El Kala, North-East of Algeria*, *Journal de Mycologie Medicale*, 25(1), 2-10, 2015.
- [43] Park, E.J., Jang, H.J., Park, C.S., Lee, S.J., Lee, S., Kim, K.H., Yun, B.S., Lee, S.W., Rho, M.C., *Evaluation of Nematicidal Activity of Streptomyces yatensis KRA-28 against Meloidogyne incognita*, *Journal of Microbiolog and Biotechnology*, 30(5), 700-707, 2020.
- [44] Kumar, Y., Goodfellow, M., *Reclassification of Streptomyces hygrosopicus strains as Streptomyces aldersoniae sp. nov., Streptomyces angustmyceticus sp. nov., comb. nov., Streptomyces ascomycinicus sp. nov., Streptomyces decoyicus sp. nov., comb. nov., Streptomyces milbemycinicus sp. nov. and Streptomyces wellingtoniae sp. nov.*, *International journal of systematic and evolutionary microbiology*, 60(4), 769-775, 2010.
- [45] Tokura, K., Tori, K., Yoshimura, Y., Okabe, K., Otsuka, H., Matsushita, K., Inagaki, F., Miyazawa, T., *The structure of siomycin-D1, peptide antibiotic isolated from Streptomyces sioyaensis*, *The Journal of Antibiotics*, 33(12), 1563-1567, 1980.
- [46] Alvariño, R., Alonso, E., Lacret, R., Oves-Costales, D., Genilloud, O., Reyes, F., Alfonso, A., Botana, L.M., *Caniferolide A, a macrolide from Streptomyces caniferus, attenuates neuroinflammation, oxidative stress, amyloid-beta, and tau pathology in vitro*, *Molecular Pharmaceutics*, 16(4), 1456-1466, 2019.
- [47] zkumar Sahu, M., Murugan, M., Sivakumar, K., Thangaradjou, T., Kannan, L., *Occurrence and distribution of actinomycetes in marine environs and their antagonistic activity against bacteria that is pathogenic to shrimps*, *Israeli Journal of Aquaculture-Bamidgeh*, 59(3), 155-161, 2007.
- [48] Selbmann, L., Zucconi, L., Ruisi, S., Grube, M., Cardinale, M., Onofri, S., *Culturable bacteria associated with Antarctic lichens: affiliation and psychrotolerance*, *Polar biology*, 33, 71-83, 2010.
- [49] Davies, J., Wang, H., Taylor, T., Warabi, K., Huang, X.H., Andersen, R.J., *Uncialamycin, a new enediyne antibiotic*, *Organic letters*, 7(23), 5233-5236, 2005.
- [50] Williams, D.E., Davies, J., Patrick, B.O., Bottriell, H., Tarling, T., Roberge, M., Andersen, R.J., *Cladoniamides A–G, tryptophan-derived alkaloids produced in culture by Streptomyces uncialis*, *Organic letters*, 10(16), 3501-3504, 2008.
- [51] Parrot, D., Antony-Babu, S., Intertaglia, L., Grube, M., Tomasi, S., Suzuki, M.T., *Littoral lichens as a novel source of potentially bioactive Actinobacteria*, *Scientific Reports*, 5(1), 15839, 2015.
- [52] Herrera, H., Fuentes, A., Soto, J., Valadares, R., Arriagada, C., *Orchid-associated bacteria and their plant growth promotion capabilities*, In *Orchids phytochemistry, biology and horticulture: fundamentals and applications*, 175-200, 2022.

[53] Alibrandi, P., Schnell, S., Perotto, S., Cardinale, M., *Diversity and structure of the endophytic bacterial communities associated with three terrestrial orchid species as revealed by 16S rRNA gene metabarcoding*, *Frontiers in Microbiology*, 11, 604964, 2020.

[54] Saikia, J., Mazumdar, R., Thakur, D., *Phylogenetic affiliation of endophytic actinobacteria associated with selected orchid species and their role in growth promotion and suppression of phytopathogens*, *Frontiers in Plant Science*, 13, 1058867, 2022.

[55] Chater, K.F., *Streptomyces inside-out: a new perspective on the bacteria that provide us with antibiotics*, *Philosophical Transactions of the Royal Society B: Biological Sciences*, 361(1469), 761-768, 2006.

[56] Bull, A.T., Stach, J.E., *Marine actinobacteria: new opportunities for natural product search and discovery*, *Trends in microbiology*, 15(11), 491-499, 2007.

[57] Sharma, S. B., Gupta, R., *Drug development from natural resource: a systematic approach*, *Mini reviews in medicinal chemistry*, 15(1), 52-57, 2015.



## A Numerical Application of the Chebyshev Operational Matrix Method for HIV Infection of CD4+T-cells

Yalçın ÖZTÜRK<sup>1,\*</sup>, Ayşe Anapalı ŞENEL<sup>2</sup>, Ceren LİMONCU<sup>3</sup>, Mustafa GÜLSU<sup>4</sup>

<sup>1</sup>Muğla Sıtkı Koçman University, Ula Ali Koçman Vocational High School, 48600, Muğla, Türkiye  
yozturk@mu.edu.tr, ORCID: 0000-0002-4142-5633

<sup>2,3,4</sup>Muğla Sıtkı Koçman University, Faculty of Science, Department of Mathematics, 48000, Muğla, Türkiye

ayseanapali@mu.edu.tr, ORCID: 0000-0002-0198-1862  
cerenlimoncu@posta.mu.edu.tr, ORCID: 0000-0002-8396-5945  
mgulsu@mu.edu.tr, ORCID: 0000-0001-6139-0266

Received: 28.08.2023

Accepted: 20.10.2023

Published: 31.12.2023

### Abstract

In this research study, we aim to approximate a solution for the mathematical model of the Human Immunodeficiency Virus (HIV) infection of CD4+T-cells. An operational matrix method based on Chebyshev orthogonal polynomials has been adapted to obtain numerical solutions for the model of HIV infection of CD4+T-cells. The proposed numerical scheme is built on a system of a nonlinear algebraic equation, including coefficients of a finite Chebyshev series that represent the approximate solutions of the model. Results are compared to existing methods to verify the accuracy of the numerical scheme.

**Keywords:** Model of the HIV infection; CD4+T cells; Operational matrix method; Chebyshev polynomials; Nonlinear system of differential equations.

### CD4+T Hücrelerindeki HIV Enfeksiyonunun Yayılım Modelinin Chebyshev Operasyonel Matris Metodu ile bir Nümerik Uygulaması



## Öz

Bu çalışma, CD4+T hücrelerinde HIV virüsünün matematiksel yayılım modeli için yaklaşık çözümler elde etmeyi amaçlamaktadır. Nümerik çözümler Chebyshev polinomları ile operasyonel matris metodunun CD4+T hücrelerinde HIV virüsünün matematiksel yayılım modeline uygulanması ile elde edilecektir. Önerilen method modele ait nümerik çözümlerin bir Chebyshev serisi formunda yazılarak, Chebyshev serisi içindeki bilinmeyen katsayıları içeren lineer olmayan bir denklem sistemi inşa atmayı amaçlar. Yöntemin doğruluğunu kontrol etmek için nümerik sonuçlar var olan nümerik yöntemlerle karşılaştırılmıştır.

**Anahtar Kelimeler:** HIV Enfeksiyon Modeli; CD4+T hücreleri; Operasyonel matris metod; Chebyshev polinomları; Lineer olmayan diferansiyel denklem sistemleri.

## 1. Introduction

Applied mathematics is modeled to interpret natural events. These models and their numerical solutions obtain valuable information about those events. For example, a crucial event for public health is the dynamics of HIV infection of CD4+T-cells. Firstly, Perelson developed a system of nonlinear differential equations to describe HIV infection of CD4+T-cells in 1989 [1-5]. Nowadays, humanity spends millions of dollars on the treatment of this disease.

The mathematical model of infection of HIV of CD4+T cells is given by [6-9]

$$\begin{aligned}\frac{dT}{dt} &= q - \alpha T + rT \left(1 - \frac{T+I}{T_{\max}}\right) - kVT \\ \frac{dI}{dt} &= kVT - \beta I \\ \frac{dV}{dt} &= \mu\beta I - \gamma V\end{aligned}\tag{1}$$

with the conditions

$$T(0) = r_1, \quad I(0) = r_2, \quad V(0) = r_3\tag{2}$$

where  $T(t)$  is denoted as the concentration of healthy CD4+ T cells,  $I(t)$  infected CD4+ T cells,  $V(t)$  and free H.I.V. at a time  $t$  in blood. In addition,  $q$  is the source term for uninfected CD4+

T cells,  $\alpha$  is the natural death rate of the CD4+ T cell concentration,  $r$  is the growth rate of CD4+ T cells,  $k$  is the rate at which CD4+ T cells become infected with a virus,  $\beta$  is the total death rate of infected CD4+ T cells,  $\mu$  is the number of virions produced by infected CD4+ T cells.  $\gamma$  is the death rate of the free virus.  $k > 0$  indicates the infection rate, and  $kVT$  indicates the infection rate of healthy CD4+ T cells. The termination  $T_{\max}$ , in the denominator of the logistic term in the equation for healthy T4 cell density, indicates the total T4 cell density that can be found stably in the blood; in other words, the carrying capacity of the blood for T4 cells. It will be assumed that each infected CD4+T cell produces. This model's global stability and a periodic solution are achieved in [10].

In this paper, we will take the numerical data as  $q = 0.1$ ,  $\alpha = 0.02$ ,  $r = 3$ ,  $\beta = 0.3$ ,  $k = 0.0027$ ,  $\gamma = 2.4$ ,  $\mu = 10$ ,  $T_{\max} = 1500$  and initial conditions data  $r_1 = 0.1$ ,  $r_2 = 0$ ,  $r_3 = 0.1$ . Since the mathematical model of H.I.V. infection HIV CD4+T cells (1) are nonlinear differential equations with three terms, the exact solution to this problem cannot be obtainable or nonexistent. A resolution to this problem is needed to analyze its epidemiology and stability and to predict advances in AIDS treatment. In this stage, numerical solution methods become crucial to solve Eq. (1) with the conditions. Many numerical methods for approximating H.I.V. in CD4+ T cells have been improved over the last twenty years. Ghoreishi [11] presents the homotopy analysis method for H.I.V. infection of CD4+T-cells. The homotopy analysis method accepts the solution as an infinite series with auxiliary parameters. All calculations are investigated in six terms in this method. Ongun [12] implement the Laplace Adomain Decomposition Method to get numerical results for H.I.V. infection of CD4+T-cells. To obtain approximate solutions to the H.I.V. infection of the CD4+ T cells model, Merdan [13] applied the variational iteration method. Yüzbaşı [14] developed a Bessel collocation method for finding numerical solutions of this model. Beler [15] analyzed to find approximate solutions of the proposed model by using Laguerre wavelets. In addition, we have access to more numerical papers to obtain such a class of nonlinear ordinary differential equation systems [16-29].

In this study, we have obtained the approximate solutions of the mathematical model (1) by developing the Chebyshev operational matrix method (COMM). Chebyshev polynomial is the cornerstone of numerical analysis. Those polynomials adapted almost all numerical methods. For example, in [30-32], Chebyshev polynomials combined the operational matrix method to solve the linear Fredholm-Volterra integro-differential [33], Lane-Emden equations [34-35], for fractional differential equations involving non-singular Mittag-Leffler kernel [36], fractional differential equations [37], mixed Volterra-Fredholm delay integro differential equations [38].

## 2. Materials and Methods

### 2.1. Shifted Chebyshev polynomials of the first kind

Chebyshev polynomials mainly admit to the approximation of continuous functions. Chebyshev polynomials have crucial properties to perform nearly all numerical methods [26]. We have four kinds of Chebyshev polynomials, which are defined in interval  $[-1,1]$ . If we choose the interval  $[0,1]$ , they called shifted Chebyshev polynomials [30]. While readers can find the definition of Chebyshev polynomials in many books [30-32], we want to take the recurrence relation

$$T_n^*(t) = 2(2t - 1)T_{n-1}^*(t) - T_{n-2}^*(t)$$

with the following initial conditions

$$T_0^*(t) = 1, T_1^*(t) = 2t - 1$$

Those polynomials have the following property [30-32]

$$t^n = 2^{-2n+1} \sum_{k=0}^n \binom{2n}{k} T_{n-k}^*(t), \quad 0 \leq t \leq 1 \tag{3}$$

and the orthogonality condition is

$$\langle T_j^*(t), T_k^*(t) \rangle_w = \int_0^1 T_j^*(t) T_k^*(t) w(t) dt = \begin{cases} \pi, & j = k = 0, \\ \pi/2, & j = k \neq 0, \\ 0, & j \neq k, \end{cases}$$

where  $w(t) = (t - t^2)^{-1/2}$ .  $\{T_0^*(t), T_1^*(t), T_2^*(t), \dots, T_n^*(t)\}$  is an orthogonal basis of  $n$ -dimensional polynomial space  $P_n$ , for  $j \neq k$ ,  $\langle T_j^*(t), T_k^*(t) \rangle_w = 0$ , for  $j = k$ ,  $\langle T_j^*(t), T_k^*(t) \rangle_w > 0$ . In addition, if  $p_k \in P_k$ , for  $k < n$ , then  $\langle p_k(t), T_n^*(t) \rangle_w = 0$  for all  $n > k$  [30-32].

Any given function  $y(t) \in L^2[0,1]$  can be approximated as a sum of shifted Chebyshev polynomials in the following way [30-32]:

$$y(t) = \sum_{n=0}^{\infty} a_n T_n^*(t)$$

where

$$a_n = \langle y(t), T_n^*(t) \rangle_w = \int_0^1 y(t) T_n^*(t) w(t) dt, \quad n = 0, 1, \dots$$

Our study aims to achieve the approximate solution of Eq. (1) as a truncated shifted Chebyshev series defined by:

$$y_N^j(t) = \sum_{r=0}^N a_r^j T_r^*(t) \tag{4}$$

where is used to denote the first kind of Chebyshev polynomials,  $a_r^j$  are referred to as unknown Chebyshev coefficients, and are chosen to be any positive integer.

### 3. Relations and Methods

#### 3.1. Matrix relations

In this part, we shall obtain the matrix-vector form of Eq. (1). For this purpose, let us consider the truncated Chebyshev polynomials  $T_N(t)$ ,  $I_N(t)$  and  $V_N(t)$  are the numerical solutions of the Eq. (1) and so those solutions can be written like this:

$$T_N(t) = \sum_{r=0}^N a_r T_r^*(t) \tag{5}$$

$$I_N(t) = \sum_{r=0}^N b_r T_r^*(t) \tag{6}$$

$$V_N(t) = \sum_{r=0}^N c_r T_r^*(t) \tag{7}$$

The matrix-vector shape of the numerical solution polynomials can be written as:

$$T_N(t) = \mathbf{T}^*(t)\mathbf{A} \tag{8}$$

$$I_N(t) = \mathbf{T}^*(t)\mathbf{B} \tag{9}$$

$$V_N(t) = \mathbf{T}^*(t)\mathbf{C} \tag{10}$$

where

$$\mathbf{T}^*(t) = [T_0^*(t) \ T_1^*(t) \ \dots \ T_N^*(t)]$$

$$\mathbf{A} = \left[\frac{1}{2} a_0 \ a_1 \dots a_N\right]^T \quad \mathbf{B} = \left[\frac{1}{2} b_0 \ b_1 \dots b_N\right]^T \quad \mathbf{C} = \left[\frac{1}{2} c_0 \ c_1 \dots c_N\right]^T$$

and where the dimension of  $\mathbf{A}$ ,  $\mathbf{B}$ ,  $\mathbf{C}$  matrices are  $(N + 1) \times 1$ , dimension of the  $\mathbf{T}^*(t)$  matrix is  $1 \times (1 + N)$ .

The property Eq. (3) permits us to write the below essential relation

$$(\mathbf{X}(t))^T = \mathbf{D}(\mathbf{T}^*(t))^T \quad \text{and} \quad \mathbf{X}(t) = \mathbf{T}^*(t)\mathbf{D}^T \tag{11}$$

where

$$\mathbf{X}(t) = [1 \ t \ \dots \ t^N],$$

it is a lower triangle matrix, for  $i, j = 0, 1, 2, \dots, N$

$$\mathbf{D} = [d_{ij}]$$

where

$$d_{ij} = \begin{cases} 2^{-2(i-j)} \binom{2((i-1))}{i-j}, & j \leq i \\ 0, & j > i \end{cases}$$

Moreover,  $\mathbf{D}$  is an invertible square matrix with  $(N + 1) \times (N + 1)$  dimensional and the dimension of  $\mathbf{X}(t)$  is  $1 \times (N + 1)$ .

From Eq. (11), we obtain the following matrix relation

$$\mathbf{T}^*(t) = \mathbf{X}(t)(\mathbf{D}^{-1})^T \tag{12}$$

and

$$(\mathbf{T}^*(t))^{(1)} = \mathbf{X}^{(1)}(t)(\mathbf{D}^{-1})^T$$

So, the basic matrix-vector forms of the differential of approximate solutions of Eq. (1) are

$$T_N^{(1)}(t) = \mathbf{X}(t)\mathbf{Y}(\mathbf{D}^T)^{-1} \mathbf{A} \tag{13}$$

$$I_N^{(1)}(t) = \mathbf{X}(t)\mathbf{Y}(\mathbf{D}^T)^{-1} \mathbf{B} \tag{14}$$

$$V_N^{(1)}(t) = \mathbf{X}(t)\mathbf{Y}(\mathbf{D}^T)^{-1} \mathbf{C} \tag{15}$$

where

$$\mathbf{X}^{(1)}(t) = \mathbf{X}(t)\mathbf{Y} \tag{16}$$

and for  $i, j = 0, 1, 2, \dots, N$ ,

$$\mathbf{Y} = [y_{ij}] = \begin{cases} i+1, & j = i+1 \\ 0, & otherwise \end{cases}$$

For example,  $N = 3$ , it can be written as

$$\mathbf{Y} = \begin{bmatrix} 0 & 1 & 0 & 0 \\ 0 & 0 & 2 & 0 \\ 0 & 0 & 0 & 3 \\ 0 & 0 & 0 & 0 \end{bmatrix}$$

### 3.2. Solution method

The numerical scheme is constructed to find the unknown coefficients in Eqs. (5-7) to obtain the numerical result of Eq. (1). To constitute the numerical scheme, firstly, Eq. (1) and initial conditions are turned into a matrix-vector form with shifted Chebyshev series. Using the matrix relations in Section 3, Eq. (1) can be written in matrix form:

$$\begin{aligned} &\mathbf{X}(t)\mathbf{Y}(\mathbf{D}^T)^{-1} \mathbf{A} + [\alpha - r]\mathbf{X}(t)(\mathbf{D}^T)^{-1} \mathbf{A} + \frac{r}{T_{\max}}(\mathbf{X}(t)(\mathbf{D}^T)^{-1} \mathbf{A})[\mathbf{X}(t)(\mathbf{D}^T)^{-1} \mathbf{A} + \mathbf{X}(t)(\mathbf{D}^T)^{-1} \mathbf{B}] \\ &+ k(\mathbf{X}(t)(\mathbf{D}^T)^{-1} \mathbf{C})(\mathbf{X}(t)(\mathbf{D}^T)^{-1} \mathbf{A}) = q \\ &\mathbf{X}(t)\mathbf{Y}(\mathbf{D}^T)^{-1} \mathbf{B} - k(\mathbf{X}(t)(\mathbf{D}^T)^{-1} \mathbf{C})(\mathbf{X}(t)(\mathbf{D}^T)^{-1} \mathbf{A}) + \beta\mathbf{X}(t)(\mathbf{D}^T)^{-1} \mathbf{B} = 0 \\ &\mathbf{X}(t)\mathbf{Y}(\mathbf{D}^T)^{-1} \mathbf{C} - \mu\beta\mathbf{X}(t)(\mathbf{D}^T)^{-1} \mathbf{B} + \gamma\mathbf{X}(t)(\mathbf{D}^T)^{-1} \mathbf{C} = 0 \end{aligned} \tag{17}$$

The residuals  $R_i(t)$  for  $i = 1,2,3$  form can be written as

$$R_1(t) \approx \mathbf{X}(t)\mathbf{Y}(\mathbf{D}^T)^{-1}\mathbf{A} + [\alpha - r]\mathbf{X}(t)(\mathbf{D}^T)^{-1}\mathbf{A} + \frac{r}{T_{\max}}(\mathbf{X}(t)(\mathbf{D}^T)^{-1}\mathbf{A})[\mathbf{X}(t)(\mathbf{D}^T)^{-1}\mathbf{A} + \mathbf{X}(t)(\mathbf{D}^T)^{-1}\mathbf{B}] + k(\mathbf{X}(t)(\mathbf{D}^T)^{-1}\mathbf{C})(\mathbf{X}(t)(\mathbf{D}^T)^{-1}\mathbf{A}) - q \quad (18)$$

$$R_2(t) \approx \mathbf{X}(t)\mathbf{Y}(\mathbf{D}^T)^{-1}\mathbf{B} - k(\mathbf{X}(t)(\mathbf{D}^T)^{-1}\mathbf{C})(\mathbf{X}(t)(\mathbf{D}^T)^{-1}\mathbf{A}) + \beta\mathbf{X}(t)(\mathbf{D}^T)^{-1}\mathbf{B} \quad (19)$$

$$R_3(t) \approx \mathbf{X}(t)\mathbf{Y}(\mathbf{D}^T)^{-1}\mathbf{C} - \mu\beta\mathbf{X}(t)(\mathbf{D}^T)^{-1}\mathbf{B} + \gamma\mathbf{X}(t)(\mathbf{D}^T)^{-1}\mathbf{C} \quad (20)$$

$3 \times N$  -times nonlinear systems of the equation are obtained by applying the operational matrix method in the following form, for  $i = 1,2,3$

$$\langle R_i(t), T_n^*(t) \rangle = \int_0^1 R_i(t)T_n^*(t)dt = 0, \quad n = 0,1,\dots,N-1 \quad (21)$$

The initial conditions Eq. (2) give us three equations:

$$\begin{aligned} [T(0)] &= \mathbf{X}(0)(\mathbf{D}^T)^{-1}\mathbf{A} = [r_1] \\ [I(0)] &= \mathbf{X}(0)(\mathbf{D}^T)^{-1}\mathbf{B} = [r_2] \\ [V(0)] &= \mathbf{X}(0)(\mathbf{D}^T)^{-1}\mathbf{C} = [r_3] \end{aligned} \quad (22)$$

As a result, we get the  $3 \times (N + 1)$  sets of nonlinear equation systems with  $3 \times (N + 1)$  unknowns by Eqs. (21-22). Then, finally, those systems are puzzled out by the mathematical program Maple 13, and Eqs. (5-7) coefficients are achieved.

#### 4. Numerical Results

In this part, we applied this proposed method (PM) to the given numerical data for the proposed method  $N=7$ . Numerical solutions are obtained by the proposed method; other numerical methods are given in Table 1 for the uninfected population  $T$ , Table 2 for infected CD+4 T-cell concentration  $I$ , and Table 3 for the concentration of free H.I.V. virus  $V$ . All tables show that PM agrees well with the solutions of other numerical results. Figures 1-2 show the uninfected population  $T$ , infected CD+4 T-cell concentration  $I$ , and concentration of free H.I.V. virus  $V$  versus time. As time increases, the uninfected population  $T$  increases, the infected CD+4 T-cells concentration  $I$  increases, and the concentration of free H.I.V. virus

decreases. The amount of infected CD+4 T-cells concentration  $I$  is slower to increase than the uninfected population  $T$ , and H.I.V. infection disease may end at any  $t$  time. In Figures 3-5, we compare the numerical results by obtained Adomian Decomposition Method, Pade approximation, Inverse Laplace transformation method, and present method. All results nearly resemble each other.

**Table 1:** Numerical results for  $T$  PM and other numerical methods.

t	The method in [13]	The method in [11]	The method in [12]	The method in [17]	PM N=5	PM N=7
0.0	0.1	0.1	0.1	0.1	0.1	0.1
0.2	0.2038616561	0.2088072731	0.2088073214	0.2088080849	0.208458510	0.2088072279
0.4	0.3803309335	0.4061052652	0.4061346587	0.4062405440	0.406339373	0.4062410095
0.6	0.6954623767	0.7611467713	0.7624530350	0.7644239007	0.764734581	0.7644229384
0.8	1.2759624442	1.3773198590	1.3978805880	1.4140468559	1.413686781	1.4140470895
1.0	2.382277428	2.3291697610	2.5067466690	2.5915948594	2.591645820	2.5915948594

**Table 2:** Numerical results for  $I$  PM and other numerical methods.

t	The method in [13]	The method in [11]	The method in [12]	The method in [17]	PM N=5	PM N=7
0.0	0.0	0.0	0.0	0.0	0.0	0.0
0.2	0.624787210E-5	0.60327072E-5	0.603263436E-5	0.603270226E-5	0.6034893E-5	0.63517134E-5
0.4	0.129355222E-4	0.13159114E-4	0.131487854E-4	0.131583409E-4	0.1315659E-4	0.12751088E-4
0.6	0.203526718E-4	0.21268368E-4	0.210141719E-4	0.212237855E-4	0.2122560E-4	0.21636848E-4
0.8	0.283730212E-4	0.30069186E-4	0.279513045E-4	0.301778550E-4	0.3017857E-4	0.29847613E-4
1.0	0.369084236E-4	0.39873654E-4	0.243156231E-4	0.400378145E-4	0.4003936E-4	0.37812697E-4

**Table 3:** Numerical results for  $V$  PM and other numerical methods.

t	The method in [13]	The method in [11]	The method in [12]	The method in [17]	PM N=5	PM N=7
0.0	0.1	0.1	0.1	0.1	0.1	0.1
0.2	0.06187991856	0.06187996025	0.06187995314	0.06187984322	0.061874446	0.0618798985
0.4	0.03829493490	0.03831324883	0.03830820126	0.03829488777	0.038298806	0.0382948388
0.6	0.02370431860	0.02439174349	0.02392029257	0.02370455004	0.023706103	0.0237045399
0.8	0.01467956982	0.00996721893	0.01621704553	0.01468036368	0.014675339	0.0148040545
1.0	0.02370431861	0.00033050764	0.01608418711	0.00910084499	0.009100830	0.0091000845

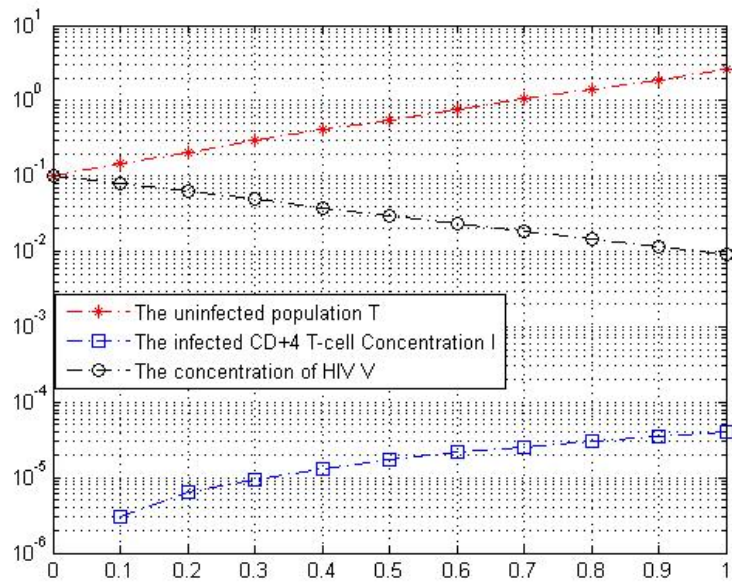


**Figure 1:** Comparison of the numerical results for  $N=5$ .

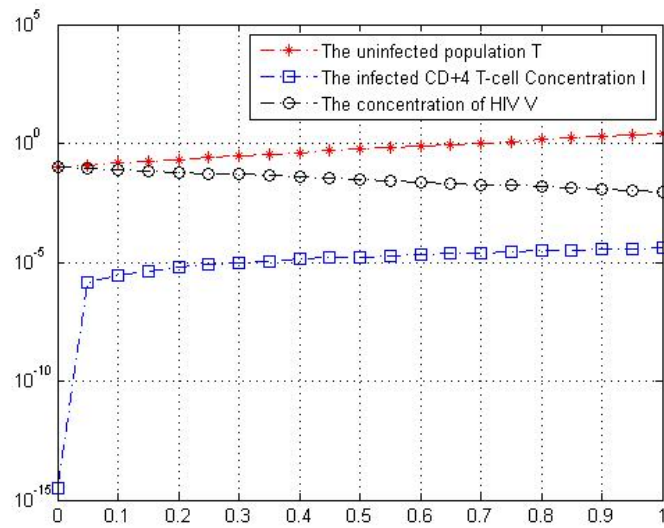


**Figure 2:** Comparison of the numerical results for  $N=7$ .

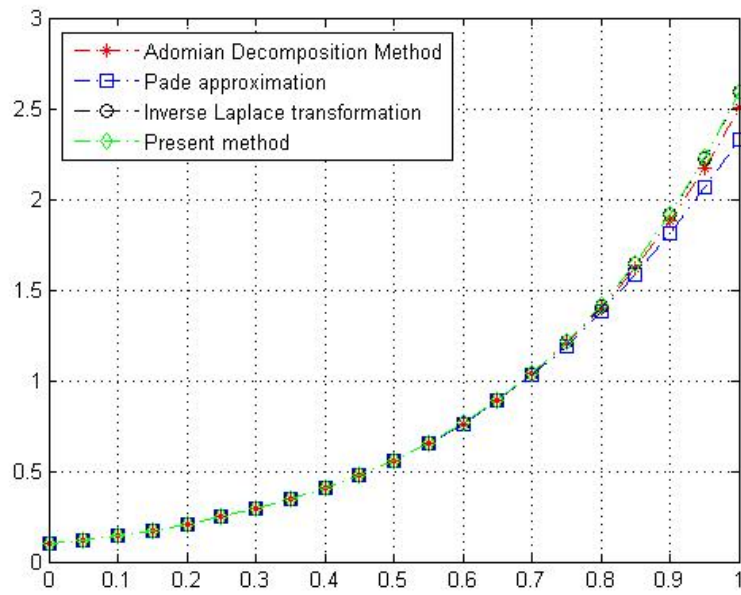


**Figure 3:** Comparison of numerical method solution of  $T$

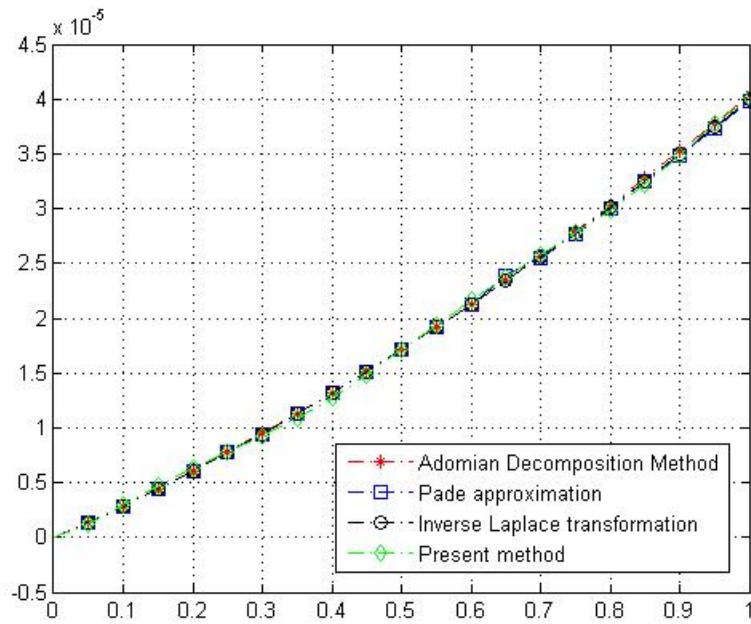


**Figure 4:** Comparison of numerical method solution of  $I$

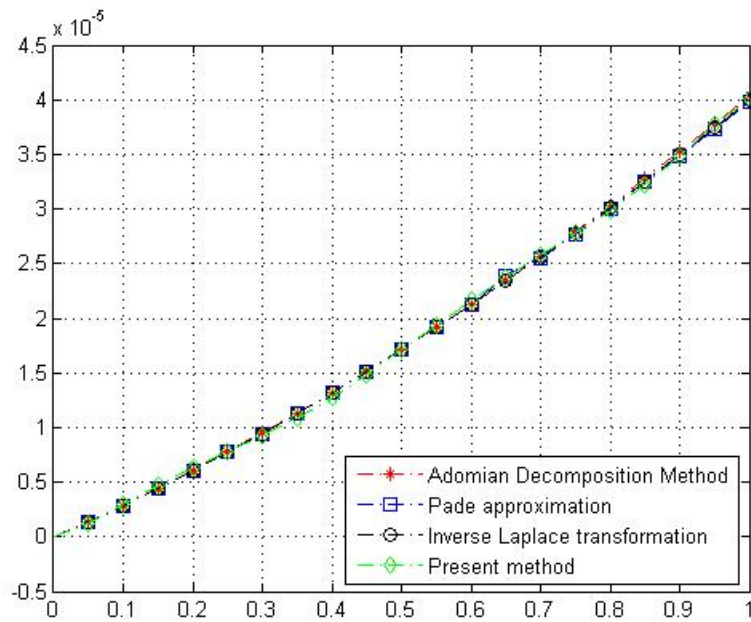


**Figure 5:** Comparison of numerical method solution of  $V$

### 5. Conclusion

This paper uses the Chebyshev operational matrix method to solve the mathematical model of HIV infection of CD4+ T-cells. The uninfected population  $T$  infected CD+4 T-cell concentration  $I$ , and free H.I.V. virus values concentration are compared with other methods in Table 1, Table 2, and Table 3, respectively. Also, with figures, the efficiency and accuracy of the method are demonstrated. The proposed method has a lower operation, so cumulative errors are minor. Moreover, the solution code of the method is easily written in Maple. The results show that the present method is accurate compared to Bessel collocation, the Adomian decomposition, the Pade approximation, and the inverse Laplace transformation with five and seven terms.

### Acknowledgments

Muğla Sıtkı Kocman University Research Projects Coordination Office has granted this paper. Project Grant Number 22/139/05/1 and title “Extending the Operational Matrix Method to Nonlinear System Models.”

### References

[1] Perelson, A.S., *Modelling the interaction of the immune system with H.I.V.*, in: C. Castillo-Chavez (Ed.), *Mathematical and Statistical Approaches to AIDS Epidemiology*, Springer, Berlin, 1989.

- [2] Perelson, A.S., Kirschner, D.E., De Boer, R., *Dynamics of H.I.V. infection of CD4+ T-cells*, *Mathematical Biosciences*, 114: 81, 1983.
- [3] Zapata, H.D., Salazar C.A., Mayorga, E.M., *Mathematical model describing HIV infection with time-delayed CD4 T-cell activation*, *Processes*, 8(7), 782, 2020.
- [4] Arafa, A.A.M., Rida, S.Z., Khalil, M., *Fractional modeling dynamics of H.I.V. and CD4+ T-cells during primary infection*, *Nonlinear Biomed. Phys.*, 6(1), 1–7, 2012.
- [5] Huo, H.F., Chen, R., Wang, X.Y., *Modelling and stability of HIV/AIDS epidemic model with treatment*, *Appl. Mathe. Model.* 40(13–14), 6550–6559, 2016.
- [6] Wang, L., Li, M.Y., *Mathematical analysis of the global dynamics of a model for H.I.V. infection of CD4+ T cells*, *Math. Biosci.*, 200(1), 44–57, 2006.
- [7] Iba-Pérez, J., Macías-Díaz, J.E., *A finite-difference discretization preserving the structure of solutions of a diffusive model of type-1 human immunodeficiency virüs*, *Advances in Difference Equations*, (1):1–19, 2021.
- [8] Crandall, K.A., *The Evolution of H.I.V.*, Johns Hopkins University Press, Baltimore, Maryland, 1999.
- [9] Culshaw, R.V., Ruan, S., *A delay-differential equation model of H.I.V. infection of CD4+ T-cells*, *Mathematical Biosciences*, 165, 27–39, 2000.
- [10] Wang, X., Song, X., *Global stability and periodic solution of a model for H.I.V. infection of CD4+ T-cells*, *Appl. Math. Model.*, 189, 1331–1340, 2007.
- [11] Ghoreishi, M., Ismail, A.I., Alomari, A.K., *Application of the homotopy analysis method for solving a model for H.I.V. infection of CD4(+) T-cells*, *Math. Comp. Model.*, 54, 3007–3015, 2011.
- [12] Ongun, M.Y., *The Laplace adomian decomposition method for solving a model for H.I.V. infection of CD4+T cells*, *Math. Comput. Model.*, 53(6), 597–603, 2011.
- [13] Merdan, M., Gökdoğan, A., Yıldırım, A., *On the numerical solution of the model for H.I.V. infection of CD4+ T cells*, *Comput. Math. Appl.* 62(1), 118-123, 2011.
- [14] Yüzbaşı, Ş., *A numerical approach to solve the model for H.I.V. Infection of CD4+T cells*, *Appl. Math. Model.*, 36(12), 2576-5890, 2012.
- [15] Beler, A., Şimşek, G.Ö., Gümgüm, S., *Numerical solutions of the HIV infection model of CD4+ cells by Laguerre wavelets*, *Math. Comp. Simulat.*, 209, 205-219, 2023.
- [16] Mehregan, F.S., Assari, P., Dehghan, M., *On the approximate solution of dynamic systems derived from the HIV infection of CD4+ T-cells using the LRBF-collocation scheme*, *Engin. Anal. Bound. Elem.*, 153, 39-50, 2023.
- [17] Parand, K., Kalantari, Z., Delkhosh, D., *Quasilinearization-Lagrangian method to solve the H.I.V. infection model of CD4+ T cells*, *SeMA J.*, 75(2), 271-283, 2007.

- [18] Guerrero–Sánchez, Y., Umar, M., Sabir, Z., Juan, L.G., Raja, M.A.Z., *Solving a class of biological HIV infection model of latently infected cells using heuristic approach*, *Discrete and Continuous Dynamical Systems - S*, 14(10), 3611-3628, 2021.
- [19] Yüzbaşı, Ş., Ismailov, N., *A numerical method for the solutions of the H.I.V. infection model of CD4+ T-cells*, *Int. J. Biomath.* 10(7), 1750098, 2017.
- [20] Khan, H., Shah, R., Arif, M., Bushnaq, S., *The Chebyshev wavelet method for the numerical solution of fractional H.I.V. infection of CD4+T cells model*, *Int. J. Appl. Comput. Math.*, 6, 34, 2020.
- [21] Merdan, M., *Homotopy perturbation method for solving a model for hiv infection of CD4+ T-cells*, *Istanbul Commerce University Journal of Science*, 12, 39–52, 2007.
- [22] Ali, N., Ahmad, S., Aziz, S., Zaman, G., *The Adomian decomposition method for solving HIV infection model of latently infected cells*, *Matrix Science Mathematic*, 3, 5-8, 2019.
- [23] N. Doğan, *Numerical treatment of the model for H.I.V. infection of CD4+T-cells by using multistep Laplace Adomian decomposition method*, *Discrete Dyna. Mature Soci.*, 976352, 2012.
- [24] Khalid, M., Sultana, M., Zaidi, F., Khan, F.S., *A numerical solution of a model for H.I.V. infection CD4+ T-cell*, *Inter. J. Inno. Scie. Rese.*, 16(1), 79-85, 2015.
- [25] Gandomani, M.R., Kajani, M.T., *Numerical solution of a fractional order model of H.I.V. infection of CD4+T cells using Müntz-Legendre polynomials*, *Int. J. Bioa.*, 20(2), 193-204 2016.
- [26] Ullah, R., Ellahi, R., Said M.S., Din, S.T., *On the fractional-order model of HIV infection of CD4+ T\*cells under the influence of antiviral drug treatment*, *Journal of Taibah University for Science*, 1, 50-59, 2020.
- [27] Deniz, S., *Semi-analytical approach for solving a model for HIV infection of CD4+ T-cells*, *TWMS J. Appl. And Eng. Math.* 1,273-281, 2021.
- [28] Kumbinarasaiah, S., Manohara, G., *Modified Bernoulli wavelets functional matrix approach for the HIV infection of CD4+ cells model*, *Results in Control Optim.*, 10, 100197, 2023.
- [29] Attaullah, A., Muhammad, S., *Mathematical modeling and numerical simulation of HIV infection model*, *Results in Control Optim.*, 7, 100118, 2022.
- [30] Mason, J.C., Handscomb, D.C., *Chebyshev polynomials*, Chapman and Hall/C.R.C., New York, 2003.
- [31] Body, J.P., *Chebyshev and fourier spectral methods*, University of Michigan, New York, 2000.
- [32] Epperson, J.F., *An Introduction to numerical methods and analysis*, Second Edition, Jhon Wiley & Sons, New Jersey, 2013.

[33] Öztürk, Y., Gülsu, M., *An operational matrix method to solve linear Fredholm-Volterra integro-differential equations with piecewise intervals*, *Math. Scie.* 15, 189-197, 2021.

[34] Öztürk, Y., Gülsu, M., *An operational matrix method for solving Lane-Emden equations arising in astrophysics*, *Mathematical Methods in Applied Sciences* 37, 2227-2235, 2014.

[35] Öztürk, Y., *An efficient numerical algorithm for solving system of Lane-Emden type equations arising in engineering*, *Nonlinear Engineering* 8, 429-439, 2019.

[36] Baleanu, D., Shiri, B., Srivasta H.M., Qurashi, *A Chebyshev spectral method based on operational matrix for fractional differential equations involving non-singular Mittag-Leffler kernel*, *Advances in Difference Equations*, 353, 2017.

[37] Doha, E. H., Bhrawy, A. H., Ezz-Eldien, S. S., *A Chebyshev spectral method based on operational matrix for initial and boundary value problems of fractional order*, *Computers & Mathematics with Applications*, 62(5), 2364–2373, 2011.

[38] Raslan, K.R., Ali, K.K., Mohammed, E.M., Younis, J.A., Elsalam, M.A., *An operational matrix technique based on Chebyshev polynomials for solving mixed Volterra-Fredholm delay integro differential equations of variable-order*, *Advan. Frac. Func. Anal.*, 6203440, 2023.



## Structural, Magnetic and Catalytic Properties of FeCo Nanoparticles Synthesized by Polyol Process

Emre Can TAYFUN<sup>1</sup>, Kaan ERMAN<sup>2</sup>, Dogan KAYA<sup>3,4,\*</sup>, Faruk KARADAG<sup>5</sup>, Ahmet EKICIBIL<sup>6</sup>

<sup>1</sup>*Cukurova University, Faculty of Art and Sciences, Department of Physics, Adana, Türkiye*  
*emrecontayfun@gmail.com, ORCID: 0009-0007-9343-7349*

<sup>2</sup>*Imperial College London, Faculty of Natural Sciences, Department of Physics, London, United Kingdom*  
*kaanerman11@gmail.com, ORCID: 0009-0004-7541-8820*

<sup>3</sup>*Cukurova University, Faculty of Art and Sciences, Department of Physics, Adana, Türkiye*

<sup>4</sup>*Cukurova University, Graduate School of Sciences, Department of Advance Materials and  
Nanotechnology, Adana, Türkiye*  
*dogankaya@cu.edu.tr, ORCID: 0000-0002-6313-7501*

<sup>5</sup>*Cukurova University, Faculty of Art and Sciences, Department of Physics, Adana, Türkiye*  
*fkaradag@cu.edu.tr, ORCID: 0000-0001-7862-9085*

<sup>6</sup>*Cukurova University, Faculty of Art and Sciences, Department of Physics, Adana, Türkiye*  
*ahmetcan@cu.edu.tr, ORCID: 0000-0003-3071-0444*

**Received:** 07.08.2023

**Accepted:** 31.10.2023

**Published:** 31.12.2023

### Abstract

Multi-functional FeCo nanoparticles (NPs) exhibit unique structural, magnetic, and catalytic properties, making them versatile materials with potential applications in diverse fields. In this work, we investigated the structural, electrochemical, and magnetic properties of as-prepared FeCo NPs synthesis by polyol method. X-ray diffraction analysis revealed multiphase structures: FeCo and  $\alpha$ -Fe<sub>2</sub>O<sub>3</sub> phases and scanning electron microscopy images confirmed spherical-like structures of FeCo NPs with an average size of  $12.4 \pm 0.1$  nm. The electrochemical properties of FeCo NPs were investigated using a three-electrode setup in a 1 M KOH electrolyte at room temperature. The onset potentials for FeCo catalysts were found to be -0.15 V for ORR,



0.25 V for OER, and -1.26 V for HER. Tafel measurements further elucidated the reaction mechanism, revealing corrosion potentials of -0.165 V for ORR and 0.215 V for OER, with Tafel slopes of 228 mV dec<sup>-1</sup> and 48 mV dec<sup>-1</sup>, respectively. A significant increase in magnetization was observed below 25 K in both zero-field-cooled and field-cooled curves, a magnetic transition temperature,  $T_s$ , occurs at 15 K, possibly indicating a ferromagnetic-to-antiferromagnetic phase transition. The hysteresis loop measurements revealed coercive field values ranging from 968 Oe at 5 K to approximately 206 Oe at 320 K, indicating a relaxation in magnetic spin orientation with increasing temperature. The saturation magnetization ( $M_s$ ) values were recorded as 15.2 emu/g under a 5 T magnetic field, and the remanent magnetization ( $M_r$ ) showed dominant ferromagnetic properties at 5 K with an  $M_r/M_s$  ratio indicating soft magnetic behavior. The magnetic susceptibility of FeCo NP exhibited a peak at approximately 25 K, and the Curie-Weiss law provided an estimated  $\theta$  angle of -9.58°, suggesting antiferromagnetic interactions.

**Keywords:** FeCo NPs; Polyol; Structural; Magnetic; Catalytic.

### **Poliol Yöntemi ile Sentezlenen FeCo Nanopartiküllerinin Yapısal, Manyetik ve Katalitik Özellikleri**

#### **Öz**

Çok işlevli FeCo nanoparçacıkları (NP'ler), manyetik, katalitik ve yapısal özelliklerin bir kombinasyonunu sergileyerek, çeşitli alanlarda potansiyel uygulamalara sahip çok yönlü malzemelerdir. Bu çalışmada, polioli yöntemi ile sentezlenen FeCo NP'lerin yapısal, elektrokimyasal ve manyetik özelliklerini araştırdık. X-ışını kırınım analizi, FeCo ve  $\alpha$ -Fe<sub>2</sub>O<sub>3</sub> fazlarını gösteren çoklu yapılar ortaya çıkardı ve taramalı elektron mikroskobu görüntüleri, ortalama boyutu  $12.4 \pm 0.1$  nm olan küresel yapıları doğruladı. FeCo NP'lerin elektrokimyasal özellikleri, oda sıcaklığında 1 M KOH elektroliti içinde üç elektrot düzeneği kullanılarak incelendi. FeCo katalizörleri için başlangıç potansiyelleri, ORR (Oksijen indirgeme reaksiyonu) için -0.15 V, OER (Oksijen oluşum reaksiyonu) için 0.25 V ve HER (Hidrojen oluşum reaksiyonu) için -1.26 V olarak bulundu. Tafel ölçümleri, ORR için -0.165 V ve OER için 0.215 V'lik korozyon potansiyellerini ve sırasıyla 228 mV dec<sup>-1</sup> ve 48 mV dec<sup>-1</sup>'lik Tafel eğimlerini ortaya çıkardı. Hem manyetik alanla soğutulmuş hem de manyetik alansız soğutulmuş eğrilerde 25 K'nin altında belirgin bir manyetizasyon artışı gözlemlendi ve 15 K'de bir manyetik bir geçiş sıcaklığı,  $T_s$ , gözlemlendi, bu da ferromanyetikten antiferromanyetik bir faz geçişini gösterebilir. Histeresis döngüsü ölçümleri, 5 K'de 968 Oe'den 320 K'de yaklaşık 206 Oe'ye kadar olan koersiv alan değerleri göstererek manyetik spin yönelmesinde bir gevşeme olduğunu gösterdi. 5 T manyetik alan altında doyum mıknatıslanması ( $M_s$ ) değerleri 15.2 emu/g olarak kaydedildi ve 5

K'de kalıcı mıknatıslanma ( $M_r$ ), domine ferromanyetik özellikleri gösterirken  $M_r/M_s$  oranı yumuşak manyetik davranışı gösterdi. Manyetik duyarlılık analizi, yaklaşık 25 K'de bir pik gösterdi ve Curie-Weiss yasası  $-9.58^\circ\text{K}$ 'lik tahmini bir  $\theta$  açısı sağlayarak antiferromanyetik etkileşimleri düşündürdü.

**Anahtar Kelimeler:** FeCo nanoparçacıklar; Poliöl; Yapısal; Manyetik; Katalitik.

## 1. Introduction

The development of advanced materials with tailored properties has become a key focus in scientific research, driven by the need for efficient and sustainable solutions to address contemporary challenges [1, 2]. In recent years, the synthesis and characterization of magnetic NPs have garnered significant attention due to their potential applications in various fields, including catalysis, biomedicine, and information storage [3, 4]. Iron-cobalt (FeCo) alloys have attracted significant attention due to their exceptional combination of magnetic and catalytic properties, rendering them promising candidates for a broad range of applications, including data storage, sensors, energy conversion, and catalysis [5-7]. FeCo NPs usually form an Fe-rich metallic core and a Co-rich surface layer composition [8] and this phenomenon can be attributed to the difference in the reduction potentials of Fe and Co [9]. FeCo NPs mostly used for oxygen evolution reaction (OER) and oxygen reduction reaction (ORR) activities. In a recent work by Park et al. [10] revealed that the overpotential for  $\text{Fe}_{59}\text{Co}_{41}$  was significantly lower, measuring 285 mV at 10 mA  $\text{cm}^{-2}$  in a 1 M KOH solution, compared to the other samples. Furthermore, following chronopotentiometry at 10 mA  $\text{cm}^{-2}$  for 24 hours in 1 M KOH, the overpotential at 10 mA  $\text{cm}^{-2}$  increased slightly from 285 to 294 mV. The improved catalyst properties were attributed not only to the synergistic effect of the metal core and oxide layer but also to the beneficial influence of optimal iron doping.

Notably, there have been recent research efforts focused on studying FeCo soft magnetic nanomaterials [11, 12], which hold promise for diverse applications due to their exceptional magnetic characteristics, such as high saturation magnetization, large permeability, low coercivity, and ferromagnetic behavior up to 1073 K [13]. To fully exploit the potential of FeCo alloys, various synthesis methods have been explored, and the polyol process has emerged as a versatile and effective technique for the fabrication of FeCo NPs. The polyol process is a solution-based method that utilizes polyols, such as ethylene glycol, the solvent and reducing agent [14]. This approach offers several advantages, including precise control over the size, shape, and composition of nanoparticles, as well as a high degree of scalability. Moreover, the polyol process allows for the incorporation of stabilizers and dopants, further enhancing the properties and

functionalities of the resulting FeCo NPs [11]. In the literature, there are some studies reported for FeCo nanomaterials. For instance, FeCo prepared surfactant-assisted ball milling method with a size of 23 nm and saturation magnetization was recorded as  $209 \text{ Am}^2 \cdot \text{kg}^{-1}$  (emu/g) [15]. Similarly, FeCo NPs synthesised using the polyol method and ethylene glycol (EG) as the solvent with a size of 30 nm and a saturation magnetization were recorded  $200 \text{ Am}^2 \cdot \text{kg}^{-1}$  [11]. In other similar work, when the particle size is about 8  $\mu\text{m}$ , the saturation magnetization was found to be  $220 \text{ Am}^2 \cdot \text{kg}^{-1}$  [16].

In this paper, we aim to provide the structural, magnetic, and catalytic properties of FeCo NP prepared using the polyol process. Structural analysis provided multiphase structure FeCo formation with narrow particle size distribution. With this structural formation, FeCo catalyst exhibited promising results for ORR and OER activities. Moreover, a detailed investigation of magnetic properties using *M-T* and *M-H* curves revealed a large coercive field and relatively low saturation magnetization.

## 2. Materials and Methods

### 2.1. Chemicals

Iron(III) acetylacetonate ( $\text{Fe}(\text{acac})_3$ ,  $\geq 97\%$ ), cobalt acetylacetonate ( $\text{Co}(\text{acac})_2$ ,  $\geq 99.0\%$ ) metal salts, polyvinylpyrrolidone (PVP, average mol wt. 40000) surfactant, N, N-dimethylformamide (DMF  $\geq 99.0\%$ ), ethylene glycol (EG  $\geq 99.0\%$ ), sodium hydroxide (NaOH  $\geq 99.0\%$ ), dichloromethane ( $\geq 99.0\%$ ), ethanol absolute ( $\geq 99.9\%$ ), and sodium borohydride ( $\text{NaBH}_4$   $\geq 98.0\%$ ) were purchased from Sigma Aldrich. All chemicals were used as received without further purification.

### 2.2. Synthesis of FeCo NPs

The synthesis process and chemicals used for FeCo NPs are presented in Figure 1. 1.7 mmol Fe and 1.7 mmol Co metal salts were dissolved in 25 ml of DMF. The resulting mixture was then poured into a three-necked round-bottom flask containing 60 ml EG (with an EG/FeCo mole ratio of 300), serving as a low-temperature reducing agent. The solution mixed with PVP to prevent agglomeration (with an EG/FeCo mole ratio of 4), and NaOH (with an EG/FeCo mole ratio of 15) to stabilize pH (orange like color). The reaction was carried out at 30 °C under a constant flow of Ar gas and vigorous magnetic stirring. Subsequently, the mixture temperature was raised to 130 °C, and the secondary reducing agent  $\text{NaBH}_4$  (with an EG/FeCo mole ratio of 24), previously dissolved in 25 ml DMF, was slowly added dropwise into the mixture over 5 minutes (brown-black color). The solution was then refluxed at 150 °C for 60 minutes, during

which the black color indicated the successful reduction of the FeCo NPs. Afterward, the solution was cooled down to room temperature, washed with ethanol to remove most of the by-products, and subjected to sanctification cycles at 9000 rpm. Finally, the resulting product was dried at 55 °C for 24 hours.

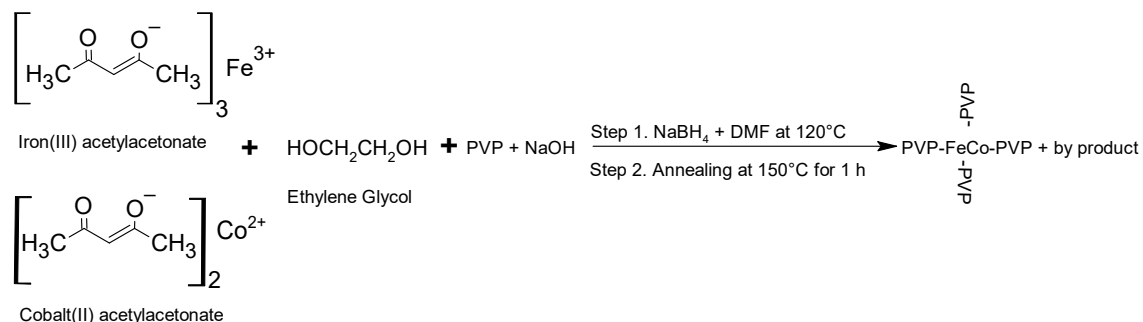


**Figure 1:** Chemical process of the synthesis of PVP decorated FeCo NPs

### 2.3. Characterizations of FeCo NPs

X-ray diffraction (XRD, using Cu- $K\alpha$  radiation ( $\lambda=1.54 \text{ \AA}$ )), was obtained for the structural analysis of the samples, and subsequently, Scanning electron microscopy (SEM) and energy-dispersive x-ray spectroscopy (EDS) data were collected to determine the morphology, the average size distribution and the chemical composition of FeCo NPs through stoichiometric calculations, respectively. The magnetic properties of FeCo NPs were investigated using a physical property measurement system with a vibrating sample magnetometer, as a function of temperature in a range of 5–380 K and applied field of  $\pm 5 \text{ T}$  at 5 K, 100 K, 300 K and 320 K.

### 2.4. Electrochemical measurements of FeCo NPs

The Gamry 1010E potentiostat was utilized for all electrochemical measurements. The system featured a conventional three-electrode setup, comprising a reference electrode with a 3 M KCl-saturated Ag/AgCl, a counter electrode with a  $6 \times 6 \text{ mm}^2$  platinum (99.95% pure) and a working electrode with a carbon rod of 5 mm diameter. To prepare the working electrode, 1 mg of FeCo NPs was mixed with  $7 \mu\text{l}$  EG,  $5 \mu\text{l}$  DMF, and  $2 \mu\text{l}$  of 5% Nafion. The mixture was sonicated for 15 minutes and then vortexed for 2 minutes. Following, this ink was dropped onto a carbon electrode and dried in a furnace for 16 hours. Cyclic voltammetry (CV) measurements were performed in a 1 M KOH alkaline solution with a scan rate of 5, 25, 50, 75, and  $100 \text{ mV s}^{-1}$  and a step size of 2 mV, within the potential range between -1.2 and 1.2 V vs. Ag/AgCl. Additionally, linear sweep

voltammetry (LSV) measurements were carried out to investigate the ORR, OER and hydrogen evolution reaction (HER) activities, with a fixed scan rate of 50 mV s<sup>-1</sup>.

### 3. Results and Discussion

#### 3.1. Characterization of FeCo NPs

The structural properties of the as-prepared FeCo NPs were determined using XRD. Figure 2(a) displays the experimental XRD data of FeCo NPs (black line), which was measured for  $2\theta$  ranging from 20° to 100° using Cu- $K\alpha$  radiation. The XRD analysis revealed a multiphase structure for the NPs, with peaks at  $2\theta=35.6^\circ$ ,  $59^\circ$  corresponding to the FeCo phase (CoFe<sub>2</sub>O<sub>4</sub>) [17] and a peak at  $2\theta=33.8^\circ$  assigned to the  $\alpha$ -Fe<sub>2</sub>O<sub>3</sub> phase [18]. This indicates that FeCo NPs were partially oxidized, forming the  $\alpha$ -Fe<sub>2</sub>O<sub>3</sub> phase in the structure [17]. In Figure 2(b), EDS data for FeCo NPs with elemental analysis for Fe, Co, O and C elements and their energy shells are illustrated [5]. The stoichiometry of Fe and Co elements was calculated by collecting EDS data from five different areas, as shown in the inset table of Figure 2(b) [19]. The counts of oxygen atoms were highest compared to Fe and Co due to oxide phases in the structure, as revealed by the XRD profile, and the C signal originated from the carbon tape sample holder. The stoichiometry analysis showed the K and L shells of Fe and Co, respectively. The entry ratio of Fe and Co precursors aimed for Fe<sub>0.50</sub>Co<sub>0.50</sub>, and the obtained stoichiometry was Fe<sub>0.49</sub>Co<sub>0.51</sub>, which was quite similar to the entry ratio [20]. Additional peaks observed at 1.04 keV and 2.121-9.67 keV belonged to sodium (Na) [21] and gold (Au) elements [22], respectively. These peaks originated from residue chemicals in the structure, where NaBH<sub>4</sub> was used as a secondary reducing agent, and NaOH served as a pH stabilizer to reduce the particle size. The presence of Au peaks was due to the Au-covered surface to improve SEM resolution before the imaging process. In Figure 2(c), SEM images of the FeCo NPs are presented. The average size distribution of FeCo NPs is shown in Figure 2(d), where approximately 250 particles were counted by analyzing several SEM images at a magnification of 600000X. The observed spherical-like structures in SEM images were due to the presence of PVP molecules. The size distribution of FeCo NPs ranged from 8 to 18 nm, as seen in Figure 2(d). To determine the average size of the NPs, a log-normal fit function was applied, yielding an average size of 12.4 ± 0.1 nm.

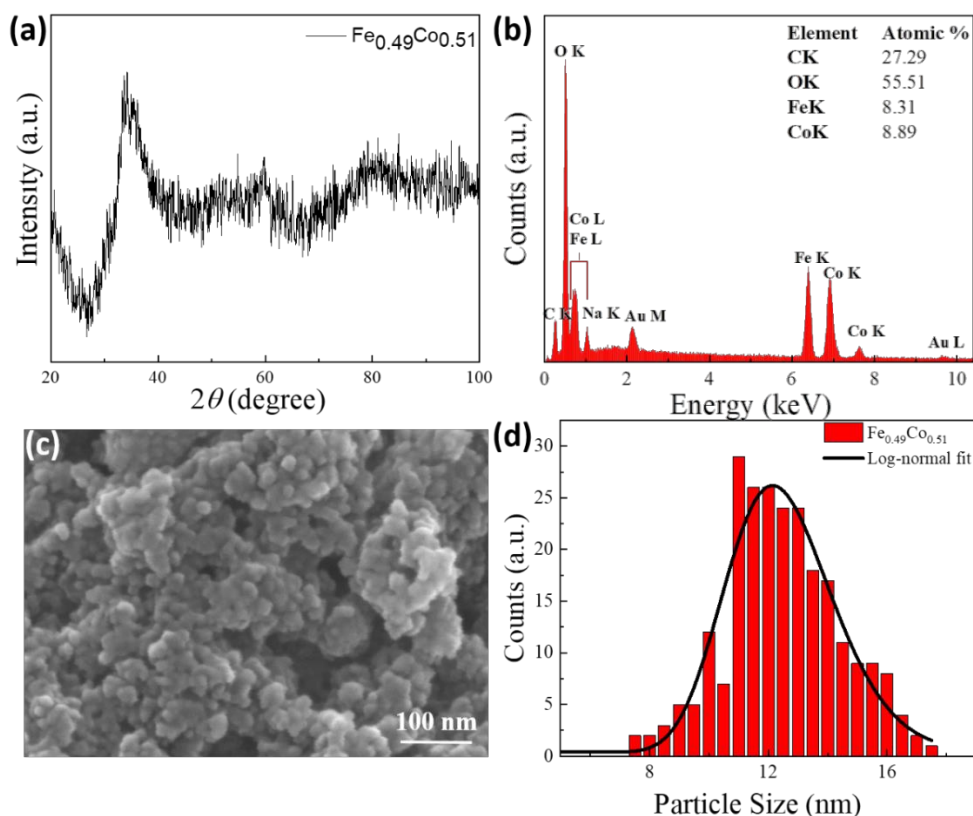


**Figure 2:** (a) XRD profile of FeCo NPs, (b) EDS data showing elemental analysis for Fe, Co, O and C, (c) SEM image, (d) The average particle size (red bar) dispersion fitted by a log-normal dispersion (dark black line) for sample

### 3.2. Electrochemical Properties of FeCo NPs

The electrochemical properties of FeCo NPs were investigated using a three-electrode setup in 1 M KOH at room temperature. Initially, the CV curves of FeCo NPs were recorded in the voltage range of -1.2 V to +1 V (vs. Ag/AgCl) to elucidate the adsorption/desorption mechanism of O and H atoms, as well as the reduction/evolution steps. Figure 3(a) illustrates the CV results, indicating weak H<sub>2</sub> gas desorption below -1.2 V and clear O<sub>2</sub> gas evolution after OH adsorption/O formation around 0.4 V. Additionally, FeCo NPs exhibited an enhanced oxygen reduction peak around -0.5 V. Furthermore, CV measurements were conducted at various scan rates of 5 mV s<sup>-1</sup> (grey line), 25 mV s<sup>-1</sup> (red line), 50 mV s<sup>-1</sup> (blue line), 75 mV s<sup>-1</sup> (green line), and 100 mV s<sup>-1</sup> (purple line), as shown in Figure 3(b). With an increase in scan rate from 5 mV s<sup>-1</sup> to 100 mV s<sup>-1</sup>, the anodic peak potential shifted slightly towards a more positive potential. The measurements were normalized for comparison, and the results indicated that as the scan rate increased, the current response to potential also increased, confirming the faradaic behavior of the FeCo electrode [23].

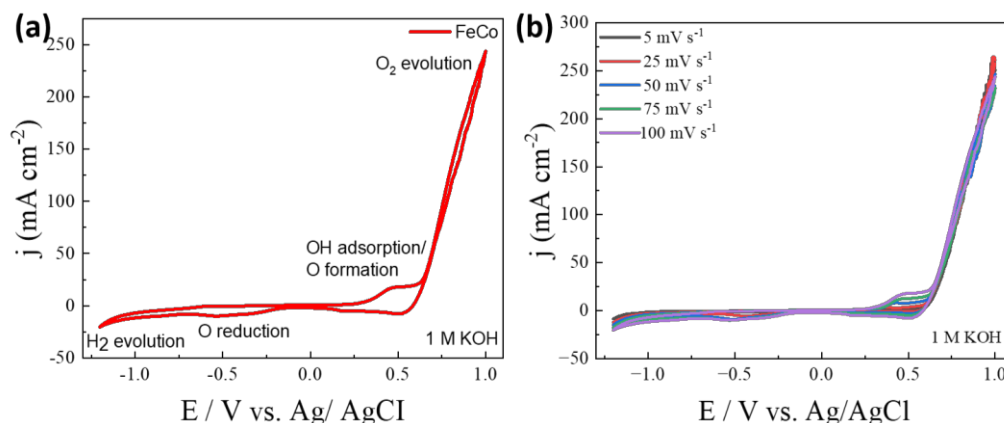


**Figure 3:** (a) CV curves of  $\text{Fe}_{0.49}\text{Co}_{0.51}$  (red line), alloys in 1 M KOH at room temperature with a scan rate of  $100 \text{ mV s}^{-1}$ , (b) CV graph at different scan rates are  $5 \text{ mV s}^{-1}$  (grey line),  $25 \text{ mV s}^{-1}$  (red line),  $50 \text{ mV s}^{-1}$  (blue line),  $75 \text{ mV s}^{-1}$  (green line), and  $100 \text{ mV s}^{-1}$  (purple line), respectively

Further, detailed investigation of FeCo NPs was conducted through ORR (orange line), OER (green line), and HER (blue line) polarization curves at a scan rate of  $50 \text{ mV s}^{-1}$  in 1 M KOH (see Figure 4(a, b and c), respectively). The onset potentials for FeCo catalysts were determined to be  $-0.15 \text{ V}$  for ORR,  $0.25 \text{ V}$  for OER and  $-1.26 \text{ V}$  for HER, respectively. Remarkably, FeCo catalyst exhibited a promising potential for ORR, surpassing commercially available Pt/C with an onset potential of  $-0.05 \text{ V}$  [24]. Notably, the current density of FeCo catalyst recorded above  $10 \text{ mA cm}^{-2}$  for ORR, which is twice as high as the commercial Pt/C catalyst at  $5 \text{ mA cm}^{-2}$  in 1 M KOH. In terms of OER, FeCo catalyst demonstrated superior performance with a  $0.25 \text{ V}$  improvement compared to commercially available  $\text{IrO}_2$  and  $\text{RuO}_2$  catalysts with  $0.3 \text{ V}$  [25, 26]. The overpotentials at  $50 \text{ mA cm}^{-2}$  and  $100 \text{ mA cm}^{-2}$  were found to be  $0.48 \text{ V}$  and  $0.71 \text{ V}$ , respectively. However, it is evident that the catalysis activity of FeCo for HER exhibited a high onset potential due to the oxide formation in the FeCo structure. To further elucidate the reaction mechanism, Tafel measurements were conducted in 1 M KOH at room temperature for ORR (red line) and OER (black line) processes (see Figure 4(d)). The corrosion potentials were recorded  $-0.165 \text{ V}$  and  $0.215 \text{ V}$  for ORR and OER, respectively. The corrosion potentials were recorded as  $-0.165 \text{ V}$  and  $0.215 \text{ V}$  and with Tafel slopes of  $228 \text{ mV dec}^{-1}$  and  $48 \text{ mV dec}^{-1}$  for ORR and OER, respectively.

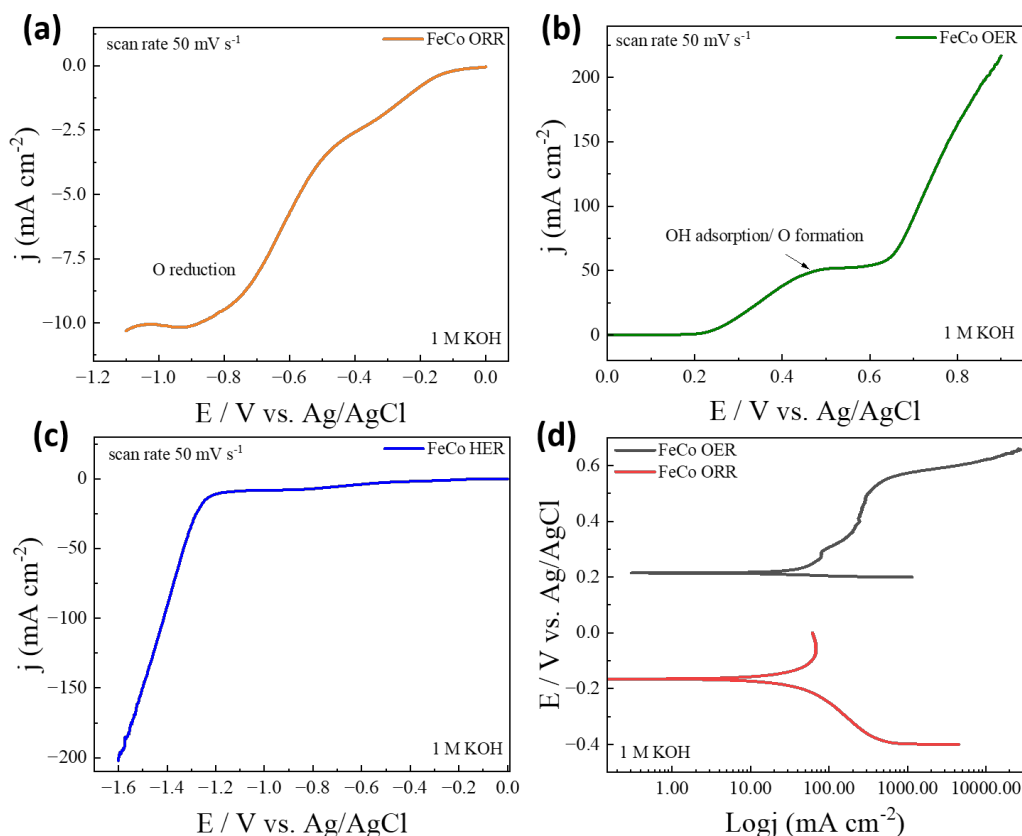
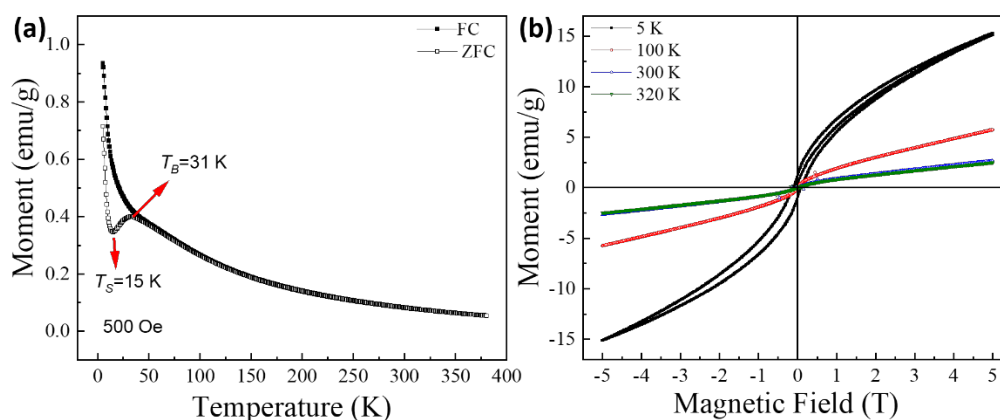


**Figure 4:** (a-c) The LSV curves shown in  $50 \text{ mVs}^{-1}$  in 1 M KOH are ORR (orange line), OER (green line), HER (blue line), respectively, (d) Tafel OER (black line) and OER (red line) curves

### 3.2. Magnetic Properties of FeCo NPs

Figure 5(a) depicts the magnetic moment as a function of temperature ( $M-T$ ) in the range of 5-380 K for ZFC (hollow circle) and FC (solid circle) curves with an applied field of 500 Oe. The magnetization of FeCo NPs increased as the temperature decreased from 380 K to 5 K, and a significant increase was observed below 25 K in the FC curve. Similarly, the ZFC curve also showed an increase with decreasing temperature between 380 K and 31 K, which is referred to as the blocking temperature,  $T_B$ . At this point, thermal energy decreases, leading to a net alignment of spins in the ferromagnetic FeCo NPs. This alignment is attributed to the presence of small particles in the sample [6]. Subsequently, the magnetization decreased, and a sudden increase was observed below 15 K, indicating a magnetic phase transition, at a temperature of  $T_s$ . This magnetic phase transition at below 15 K force the spins alignment to applied magnetic field which results in ferromagnetic contribution so that magnetization increases with decreasing temperature. There is a reduction in ZFC magnetization below  $T_B$  which is the presence of an antiferromagnetic signal in the sample surface may arise from the  $\alpha\text{-Fe}_2\text{O}_3$  phase. The magnetization behavior of Fe-oxide varies with particle size, influenced by the surface spin effect, which leads to decreased

magnetization for smaller nanoparticles [27]. Additionally, changes in particle size or fluctuations in temperature can also control this behavior.



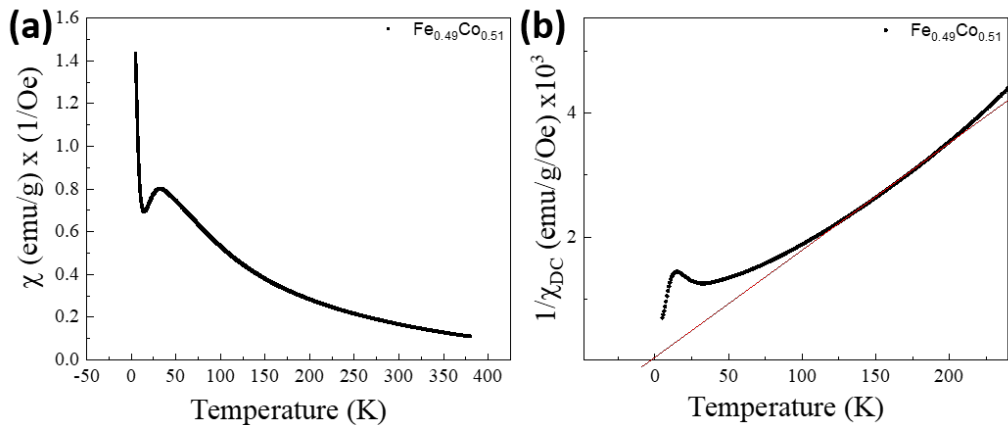
**Figure 5:** (a)  $M$ - $T$  plot in range of 5-380 K for ZFC (hollow circle) and FC (solid circle) curves showing temperature transitions at  $T_B=31$  K and  $T_S=15$  K under magnetic field of 500 Oe, (b)  $M$ - $H$  plot recorded at 5 K (black), 100 K (red), 300 K (blue) and 320 K (green) between  $\pm 5$  T

Figure 5(b) illustrates the hysteresis loop measurements as a function of temperature for the  $\text{Fe}_{0.49}\text{Co}_{0.51}$  sample. The magnetic behavior was investigated at temperatures of 5 K (black line), 100 K (red line), 300 K (blue line), and 320 K (green line). Clear hysteresis loop gaps were observed, indicating the presence of a coercive field ( $H_c$ ) at all temperatures. The  $H_c$  values were found to be 968 Oe at 5 K, gradually decreasing to approximately 206 Oe with increasing temperature, which suggests a relaxation in magnetic spin orientation [6, 28]. Additionally, while a dominant ferromagnetic effect was observed below  $T_S=15$  K, an antiferromagnetic contribution was observed as the temperature increased, providing an explanation for the behavior of  $H_c$  [29]. The substantial coercivity measuring 968 Oe, which is notably higher than the typically low coercivities observed in soft magnetic FeCo, serves as evidence indicating that the particles do not exhibit superparamagnetic behavior [30].

The saturation magnetization ( $M_s$ ) value was recorded as approximately 15.2 emu/g under a 5 T magnetic field. The decrease in  $M_s$  relative to the bulk is ascribed to the existence of a thin oxide layer of the  $\alpha\text{-Fe}_2\text{O}_3$  phase on the surface of the particles, which forms rapidly upon exposure to air. However, the hysteresis curve indicated that the sample did not reach full-saturation magnetization at 5 K. This suggests that the magnetic field strength and magnetization increase at the same rate as the temperature applied to the material increases. Similar results were obtained for  $\text{Fe}_{0.49}\text{Co}_{0.51}$  NPs, with a maximum  $M_s$  of 60 emu/g, attributed to oxidation-free synthesis and small particle size in the range of 1.34 to 2.47 nm [13, 31]. Consequently, as the temperature approaches 5 K, entropy decreases, thermal degradation does not occur, and the

material exhibits regularity, leading to an increase in the magnetic moment of the material and thereby increasing the magnetization [32, 33].

Moreover, the remanent magnetization ( $M_r$ ) of the material was determined as 1.08 emu/g at 5 K and 0.03 emu/g at 300 K and 320 K, yielding approximately the same value. Therefore, the result of about 1.08 emu/g at 5 K indicates that the material exhibits dominant ferromagnetic properties at 5 K, which can be attributed to oxidation. The  $M_r/M_s$  ratio was calculated to provide information about the magnetic characterization of the material, indicating that the resulting compound possesses soft magnetic properties. The  $M_p$  values shifted positively at 5 and 100 K, but negatively at 300 and 320 K. Detailed magnetization results of the sample are recorded in Table 1.



**Figure 6:** (a)  $\chi$ - $T$  graph, and (b)  $1/\chi$ - $T$  and with linear fit

Magnetic susceptibility measurements for FeCo NPs are presented in Figure 6(a and b), which depicts the  $\chi$  and  $1/\chi_{DC}$  graphs with a linear fit (red line) applied to these curves. The data were calculated using the Curie-Weiss law with the aid of a linear fit for  $1/\chi_{DC} = (T - \theta)/C$ . In Figure 6(a), the magnetic susceptibility decreases from 380 K, reaches a peak at approximately 25 K, and then decreases to 0 K. Consequently, the value of the  $\theta$  angle was determined as  $-9.58^\circ$  based on the linear slope of this graph. Furthermore, upon further examination of Figure 6(b), it is observed that the magnetic susceptibility experiences a decrease of  $0.7 \text{ Oe}^{-1}$ , followed by another peak, indicating an initial increase and then a subsequent decrease, ultimately converging to a descending curve toward 380 K [34].

**Table 1:** Measured values of the magnetic properties of FeCo

$\text{Fe}_{0.49}\text{Co}_{0.51}$	$H_c$ (Oe)	$H_e$ (Oe)	$M_s$ (emu/g)	$M_r$ (emu/g)	$M_p$ (emu/g)	$M_r/M_s$
5 K	968.4	94.3	15.20	1.08	0.136	0.071
100 K	214.5	8.5	5.74	0.12	0.001	0.021
300 K	192.5	13.5	2.64	0.03	-0.001	0.012
320 K	206.5	11.5	2.49	0.03	-0.001	0.012

#### 4. Conclusion

In conclusion, the multi-functional FeCo nanoparticles (NPs) synthesized through the polyol method display a diverse range of magnetic, catalytic, and structural properties, making them highly versatile materials with significant potential for various applications. The investigation of their structural, electrochemical, and magnetic characteristics revealed multiphase structures consisting of FeCo and  $\alpha$ -Fe<sub>2</sub>O<sub>3</sub> phases. The spherical-like structures of FeCo NPs, with an average size of  $12.4 \pm 0.1$  nm, were confirmed through scanning electron microscopy. The electrochemical studies demonstrated promising catalytic activities of FeCo NPs for oxygen reduction reaction (ORR), oxygen evolution reaction (OER), and hydrogen evolution reaction (HER), with onset potentials of -0.15 V, 0.25 V, and -1.26 V, respectively. Tafel measurements provided further insights into the reaction mechanism, unveiling corrosion potentials of -0.165 V for ORR and 0.215 V for OER, along with respective Tafel slopes. Additionally, magnetization studies exhibited intriguing behavior below 25 K, indicating a magnetic transition at  $T_s=15$  K, possibly implying a ferromagnetic-to-antiferromagnetic phase transition. The hysteresis loop measurements revealed temperature-dependent  $H_c$  values, indicative of magnetic spin orientation relaxation. Furthermore, the  $M_s$  values recorded at 5 T magnetic field and the  $M_r$  at 5 K highlighted the dominant ferromagnetic properties of the FeCo NPs, suggesting soft magnetic behavior. The magnetic susceptibility analysis further supported the presence of antiferromagnetic interactions with a peak at approximately 25 K. Overall, these findings contribute valuable insights into the multi-faceted properties of FeCo NPs and their potential for a wide range of applications in various fields.

#### Acknowledgements

This work was primarily supported by Cukurova University, Adana, Turkey, under Scientific Research Funding Grand No: FBA-2021-13479.

#### References

- [1] Zhang, H.-M., Wang, J.-J., Meng, Y., Sun, J., *Recent advances in amorphous metal phosphide electrocatalysts for hydrogen evolution reaction*, International Journal of Hydrogen Energy, 47(85), 36084-36097, 2022.
- [2] Kim, J.S., Kim, B., Kim, H., Kang, K., *Recent progress on multimetal oxide catalysts for the oxygen evolution reaction*, 8(11), 1702774, 2018.
- [3] Litvinov, D., Chunseng, E., Parekh, V., Smith, D., Rantschler, J., Zhang, S., Donner, W., Lee, T.R., Ruchhoeft, P., Weller, D., Khizroev, S., *Design and fabrication of high anisotropy nanoscale bit-patterned magnetic recording medium for data storage applications*, ECS Transactions, 3(25), 249-258, 2019.

[4] Liu, Y., Li, D., Sun, S., *Pt-Based composite nanoparticles for magnetic, catalytic, and biomedical applications*, *Journal of Materials Chemistry*, 21(34), 12579-12587, 2011.

[5] Koutsopoulos, S., Barfod, R., Eriksen, K.M., Fehrmann, R., *Synthesis and characterization of iron-cobalt (FeCo) alloy nanoparticles supported on carbon*, *Journal of Alloys and Compounds*, 725, 1210-1216, 2017.

[6] Shokuhfar, A., Afghahi, S.S.S., *Size controlled synthesis of FeCo alloy nanoparticles and study of the particle size and distribution effects on magnetic properties*, *Advances in Materials Science and Engineering*, 2014, 1-10, 2014.

[7] Liu, X.G., Geng, D.Y., Ma, S., Meng, H., Tong, M., Kang, D.J., Zhang, Z.D., *Electromagnetic-wave absorption properties of FeCo nanocapsules and coral-like aggregates self-assembled by the nanocapsules*, *Journal of Applied Physics*, 104(6), 064319, 2008.

[8] Park, J.-H., Woo, S., Lee, J., Jung, H.Y., Ro, J.C., Park, C., Lim, B., Suh, S.-J., *Facile modified polyol synthesis of FeCo nanoparticles with oxyhydroxide surface layer as efficient oxygen evolution reaction electrocatalysts*, *International Journal of Hydrogen Energy*, 46(29), 15398-15409, 2021.

[9] Larcher, D., Patrice, R., *Preparation of metallic powders and alloys in polyol media: a thermodynamic approach*, *Journal of Solid State Chemistry*, 154(2), 405-411, 2000.

[10] Park, J.-H., Ro, J.C., Suh, S.-J., *FeCo nanoparticles with different compositions as electrocatalysts for oxygen evolution reaction in alkaline solution*, *Applied Surface Science*, 589, 153041, 2022.

[11] Zamanpour, M., Chen, Y., Hu, B., Carroll, K., Huba, Z.J., Carpenter, E.E., Lewis, L.H., Harris, V.G., *Large-scale synthesis of high moment feco nanoparticles using modified polyol synthesis*, *Journal of Applied Physics*, 111(7), 2012.

[12] Rafique, M.Y., Pan, L., Zubair Iqbal, M., Javed, Q.-u.-a., Qiu, H., Rafi ud, d., Farooq, M.H., Guo, Z., *3-D flower like FeCo alloy nanostructures assembled with nanotriangular prism: facile synthesis, magnetic properties, and effect of NaOH on its formation*, *Journal of Alloys and Compounds*, 550, 423-430, 2013.

[13] Yang, F.J., Yao, J., Min, J.J., Li, J.H., Chen, X.Q., *Synthesis of high saturation magnetization FeCo nanoparticles by polyol reduction method*, *Chemical Physics Letters*, 648, 143-146, 2016.

[14] Fiévet, F., Ammar-Merah, S., Brayner, R., Chau, F., Giraud, M., Mammeri, F., Peron, J., Piquemal, J.Y., Sicard, L., Viau, G., *The polyol process: a unique method for easy access to metal nanoparticles with tailored sizes, Shapes And Compositions*, *Chemical Society Reviews*, 47(14), 5187-5233, 2018.

[15] Poudyal, N., Rong, C.-b., Liu, J.P., *Morphological and magnetic characterization of Fe, Co, and FeCo nanoplates and nanoparticles prepared by surfactants-assisted ball milling*, *Journal of Applied Physics*, 109, 07B526, 2011.

[16] Hiyama, H., Kodama, D., Matsumoto, T., Shinoda, K., Kasuya, R., Balachandran, J., *Synthesis and magnetic properties of platelet Fe-Co particles*, *Journal of Applied Physics*, 107(9), 2010.

- [17] Zehani, K., Bez, R., Moscovici, J., Mazaleyrat, F., Mliki, N., Bessais, L., *High magnetic moment of FeCo nanoparticles produced in polyol medium*, IEEE Transactions on Magnetics, 50(4), 1-5, 2014.
- [18] Suman, S., Chahal, S., Kumar, A., Kumar, P., *Zn Doped  $\alpha$ -Fe<sub>2</sub>O<sub>3</sub>: An efficient material for UV driven photocatalysis and electrical conductivity*, 10(4), 273, 2020.
- [19] Farahmandjou, M., Honarbakhsh, S., Behrouzinia, S., *FeCo nanorods preparation using new chemical synthesis*, Journal of Superconductivity and Novel Magnetism, 31(12), 4147-4152, 2018.
- [20] Hossain, M.A., *Synthesis of carbon nanoparticles from kerosene and their characterization by SEM/EDX, XRD and FTIR*, American Journal of Nanoscience and Nanotechnology, 1(2), 2013.
- [21] Zhang, M., Lin, Y., Mullen, T.J., Lin, W.-f., Sun, L.-D., Yan, C.-H., Patten, T.E., Wang, D., Liu, G.-y., *Improving Hematite's solar water splitting efficiency by incorporating Rare-Earth upconversion nanomaterials*, The Journal of Physical Chemistry Letters, 3(21), 3188-3192, 2012.
- [22] Cappellari, P.S., Baena-Moncada, A.M., Coneo-Rodríguez, R., Moreno, M.S., Barbero, C.A., Planes, G.A., *Catalytic enhancement of formic acid electro-oxidation through surface modifications with gold on supported Pt nanoparticles*, International Journal of Hydrogen Energy, 44(3), 1967-1972, 2019.
- [23] Puratchi Mani, M., Ponnarasi, K., Rajendran, A., Venkatachalam, V., Thamizharasan, K., Jothibas, M., *Electrochemical behavior of an advanced FeCo<sub>2</sub>O<sub>4</sub> electrode for supercapacitor applications*, Journal of Electronic Materials, 49(10), 5964-5969, 2020.
- [24] Gao, F., Zhang, Y., Wu, Z., You, H., Du, Y., *Universal strategies to multi-dimensional noble-metal-based catalysts for electrocatalysis*, Coordination Chemistry Reviews, 436, 213825, 2021.
- [25] Meierhofer, F., Fritsching, U., *Synthesis of metal oxide nanoparticles in flame sprays: review on process technology, modeling, and diagnostics*, Energy & Fuels, 35(7), 5495-5537, 2021.
- [26] Yoo, H., Oh, K., Lee, Y.R., Row, K.H., Lee, G., Choi, J., *Simultaneous co-doping of RuO<sub>2</sub> And IrO<sub>2</sub> into Anodic TiO<sub>2</sub> Nanotubes: A binary catalyst for electrochemical water splitting*, International Journal of Hydrogen Energy, 42(10), 6657-6664, 2017.
- [27] Sun, S., Zeng, H., Robinson, D.B., Raoux, S., Rice, P.M., Wang, S.X., Li, G., *Monodisperse MFe<sub>2</sub>O<sub>4</sub> (M = Fe, Co, Mn) nanoparticles*, Journal of the American Chemical Society, 126(1), 273-279, 2004.
- [28] Wesselinowa, J.M., Apostolova, I., *Size, Anisotropy and doping effects on the coercive field of ferromagnetic nanoparticles*, Journal of Physics: Condensed Matter, 19(40), 406235, 2007.
- [29] Sort, J., Nogués, J., Amils, X., Suriñach, S., Muñoz, J.S., Baró, M.D., *Room-temperature coercivity enhancement in mechanically alloyed antiferromagnetic-ferromagnetic powders*, Applied Physics Letters, 75(20), 3177-3179, 1999.

[30] Karipoth, P., Thirumurugan, A., Velaga, S., Greneche, J.-M., Justin Joseyphus, R., *Magnetic properties of FeCo alloy nanoparticles synthesized through instant chemical reduction*, Journal of Applied Physics, 120(12), 2016.

[31] Kemp, S.J., Ferguson, R.M., Khandhar, A.P., Krishnan, K.M., *Monodisperse magnetite nanoparticles with nearly ideal saturation magnetization*, RSC Advances, 6(81), 77452-77464, 2016.

[32] Kurniawan, M., Perrin, A., Xu, P., Keylin, V., McHenry, M., *Curie temperature engineering in high entropy alloys for magnetocaloric applications*, IEEE Magnetics Letters, 7, 1-5, 2016.

[33] Goya, G.F., Berquó, T.S., Fonseca, F.C., Morales, M.P., *Static and dynamic magnetic properties of spherical magnetite nanoparticles*, Journal of Applied Physics, 94(5), 3520-3528, 2003.

[34] Stipe, B.C., Rezaei, M.A., Ho, W., Gao, S., Persson, M., Lundqvist, B.I., *Single-molecule dissociation by tunneling electrons*, Physical Review Letters, 78(23), 4410-4413, 1997.



## Chen-like Inequalities on Submanifolds of Cosymplectic 3-Space Forms

Mehmet GLBAHAR<sup>1</sup>, Esra ERKAN<sup>2,\*</sup>

<sup>1</sup>Harran University, Faculty of Arts and Sciences, Department of Mathematics, 63300, Şanlıurfa, Türkiye  
mehmetgulbahar@harran.edu.tr, ORCID: 0000-0001-6950-7633

<sup>2</sup>Harran University, Faculty of Arts and Sciences, Department of Mathematics, 63300, Şanlıurfa, Türkiye  
esraerkan@harran.edu.tr, ORCID: 0000-0003-0456-6418

Received: 18.01.2023

Accepted: 02.12.2023

Published: 31.12.2023

### Abstract

In this paper, some equalities and inequalities involving the Riemannian curvature invariants are obtained on 3-semi slant submanifolds of cosymplectic 3-space forms. Obtained relations for 3-semi slant submanifolds are examined on 3-slant, invariant, and totally real submanifolds.

**Keywords:** Curvature; Submanifold; Cosymplectic 3-Space Form.

### Kosimplektik 3-Uzay Formlarının Altmanifoldları Üzerinde Chen-tipi Eşitsizlikler

### Öz

Bu çalışmada kosimplektik 3-uzay formlarının 3-semi slant altmanifoldları üzerine Riemann eğrilik invariyantları içeren bazı eşitlik ve eşitsizlikler elde edilmiştir. 3-semi slant alt manifoldlar için elde edilen bağıntılar, 3-slant, invaryant ve total reel altmanifoldlar üzerinde incelenmiştir.

**Anahtar Kelimeler:** Eğrilik; Altmanifold; Kosimplektik 3-Uzay Form.



## 1. Introduction

The concept of contact 3–manifolds was originated by Y. Kuo [1] and C. Udriște [2], independently. With the introduction of this concept, some classifications of contact 3–manifolds were presented by many authors. For mathematical and physical applications of contact 3–manifolds, we refer to [3-9], etc.

After the definition of Chen's slant submanifolds (cf. [10]), the problem of studying the geometry of slant submanifolds attracted a lot of attention. From this viewpoint, these submanifolds of almost contact metric 3–manifolds were investigated by Malek and Balgeshir in [11, 12].

In the submanifold theory, the problem of finding basic relationships between curvature invariants is one of the most basic and interesting problems. In order to compare the curvature invariants of a Riemannian manifold and its submanifold, several inequalities were established by Chen [13-16], etc. Later, this problem has been studied by many authors in various submanifolds [17-24], etc.

In the first section of this study, some main formulas and notations for a Riemannian manifold and its submanifolds are expressed. In the second section, the definitions of contact 3–manifolds and their submanifolds are given. An example of 3–semi-slant submanifolds is presented. In the third section, some relations involving Ricci curvatures of cosymplectic 3–space forms and their 3–semi-slant, 3–slant, invariant, and totally real submanifolds are examined. In the fourth section, some relations involving scalar curvatures and sectional curvatures of cosymplectic 3–space forms and their 3–semi-slant, 3–slant, invariant and totally real submanifolds are obtained.

## 2. Preliminaries

Let  $(\tilde{M}, \tilde{g})$  be a  $m$ –dimensional Riemannian manifold. The sectional curvature of  $\Pi = \text{Span}\{Y, Z\}$  is formulated by

$$\tilde{K}(Y \wedge Z) = \frac{\tilde{g}(\tilde{R}(Y, Z)Z, Y)}{\tilde{g}(Y, Y)\tilde{g}(Z, Z) - \tilde{g}(Y, Z)^2},$$

where  $\tilde{R}$  is the Riemannian curvature tensor field of  $(\tilde{M}, \tilde{g})$ . Let  $\{e_1, e_2, \dots, e_m\}$  be an orthonormal basis of  $T_p\tilde{M}$  at  $p \in \tilde{M}$ . The Ricci curvature for  $e_l, l \in \{1, 2, \dots, m\}$  is formulated by

$$\tilde{Ric}(e_i) = \sum_{j \neq i}^m \tilde{K}(e_i \wedge e_j) \tag{1}$$

and the scalar curvature at a point  $p \in \tilde{M}$  is defined by

$$\tilde{\tau}(p) = \sum_{1 \leq i < j \leq m} \tilde{K}(e_i \wedge e_j). \tag{2}$$

Let  $\Pi_n$  be an  $n$ -dimensional subsection of  $T_p \tilde{M}$ . If  $n = m$ ,  $\Pi_n = T_p \tilde{M}$ . Let us choose an orthonormal basis  $\{e_1, e_2, \dots, e_n\}$  of  $\Pi_n$ . Then  $n$ -Ricci curvature of  $e_t$ ,  $t \in \{1, 2, \dots, n\}$ , is formulated by

$$\tilde{Ric}_{\Pi_n}(e_t) = \sum_{j \neq t}^n \tilde{K}(e_t \wedge e_j) \tag{3}$$

and  $n$ -scalar curvature of  $\Pi_n$  is formulated by

$$\tilde{\tau}_{\Pi_n}(p) = \sum_{1 \leq i < j \leq n} \tilde{K}(e_i \wedge e_j). \tag{4}$$

We note that if  $n = m$ , then  $\tilde{Ric}_{\Pi_n}(e_t) = \tilde{Ric}_{T_p \tilde{M}}(e_t)$  and  $\tilde{\tau}_{\Pi_n}(p) = \tilde{\tau}_{T_p \tilde{M}}(p)$ .

Assume that  $(M, g)$  is a  $k$ -dimensional submanifold of  $(\tilde{M}, \tilde{g})$ . The Gauss and Weingarten formulas are formulated by

$$\nabla_X Y = \nabla_X Y + \sigma(X, Y) \tag{5}$$

and

$$\nabla_X Y = -A_N X + \nabla_X^\perp N, \tag{6}$$

where  $X, Y \in T_p M$ ,  $N$  is a unit normal vector,  $\nabla_X Y, A_N X \in T_p M$  and  $\sigma(X, Y), \nabla_X^\perp N \in T_p^\perp M$ . Here,  $\sigma$  is the second fundamental form,  $A_N$  is the shape operator and  $\nabla^\perp$  is the normal connection of  $M$ . It is well known that  $\sigma$  is associated to  $A_N$  by the following formula:

$$\tilde{g}(\sigma(X, Y), N) = g(A_N X, Y). \tag{7}$$

Denote the Riemannian curvature tensor of  $M$  by  $R$ . The Gauss equation is formulated by

$$g(R(X, Y)Z, W) = \tilde{g}(\tilde{R}(X, Y)Z, W) + \tilde{g}(\sigma(X, W), \sigma(Y, Z)) - \tilde{g}(\sigma(X, Z), \sigma(Y, W)) \tag{8}$$

for any  $X, Y, Z, W \in T_p M$ .

Let  $\{e_1, e_2, \dots, e_k\}$  be an orthonormal basis of  $T_p M$ . The main curvature vector field  $\tilde{h}$  is formulated by

$$\tilde{h} = \frac{1}{k} \sum_{l=1}^k \sigma(e_l, e_l). \tag{9}$$

$M$  is said to be totally geodesic if  $\sigma = 0$ , and it is said to be minimal if  $\tilde{h} = 0$ .  $M$  is totally umbilical if and only if  $\sigma(X, Y) = g(X, Y)\tilde{h}$  is satisfied for all  $X, Y \in T_p M$ .

Let  $\{e_{k+1}, e_{k+2}, \dots, e_m\}$  be an orthonormal basis of  $T_p^\perp M$  and  $e_s$  belongs to  $\{e_{k+1}, e_{k+2}, \dots, e_m\}$ . Denote the intrinsic sectional curvature by  $K(e_l \wedge e_j)$ . In view of (8), if we put

$$\sigma_{ij}^s = \tilde{g}(\sigma(e_l, e_j), e_s) \quad \text{and} \quad \|\sigma\|^2 = \sum_{l,j=1}^k \tilde{g}(\sigma(e_l, e_j), \sigma(e_l, e_j)), \tag{10}$$

then we find

$$K(e_l \wedge e_j) = \tilde{K}(e_l \wedge e_j) + \sum_{s=k+1}^m (\sigma_{li}^s \sigma_{jj}^s - (\sigma_{lj}^s)^2). \tag{11}$$

From (11), it follows that

$$2\tau(p) = 2\tilde{\tau}(T_p M) + n^2 \|\tilde{h}\|^2 - \|\sigma\|^2, \tag{12}$$

where

$$\tilde{\tau}(T_p M) = \sum_{1 \leq l < j \leq k} \tilde{K}_{lj}.$$

Moreover, there exists the following relation:

$$\begin{aligned} \|\sigma\|^2 = & \frac{1}{2}k^2 \|\tilde{h}\|^2 + \frac{1}{2} \sum_{s=k+1}^m (\sigma_{11}^r - \sigma_{22}^r - \dots - \sigma_{kk}^s)^2 + 2 \sum_{s=k+1}^m \sum_{j=2}^k (\sigma_{1j}^s)^2 \\ & - 2 \sum_{s=k+1}^m \sum_{2 \leq l < j \leq k} (\sigma_{ll}^s \sigma_{jj}^s - (\sigma_{lj}^s)^2). \end{aligned} \tag{13}$$

For the basic concepts dealing with Riemannian manifolds, we refer to [16].

The relative null space at a point  $p$  in  $M$  is given by [14]

$$N_p = \{X \in T_p M \mid \sigma(X, Y) = 0 \text{ for all } Y \in T_p M\}. \tag{14}$$

We note that  $N_p$  is also said to be the kernel of  $\sigma$  at  $p$  [25].

The Chen invariant  $\delta_M$  for a Riemannian submanifold  $M$  is formulated by [26]

$$\delta_M(p) = \tau(p) - \inf(K)(p), \tag{15}$$

where  $\inf(K)(p) = \inf\{K(\Pi) : \Pi \text{ is a plane}\}$ .

### 3. Submanifolds of Contact 3-Space Forms

**Definition 1.** [1] A differentiable manifold  $\tilde{M}$  admitting an almost contact 3 – structure  $(\xi_l, \eta_l, \varphi_l)_{l \in \{1,2,3\}}$  is said to be an almost contact 3 – structure manifold. An almost contact 3 – structure manifold is denoted by  $(\tilde{M}, \xi_l, \eta_l, \varphi_l)_{l \in \{1,2,3\}}$ .

For  $(\tilde{M}, \xi_l, \eta_l, \varphi_l)_{l \in \{1,2,3\}}$ , the following relations hold:

$$\varphi_l \xi_j = -\varphi_j \xi_l = \xi_n, \quad \eta_l \varphi_j = -\eta_j \varphi_l = \eta_n, \quad \eta_l \xi_j = 0 \tag{16}$$

and

$$\varphi_l \circ \varphi_j - \eta_j \otimes \xi_l = -\varphi_j \circ \varphi_l + \eta_l \otimes \xi_j = \varphi_n, \tag{17}$$

where  $(l, j, n)$  is a cyclic permutation of  $(1, 2, 3)$ . If  $(\tilde{M}, \xi_l, \eta_l, \varphi_l)_{l \in \{1,2,3\}}$  includes a Riemannian metric  $\tilde{g}$  given by

$$\tilde{g}(\varphi_l Y, \varphi_l Z) = \tilde{g}(Y, Z) - \eta_l(Y)\eta_l(Z) \tag{18}$$

for any  $Y, Z \in T_p \tilde{M}$ , then  $(\tilde{M}, \tilde{g}, \xi_l, \eta_l, \varphi_l)_{l \in \{1,2,3\}}$  is said to be an almost contact metric 3 – structure manifold. From the Eq. (18), we have

$$\tilde{g}(\varphi_l Y, Z) = -\tilde{g}(Y, \varphi_l Z). \tag{19}$$

$(\tilde{M}, \tilde{g}, \xi_l, \eta_l, \varphi_l)_{l \in \{1,2,3\}}$  is called a cosymplectic 3 – manifold if

$$\tilde{\nabla} \varphi_l = 0 \tag{20}$$

is satisfied. It is said to be a Sasakian 3 – manifold if

$$(\tilde{\nabla}_Y \varphi_l)Z = \tilde{g}(Y, Z)\xi_l - \eta_l(Z)Y \tag{21}$$

is provided.

In a similar manner to the concept of holomorphic sectional curvature on Hermitian or contact metric manifolds, we can state the concept of  $\varphi_l$  – holomorphic sectional curvature on  $(\tilde{M}, \tilde{g}, \xi_l, \eta_l, \varphi_l)_{l \in \{1,2,3\}}$  in such a way:

**Definition 2.** [11] A plane  $\Pi$  is said to be a  $\varphi_l$  – section if there exists a unit vector  $X \in T_p \tilde{M}$  orthogonal to  $\xi_l$ , where  $\{X, \varphi_l X\}$  is an orthonormal basis on  $\Pi$  for some  $l \in \{1, 2, 3\}$ . The  $\varphi_l$  – holomorphic sectional curvature of a  $\varphi_l$  – section is defined by

$$\tilde{K}(X \wedge \varphi_l X) = \tilde{g}(\tilde{R}(X, \varphi_l X)\varphi_l X, X).$$

A cosymplectic 3 – manifold  $(\tilde{M}, \tilde{g}, \xi_l, \eta_l, \varphi_l)_{l \in \{1,2,3\}}$  becomes a cosymplectic 3 – space form if it is of constant  $\varphi_l$  – holomorphic sectional curvature  $c$ . A cosymplectic 3 – space form is shown by  $\tilde{M}(c)$ .

If  $\tilde{M}(c)$  is a cosymplectic 3 – space form, then the Riemannian curvature is satisfied the following relation [1]:

$$\begin{aligned} \tilde{R}(X, Y, Z, W) = & \frac{c}{4} \{g(X, W)g(Y, Z) - g(X, Z)g(Y, W) \\ & + \sum_{n=1}^3 [g(X, \varphi_n W)g(Y, \varphi_n Z) - g(X, \varphi_n Z)g(Y, \varphi_n W) \\ & - 2g(X, \varphi_n Y)g(Z, \varphi_n W) - g(X, W)\eta_n(Y)\eta_n(Z) \\ & + g(X, Z)\eta_n(Y)\eta_n(W) - g(Y, Z)\eta_n(X)\eta_n(W) \\ & + g(Y, W)\eta_n(X)\eta_n(Z)], \end{aligned}$$

(22)

for any  $X, Y, Z, W \in \tilde{M}$ .

Assume that  $(M, g)$  is a  $k$  – dimensional submanifold of  $(\tilde{M}, \tilde{g}, \xi_l, \eta_l, \varphi_l)_{l \in \{1,2,3\}}$ . For any vector field  $X$  in  $T_p M$ , we can write  $\varphi_l X$  as follows:

$$\varphi_l X = P_l X + F_l X, \tag{23}$$

where  $P_l X \in T_p M$  and  $F_l X \in T_p^\perp M$  for  $l \in \{1, 2, 3\}$ .

We can express the following:

$$\|P_l\|^2 = \sum_{j,n=1}^k g(P_l e_j, e_n)^2 \tag{24}$$

and

$$\|P_l X\|^2 = \sum_{n=1}^k g(P_l X, e_n)^2. \tag{25}$$

$(M, g)$  is said to be invariant if  $F_l = 0$  and it is said to be totally real if  $P_l = 0$  for each  $l \in \{1, 2, 3\}$ . Furthermore,  $(M, g)$  becomes 3 – slant if for each  $l \in \{1, 2, 3\}$ , the angle  $\theta$  between  $\varphi_l X$  and the tangent space  $T_p M$  is constant for every  $p$  in  $M$  and every  $X \neq 0$  which is not linearly dependent by  $\xi_l$  [12].

We remark that a 3 – slant submanifold becomes invariant when  $\theta = 0$  and it becomes totally real if  $\theta = \frac{\pi}{2}$ . Furthermore, the following classification could be stated:

**Definition 3.** [12] A submanifold  $(M, g)$  is said to be a 3 – semi-slant submanifold if we have three orthogonal distributions  $D_1, D_2, D_3$ , where  $D_3 = \text{Span}\{\xi_1, \xi_2, \xi_3\}$  and the following cases occur:

- i)  $TM = D_1 \oplus D_2 \oplus D_3$ ,
- ii)  $\varphi_i(D_1) \subset D_1, \forall i \in \{1, 2, 3\}$ ,
- iii)  $D_2$  is 3 – slant with  $\theta \neq 0$ .

It is clear that  $(M, g)$  is 3 – slant if  $D_1 = 0$  and it becomes an invariant submanifold if  $\theta = 0$ .

**Example 1.** Let us consider 11 – dimensional Euclidean space  $E^{11}$ . If we define

$$\begin{aligned} \varphi_1((x_i)_{i \in \{1, \dots, 11\}}) &= (-x_2, x_1, -x_3, x_4, -x_7, -x_8, x_5, x_6, 0, -x_{11}, x_{10}) \\ \varphi_2((x_i)_{i \in \{1, \dots, 11\}}) &= (-x_4, -x_3, x_1, x_2, -x_7, -x_8, x_5, x_6, x_{11}, 0, x_9), \\ \varphi_3((x_i)_{i \in \{1, \dots, 11\}}) &= (x_2, -x_1, x_3, -x_4, -x_7, -x_8, x_5, x_6, -x_{10}, x_9, 0) \end{aligned}$$

such that  $\xi_1 = \partial x_9, \xi_2 = \partial x_{10}, \xi_3 = \partial x_{11}$  and  $\eta_1, \eta_2, \eta_3$  are duals of  $\xi_1, \xi_2, \xi_3$ , respectively.

We find  $(E^{11}, \xi_l, \eta_l, \varphi_l)_{l \in \{1, 2, 3\}}$  is an almost contact 3 – structure manifold.

Let us define the following submanifold of  $(E^{11}, \xi_l, \eta_l, \varphi_l)_{l \in \{1, 2, 3\}}$ :

$$M = \{(u_1, u_2, u_3, u_4, u_5 \cos \alpha, u_5 \sin \alpha, u_6 \cos \beta, u_6 \sin \beta, u_7, u_8, u_9)\},$$

where  $\alpha, \beta \in [0, \frac{\pi}{2})$ . In this case, we obtain

$$\begin{aligned} Y_1 &= \partial x_1, \quad Y_2 = \partial x_2, \quad Y_3 = \partial x_3, \quad Y_4 = \partial x_4, \\ Y_5 &= \cos \alpha \partial x_5 + \sin \alpha \partial x_6, \quad Y_6 = \cos \beta \partial x_7 + \sin \beta \partial x_8, \\ \xi_1 &= \partial x_9, \quad \xi_2 = \partial x_{10}, \quad \xi_3 = \partial x_{11} \end{aligned}$$

and

$$N_1 = -\sin \alpha \partial x_5 + \cos \alpha \partial x_6, \quad N_2 = -\sin \beta \partial x_7 + \cos \beta \partial x_8,$$

where  $T_p M = \text{Span}\{Y_1, Y_2, Y_3, Y_4, Y_5, Y_6, \xi_1, \xi_2, \xi_3\}$ ,  $T_p^\perp M = \text{Span}\{N_1, N_2\}$  and  $\{\partial x_1, \dots, \partial x_{11}\}$  is the natural basis of  $E^{11}$ . If we put  $D_1 = \text{Span}\{Y_1, Y_2, Y_3, Y_4\}$ ,  $D_2 = \text{Span}\{Y_5, Y_6\}$  and  $D_3 = \text{Span}\{\xi_1, \xi_2, \xi_3\}$ , then  $M$  becomes 3 – semi invariant with  $\theta = |\alpha - \beta|$ .

#### 4. Inequalities Involving Ricci Curvatures

Let us indicate the set of all unit vectors in  $T_p M$  by  $T_p^1 M$ .

**Theorem 1.** [27] Let  $M$  be a  $k$  – dimensional submanifold of  $(\tilde{M}, \tilde{g})$ . The following cases hold:

i) For any  $X \in T_p^1 M$ , we get

$$\text{Ric}(X) \leq \frac{1}{4} k^2 \|\tilde{h}\|^2 + \tilde{\text{Ric}}_{T_p M}(X). \tag{26}$$

Here  $\tilde{\text{Ric}}_{T_p M}(X)$  is the  $k$  – Ricci curvature of  $X \in T_p^1 M$ .

ii) The equality case of (26) occurs for  $X \in T_p^1 M$  if and only if

$$\begin{cases} \sigma(X, Z) = 0, & \text{for each } Z \perp X, \\ 2\sigma(X, X) = k\tilde{h}(p). \end{cases}$$

iii) The equality case of (26) occurs for each  $X \in T_p^1 M$  if and only if either  $p$  is a totally geodesic point or  $p$  is a totally umbilical point for  $k = 2$ .

From Theorem 1, we can state:

**Corollary 1.** [28] For any Riemannian submanifold, any two of the below three cases refer to the other one:

i)  $X$  satisfies the equality case of (26).

ii)  $\tilde{h}(p) = 0$ .

iii)  $X \in N_p$ .

Now, we assume that  $\{\xi_1, \xi_2, \xi_3\}$  is tangent to  $M$  and  $X \in T_p^1M$  throughout this paper.

**Lemma 1.** For any  $k$  – dimensional submanifold of  $\tilde{M}(c)$ . We find

$$\tilde{K}(e_l \wedge e_j) = \frac{c}{4} \left\{ 1 + \sum_{n=1}^3 [3g(P_n e_l, e_j)^2 - \eta_n^2(e_j) - \eta_n^2(e_l)] \right\}, \tag{27}$$

$$\tilde{Ric}_{T_p M}(X) = \frac{c}{4} \left\{ (n-4) + \sum_{n=1}^3 [3\|P_n X\|^2 + (2-k)\eta_n^2(X)] \right\}, \tag{28}$$

$$\tilde{\tau}_{T_p M}(p) = \frac{c}{8} \left\{ (k-1)(k-6) + 3 \sum_{n=1}^3 \|P_n\|^2 \right\}. \tag{29}$$

**Proof.** From (22), we have

$$\begin{aligned} \tilde{g}(\tilde{R}(e_l, e_j)e_j, e_l) &= \frac{c}{4} \left\{ g(e_l, e_l)g(e_j, e_j) - g(e_l, e_j)g(e_j, e_l) \right. \\ &\quad + \sum_{n=1}^3 [g(e_l, \varphi_n e_l)g(e_j, \varphi_n e_j) - g(e_l, \varphi_n e_j)g(e_j, \varphi_n e_l)] \\ &\quad - 2g(e_l, \varphi_n e_j)g(e_j, \varphi_n e_l) - g(e_l, e_l)\eta_n(e_j)\eta_n(e_j) \\ &\quad + g(e_l, e_j)\eta_n(e_j)\eta_n(e_l) - g(e_j, e_j)\eta_n(e_l)\eta_n(e_l) \\ &\quad \left. + g(e_j, e_l)\eta_n(e_l)\eta_n(e_j) \right\}, \end{aligned}$$

which is equivalent to (27). In view of (1) and (27), we find

$$\tilde{Ric}_{T_p M}(e_1) = \frac{c}{4} \left\{ (k-1) + \sum_{n=1}^3 \left[ 3 \sum_{j=1}^k g(P_n e_1, e_j)^2 + (2-k) \sum_{j=1}^k \eta_n^2(e_1) \right] \right\}.$$

Putting  $e_1 = X$  and using (25) in the last equation, we obtain (28). From (2) and (28), we get

$$\tilde{\tau}_{T_p M}(p) = \frac{c}{8} \left\{ k(k-4) + \sum_{l=1}^k \sum_{n=1}^3 [3\|P_n e_l\|^2 + (2-k)\eta_n^2(e_l)] \right\}.$$

Considering (24) in the last equation, we obtain (29).

In view of Theorem 1 and (28), we obtain

**Theorem 2.** For any  $k$  – dimensional submanifold of  $\tilde{M}(c)$ , we have the following cases:

i) For any  $X \in T_p^1M$ , we get

$$Ric(X) \leq \frac{1}{4}k^2 \|\hbar\|^2 + \frac{c}{4} \left\{ (k-4) + \sum_{n=1}^3 \left[ 3\|P_n X\|^2 + (2-k)\eta_n^2(X) \right] \right\}. \tag{30}$$

ii) The equality case of (30) occurs for  $X \in T_p^1M$  if and only if

$$\begin{cases} \sigma(X, Z) = 0, & \text{for each } Z \perp X, \\ \sigma(X, X) = \frac{k}{2} \hbar(p). \end{cases}$$

iii) The equality case of (30) occurs for each  $X \in T_p^1M$  if and only if  $p$  is a totally geodesic point.

From Theorem 2, we immediately have

**Corollary 3.** For  $k$  – dimensional submanifold of  $\tilde{M}(c)$ , any two of the below three cases refer to the other one:

- i)  $X$  satisfies the equality case of (30).
- ii)  $\hbar(p) = 0$ .
- iii)  $X \in N_p$ .

**Definition 4.** Let  $D$  be a distribution on  $M$ .

- i) If  $\sigma(X, Z) = 0$  is satisfied for all  $X, Z \in D$ , then  $M$  is said to be  $D$  – geodesic.
- ii) If there exists a smooth function  $\lambda$  on  $M$  satisfying  $\sigma(X, Z) = \lambda g(X, Z)$  for each  $X, Z \in D$ , then  $M$  is called  $D$  – umbilical.

**Theorem 3.** For any  $k$  – dimensional 3 – semi-slant submanifold, the following cases occur:

i) For every unit  $X \in D_1$ , we get

$$Ric(X) \leq \frac{1}{4}k^2 \|\hbar\|^2 + \frac{c}{4}(k+5). \tag{31}$$

ii) The equality case of (31) is true for each  $X \in D_1$  at  $p \in M$  if and only if  $M$  is  $D_1$  – geodesic.

iii) For every unit  $Y \in D_2$ , we get

$$\text{Ric}(Y) \leq \frac{1}{4}k^2 \|\tilde{h}\|^2 + \frac{c}{4} \{(k-4) + 9 \cos^2 \theta\}. \tag{32}$$

iv) The equality case of (32) is true for all  $X \in D_2$  at  $p \in M$  if and only if  $M$  is  $D_2$  – geodesic.

**Proof.** If  $X \in D_1$ , we obtain

$$\|P_n X\|^2 = 1, \eta_n(X) = 0 \text{ and } \sum_{n=1}^3 \sum_{j=1}^k \eta_n(e_j) = 3.$$

Using these facts in (28), we obtain (31). The equality case of (31) occurs for each  $X \in D_1$  if and only if  $\sigma(X, Z) = 0$  for all  $X, Z \in D_1$ . This implies that  $M$  is  $D_1$  – geodesic.

If  $X$  belongs to  $D_1$ , we obtain

$$\sum_{n=1}^3 \|P_n X\|^2 = 3 \cos^2 \theta, \eta_n(X) = 0 \text{ and } \sum_{n=1}^3 \sum_{j=1}^k \eta_n(e_j) = 3.$$

Using these facts in (29), we obtain (32). The equality case of (32) occurs for each  $Y \in D_2$  if and only if  $\sigma(Y, Z) = 0$  for all  $Y, Z \in D_2$ . This implies that  $M$  is  $D_2$  – geodesic.

In view of Theorem 3, we find

**Theorem 4.** For any  $k$  – dimensional submanifold of  $\tilde{M}(c)$ , we find the following cases:

i) For the Ricci tensor  $S$  of  $M$ , we have the following table:

**Table 1:**

	$M$	Inequality
(1)	3 – slant	$S \leq \left( \frac{1}{4}k^2 \ \tilde{h}\ ^2 + \frac{c}{4} \{(k-4) + 9 \cos^2 \theta\} \right) g.$
(2)	invariant	$S \leq \left( \frac{1}{4}k^2 \ \tilde{h}\ ^2 + \frac{c}{4} (k+5) \right) g.$

(3)	totally real	$S \leq \left( \frac{1}{4}k^2 \ \tilde{h}\ ^2 + \frac{c}{4}(k-1) \right) g.$
-----	--------------	--

ii) The equality case of (1) – (3) occurs if and only if  $M$  is a totally geodesic submanifold.

### 5. Inequalities Involving Scalar Curvatures

**Lemma 2.** [29] If  $a_1, \dots, a_k$  ( $k > 1$ ) are real numbers, then

$$\frac{1}{k} \left( \sum_{l=1}^k a_l \right)^2 \leq \sum_{l=1}^k a_l^2 \tag{33}$$

is satisfied. The equality case of (33) occurs if and only if  $a_1 = a_2 = \dots = a_k$ .

**Theorem 5.** For any  $k$  – dimensional submanifold of  $\tilde{M}(c)$ . Then

$$\tau(p) \leq \frac{k(k-1)}{2} \|\tilde{h}\|^2 + \frac{c}{8} \left\{ (k-1)(k-6) + 3 \sum_{n=1}^3 \|P_n\|^2 \right\} \tag{34}$$

is satisfied. The equality case of (34) is true for  $p$  in  $M$  if and only if  $p$  is a totally umbilical point.

**Proof.** Assume that  $e_{k+1}$  is parallel to  $\tilde{h}(p)$  and  $e_1, \dots, e_k$  diagonalize  $A_{e_{k+1}}$ . In this case, we can write

$$A_{e_{k+1}} = \text{diag}(\sigma_{11}^{k+1}, \sigma_{22}^{k+1}, \dots, \sigma_{kk}^{k+1}) \tag{35}$$

and

$$A_{e_s} = (\sigma_{lj}^s), \quad \text{trace } A_{e_s} = \sum_{l=1}^k \sigma_{ll}^s = 0 \tag{36}$$

for each  $l, j = 1, \dots, k$  and  $s = k + 2, \dots, m$ . From (12), (35) and (36), we get

$$2\tau(p) = \frac{c}{4} \left\{ (k-1)(k-6) + 3 \sum_{n=1}^3 \|P_n\|^2 \right\} + k^2 \|\tilde{h}\|^2 - \sum_{l=1}^k (\sigma_{ll}^{k+1})^2 - \sum_{s=k+2}^m \sum_{l,j=1}^k (\sigma_{lj}^s)^2. \tag{37}$$

Considering Lemma 2, we arrive at

$$k \|\tilde{h}\|^2 \leq \sum_{l=1}^k (\sigma_{ll}^{k+1})^2. \tag{38}$$

From (37) and (38), the eq. (34) could be obtained. If the equality situation of (34) occurs, from Lemma 2, we find

$$\sigma_{11}^{k+1} = \sigma_{22}^{k+1} = \dots = \sigma_{kk}^{k+1} \quad \text{and} \quad A_{e_s} = 0.$$

The last equation implies that  $p$  is a totally umbilical point. The other direction of proof is easy to follow.

For any  $k$ -dimensional 3-semi-slant submanifold of  $\tilde{M}(c)$ , we put  $\dim D_1 = s_1$ ,  $\dim D_2 = s_2$  and  $k = s_1 + s_2 + 3$ . Then, we have the following:

**Theorem 6.** For any  $k$ -dimensional 3-semi-slant submanifold of  $\tilde{M}(c)$ , we find

$$\tau(p) \leq \frac{k(k-1)}{2} \|\tilde{h}\|^2 + \frac{c}{8} \{ (k-1)(k-6) + 9(s_1 + 2 + s_2 \cos^2 \theta) \}. \tag{39}$$

The equality case of (39) is true for  $p$  in  $M$  if and only if  $p$  is a totally umbilical point.

**Proof.** If  $M$  is 3-semi-slant, it can be found

$$\sum_{n=1}^3 \|P_n\|^2 = 3s_1 + 6 + 3s_2 \cos^2 \theta. \tag{40}$$

Considering (40) in Theorem 5, the proof is easy to follow.

As a result of Theorem 6, we also have the following:

**Corollary 4.** For any  $k$ -dimensional submanifold  $M$  of  $\tilde{M}(c)$ ,

i) we have the following table:

**Table 2:**

	$M$	Inequality
(1)	3 – slant	$\tau(p) \leq \frac{k(k-1)}{2} \ \tilde{h}\ ^2 + \frac{c}{8} \{(k-1)(k-6) + 9((s_1 + s_2) \cos^2 \theta + 2)\}.$
(2)	invariant	$\tau(p) \leq \frac{k(k-1)}{2} \ \tilde{h}\ ^2 + \frac{c}{8} \{(k-1)(k+3)\}.$
(3)	totally real	$\tau(p) \leq \frac{k(k-1)}{2} \ \tilde{h}\ ^2 + \frac{c}{8} \{k^2 - 7k + 24\}.$

ii) the equality case of (1)-(3) for each case is satisfied if and only if  $p$  is a totally umbilical point.

**Proof.** If  $M$  is 3 – slant, then it can be obtained

$$\sum_{n=1}^3 \|P_n\|^2 = 3(s_1 + s_2) \cos^2 \theta + 6. \tag{41}$$

Putting (41) in (34), we get the first case of Table 2.

Consider the fact that  $\varphi_l \xi_j = \xi_n$ , if  $M$  is invariant, then we find

$$\sum_{n=1}^3 \|P_n\|^2 = 3(s_1 + s_2) + 6 = 3(k-1). \tag{42}$$

Putting (42) in (34), we get the second case of Table 2.

Considering the fact that  $\varphi_l \xi_j = \xi_n$ , if  $M$  is totally real, then we find

$$\sum_{n=1}^3 \|P_n\|^2 = 6. \tag{43}$$

Putting (43) in (34), we get the third case of Table 2.

The proof of ii) is easy to follow from Theorem 6.

**Theorem 7.** For any  $k$  – dimensional submanifold of  $\tilde{M}(c)$ , we have

$$\tau(p) \leq \frac{1}{2}k^2 \|\tilde{h}\|^2 + \frac{c}{8} \left\{ (k-1)(k-6) + 3 \sum_{n=1}^3 \|P_n\|^2 \right\}. \tag{44}$$

The equality case of (44) occurs for  $p$  in  $M$  if and only if  $p$  is a totally geodesic point.

**Proof.** The proof is easy to follow by (12) and (29).

As a result of Theorem 7, we find the following:

**Corollary 5.** For any  $k$  – dimensional 3 – semi-slant submanifold of  $\tilde{M}(c)$ , we have

$$\tau(p) \leq \frac{1}{2}k^2 \|\tilde{h}\|^2 + \frac{c}{8} \{ (k-1)(k-6) + 9(s_1 + 2 + s_2 \cos^2 \theta) \}. \tag{45}$$

The equality case of (45) occurs for  $p$  in  $M$  if and only if  $p$  is a totally geodesic point.

**Corollary 6.** For any  $k$  – dimensional submanifold of  $\tilde{M}(c)$ ,

i) we have the following table:

**Table 3:**

	$M$	Inequality
(1)	3 – slant	$\tau(p) \leq \frac{1}{2}k^2 \ \tilde{h}\ ^2 + \frac{c}{8} \{ (k-1)(k-6) + 9((s_1 + s_2) \cos^2 \theta + 2) \}.$
(2)	invariant	$\tau(p) \leq \frac{1}{2}k^2 \ \tilde{h}\ ^2 + \frac{c}{8} \{ (k-1)(k+3) \}.$
(3)	totally real	$\tau(p) \leq \frac{1}{2}k^2 \ \tilde{h}\ ^2 + \frac{c}{8} \{ k^2 - 7k + 24 \}.$

ii) The equality case of (1)-(3) occurs if and only if  $p$  is a totally geodesic point.

We need the following lemma for later uses:

**Lemma 3.** Let  $a_1, \dots, a_k, a$  ( $k > 2$ ) be real numbers satisfying

$$\left( \sum_{l=1}^k a_l \right)^2 = (k-1) \left( \sum_{l=1}^k a_l^2 + a \right). \tag{46}$$

Then

$$2a_1a_2 \geq a$$

is satisfied if and only if we find

$$a_1 + a_2 = a_3 = \dots = a_k.$$

Let  $\{e_1, \dots, e_k\}$  be an orthonormal basis and  $\Pi = \text{Span}\{e_1, e_2\}$ . We define

$$\|P_n|_{\pi^\perp}\|^2 = \sum_{j,t=3}^k g(P_n e_t, e_j)^2. \tag{47}$$

Then we have

**Theorem 8.** Let  $M$  be a  $k$  – dimensional ( $k \geq 3$ ) submanifold of  $\tilde{M}(c)$ . Then, for each point  $p \in M$  and each  $\varphi_l$  – plane section  $\Pi = \text{Span}\{e_1, e_2\}$  such that  $\varphi_l e_1 = e_2$ , we have

$$\tau(p) - K(e_1 \wedge e_2) \leq \frac{k^2(k-2)}{2(k-1)} \|\tilde{h}\|^2 + \frac{c}{8} \left\{ (k^2 - 7k + 4) + 3\|P_n|_{\pi^\perp}\|^2 \right\}. \tag{48}$$

The equality case (48) occurs at  $p$  in  $M$  if and only if there exists an orthonormal basis  $\{e_{k+1}, \dots, e_m\}$  of  $T_p^\perp M$  such that the shape operators  $A_{e_s}$  take the following forms:

$$A_{e_{k+1}} = \begin{pmatrix} a & 0 & 0 \\ 0 & b & 0 \\ 0 & 0 & (a+b)I_{k-2} \end{pmatrix}, \tag{49}$$

$$A_{e_s} = \begin{pmatrix} c_s & d_s & 0 \\ d_s & -c_s & 0 \\ 0 & 0 & 0_{k-2} \end{pmatrix}, \quad s \in \{k+2, \dots, m\}. \tag{50}$$

**Proof.** Assume that  $\tilde{h}(p)$  is in the direction of  $e_{k+1}$  and  $e_1, \dots, e_k$  diagonalize  $A_{e_{k+1}}$ . In this case,  $A_{e_s}$  take the forms (35) and (36). Thus, we can write

$$\left(\sum_{l=1}^k \sigma_{ll}^{k+1}\right)^2 = (k-1)\left(\sum_{l=1}^k (\sigma_{ll}^{k+1})^2 + \sum_{l \neq j=1}^k (\sigma_{lj}^{k+1})^2 + \sum_{s=k+2}^m \sum_{l,j=1}^k (\sigma_{lj}^s)^2 + \omega\right) \tag{51}$$

such that

$$\omega = 2\tau(p) - \frac{c}{8} \left\{ (k-1)(k-6) + 3\|P_n\|^2 \right\} - \frac{k^2(k-2)}{k-1} \|\hbar\|^2. \tag{52}$$

Applying Lemma 3 to (51), we find

$$2\sigma_{11}^{k+1}\sigma_{22}^{k+1} \geq \omega + \sum_{l \neq j=1}^k (\sigma_{lj}^{k+1})^2 + \sum_{s=k+2}^m \sum_{l,j=1}^k (\sigma_{lj}^s)^2. \tag{53}$$

Using (53) in (27), it also follows that

$$\begin{aligned} K(e_1 \wedge e_2) &\geq \frac{c}{4} \left\{ 1 + \sum_{n=1}^3 [3g(\varphi_n e_1, e_2)^2 - \eta_n^2(e_1) - \eta_n^2(e_2)] \right\} \\ &\quad + \frac{1}{2} \omega + \sum_{s=k+2}^m \sum_{j>2} \{(\sigma_{1j}^s)^2 + (\sigma_{2j}^s)^2\} + \frac{1}{2} \sum_{s=k+2}^m (\sigma_{11}^s + \sigma_{22}^s)^2 \\ &\quad + \frac{1}{2} \sum_{s=k+2}^m \sum_{l,j>2} (\sigma_{lj}^s)^2 \end{aligned} \tag{54}$$

or we have

$$K(e_1 \wedge e_2) \geq \frac{c}{4} \left\{ 1 + \sum_{n=1}^3 [3g(\varphi_n e_1, e_2)^2 - \eta_n^2(e_1) - \eta_n^2(e_2)] \right\} + \frac{1}{2} \omega. \tag{55}$$

In view of (52) and (55), we get (48).

If the equality case of (48) occurs, then we find

$$\begin{cases} \sigma_{1j}^{k+1} = \sigma_{2j}^{k+1} = 0, & j = n+1, \dots, k, \\ \sigma_{lj}^s = 0, & l, j = n+1, \dots, k, \\ \sigma_{11}^s + \sigma_{22}^s = 0 \end{cases} \tag{56}$$

for  $s = k+2, \dots, m$ . From Lemma 3, it can be found

$$\sigma_{11}^{k+1} + \sigma_{22}^{k+1} = \sigma_{33}^{k+1} = \dots = \sigma_{kk}^{k+1}, \tag{57}$$

which shows that  $A_{e_s}$  becomes as in (49) and (50).

In view of Theorem 8, we get

**Corollary 7.** Let  $M$  be a  $k$  – dimensional 3 – semi-slant submanifold of  $\tilde{M}(c)$ . For each  $\varphi_l$  – plane section  $\Pi = \text{Span}\{e_1, e_2\}$ , we have

$$\tau(p) - K(e_1 \wedge e_2) \leq \frac{k^2(k-2)}{2(k-1)} \|\tilde{h}\|^2 + \frac{c}{8} \{k^2 - 7k + 14 + 9(s_1 + s_2 \cos^2 \theta)\}. \tag{58}$$

The equality case of (58) is satisfied if and only if  $A_{e_s}$  becomes as in (49) and (50).

**Proof.** Under this assumption, we find

$$\|P_n|_{\pi^\perp}\|^2 = 3(s_1 + s_2 \cos^2 \theta). \tag{59}$$

Using (59) in (48), the proof could be obtained.

**Corollary 8.** Let  $M$  be a  $k$  – dimensional submanifold of  $\tilde{M}(c)$  and  $\Pi = \text{Span}\{e_1, e_2\}$  be a  $\varphi_l$  – section.

i) We get the below table:

**Table 4:**

	$M$	Inequality
(1)	invariant	$\tau(p) - K(e_1 \wedge e_2) \leq \frac{k^2(k-2)}{2(k-1)} \ \tilde{h}\ ^2 + \frac{c}{8} \{k^2 + 2k - 15\}$
(2)	totally real	$\tau(p) - K(e_1 \wedge e_2) \leq \frac{k^2(k-2)}{2(k-1)} \ \tilde{h}\ ^2 + \frac{c}{4} \{k^2 - 7k + 32\}.$

ii) The equality case of (1)-(2) is satisfied if and only if  $A_{e_s}$  becomes as in (49) and (50).

**Proof.** Assume that  $M$  is invariant. In this case, we find

$$\|P_n|_{\pi^\perp}\|^2 = 3(s_1 + s_2) = 3(k-3). \quad (60)$$

Using (60) in (48), we obtain the first case of Table 4.

If  $M$  is totally real, then we have

$$\|P_n|_{\pi^\perp}\|^2 = 6. \quad (61)$$

Using (61) in (48), we obtain the second case of Table 4.

The proof of ii) is straightforward from Theorem 8.

### References

- [1] Kuo, Y., *On almost contact 3-structure*, Tôhoku Mathematical Journal (2) 22, 325–332, 1970.
- [2] Udriște, C., *Structure presque coquaternioniennes*, Bulletin Mathématique de la Société des Sciences Mathématiques de la République Socialiste de Roumanie, Nouvelle Série, 13, 487–507, 1969.
- [3] Balgेशir, M.B.K., *Point-wise slant submanifolds in almost contact geometry*, Turkish Journal of Mathematics, 40, 657-664, 2006.
- [4] Boyer, C. P., Galicki, K., *3-Sasakian manifolds*, arXiv preprint hep-th/9810250, 1998.
- [5] Galicki, K., Salamon, S., *Betti numbers of 3-Sasakian manifold*, Geometriae Dedicata, 63, 45-68, 1996.
- [6] Gibbons, G.W., Rychenkova, P., *Cones, tri-Sasakian structures and superconformal invariance*, Physics Letters B, 443, 138-142, 1998.
- [7] Kashiwada, T., *On a contact 3-structure*, Mathematische Zeitschrift, 238, 829-832, 2001.
- [8] Mann, B., Galicki, K., Boyer, C.P., *The geometry and topology of 3-Sasakian manifolds*, Journal für die. reine und angewandte Mathematik, 455, 183-220, 1994.
- [9] Montano, B. C., De Nicola, A., *3-Sasakian manifolds, 3-cosymplectic manifolds and Darboux theorem*, Journal of Geometry and Physics, 57, 2509-2520, 2007.
- [10] Chen, B.-Y., *Geometry of slant submanifolds*, Katholieke Universiteit Leuven, 1990.
- [11] Malek, F., Balgेशir, M.B.K., *Slant submanifolds of almost contact metric 3-structure manifolds*, Mediterranean Journal of Mathematics, 10, 1023-1033, 2013.
- [12] Malek, F., Balgेशir, M.B.K., *Semi-slant and bi-slant submanifolds of almost contact metric 3-structure manifolds*, Turkish Journal of Mathematics, 37, 1030-1039, 2013.
- [13] Chen B.-Y., *Mean curvature and shape operator of isometric immersions in real space forms*, Glasgow Mathematical Journal, 38, 87-97, 1996.

- [14] Chen B.-Y., *Relations between Ricci curvature and shape operator for submanifolds with arbitrary codimensions*, Glasgow Mathematical Journal, 41, 33-41, 1999.
- [15] Chen B.-Y., *Riemannian DNA, inequalities and their applications*, Tamkang Journal of Science and Engineering, 3, 123-130, 2000.
- [16] Chen B.-Y., *Pseudo-Riemannian geometry,  $\delta$  – invariants and applications*, World Scientific Publishing, 2011.
- [17] Akgün, A., Gülbahar, M., *Bi-slant submanifolds of an S manifold*, Arab Journal of Mathematical Sciences, 2021.
- [18] Li, Y., Khatri, M., Singh, J.P., Chaubey, S.K., *Improved Chen's inequalities for submanifolds of generalized Sasakian-space-forms*, Axioms, 11, 324, 2022.
- [19] Özgür, C., *Chen inequalities for submanifolds of a cosymplectic space form with a semi-symmetric metric connection*, Analele Stiintifice Ale Universitatii Al. I. Cuza Din Iasi-Serie Noua-Matematica, 58, 2012.
- [20] Poyraz, N.Ö., *Chen inequalities on spacelike hypersurfaces of a GRW spacetime*, Differential Geometry and its Applications, 81, 101863, 2022.
- [21] Poyraz, N.Ö., Doğan, B., Yaşar, E., *Chen inequalities on lightlike hypersurface of a Lorentzian manifold with semi-symmetric metric connection*, International Electronic Journal of Geometry, 10, 1-14, 2017.
- [22] Slesar, V., Şahin, B., Vilcu, G.E., *Inequalities for the Casorati curvatures of slant submanifolds in quaternionic space forms*, Journal of Inequalities and Applications, 2014, 1-10, 2014.
- [23] Siddiqui, A.N., Chen, B.Y., Bahadir, O., *Statistical solitons and inequalities for statistical warped product submanifolds*. Mathematics, 7, 797, 2019.
- [24] Tripathi, M.M., Gülbahar, M., Kılıç, E., Keleş, S., *Inequalities for scalar curvature of pseudo-Riemannian submanifolds*, Journal of Geometry and Physics, 112, 74-84, 2017.
- [25] Chen, B.-Y., *On Ricci curvature of isotropic and Langrangian submanifolds in complex space forms*, Archiv der Mathematik, 74, 154-160, 2000.
- [26] Chen B.-Y., *A Riemannian invariant for submanifolds in space forms and its applications* in: Geometry and Topology of Submanifolds, World Scientific Publishing, River Edge, 6, 58-81, 1994.
- [27] Hong, S., Tripathi, M. M., *On Ricci curvature of submanifolds*, International Journal Pure and Applied Mathematical Sciences, 2, 227-245, 2005.
- [28] Hong, S., Matsumoto, K., Tripathi, M.M., *Certain basic inequalities for submanifolds of locally conformal Kaehler space forms*, Sut Journal of Mathematics, 41, 75-94, 2005.
- [29] Tripathi, M.M., *Certain basic inequalities for submanifolds in  $(K, \mu)$  – spaces*, In: Recent Advances in Riemannian and Lorentzian Geometries (Baltimore, MD, 2003), Contemporary Mathematics 337, American Mathematical Society, 187—202, 2003.